UNIVERSITY OF SOUTHAMPTON

FACULTY OF SOCIAL and HUMAN SCIENCES

School of Mathematics

Modelling the Fluid Drainage Through Primary Lymphatic Valves

by

Charles William Heppell

Thesis for the degree of Doctor of Philosophy

November 2013

UNIVERSITY OF SOUTHAMPTON

ABSTRACT

FACULTY OF SOCIAL and HUMAN SCIENCES

SCHOOL OF MATHEMATICS

Doctor of Philosophy

Modelling the Fluid Drainage Through Primary Lymphatic Valves

by Charles William Heppell

This study investigates the fluid flow through tissues where lymphatic drainage occurs. Lymphatic drainage relies on two unidirectional valve systems, primary and secondary. The primary system is located in the initial lymphatics with, it is presumed, overlapping endothelial cells around the circumferential lining of lymphatic capillaries which act as unidirectional valves. The secondary lymphatic system is located in the lumen of the collecting lymphatics and is well studied in contrast to the primary system. We propose two models for the drainage of fluid by the lymphatic system that includes the primary valve system. The analysis identifies four key areas that affect lymphatic drainage. These are: the regular tissue deformations, the mechanics of the primary lymphatic valves, the fluid flow through the interstitium and that through the walls of blood capillaries. The models outline a new way of modelling the primary valve system that appears to be more relevant to experimental studies than previous models.

The first model presented in this thesis describes a permeable membrane around a blood capillary, an elastic primary lymphatic valve and the interstitium lying between the two. Here we pay special attention to the mechanics of the primary valve system, by assuming that lymphatic endothelial cells (primary valve system) deflect into the lumen (allowing fluid drainage) in response to pressure differences between the interstitium and the lumen. The model predicts a piecewise linear relation between the drainage flux and the pressure difference between the blood and lymphatic capillaries.

The second model presented in this thesis includes the regular tissue deformations in modelling lymphatic drainage. We propose a 'sliding door' theory of how lymphatic drainage occurs, which we base upon the premise that when the

interstitium expands (due to excess fluid) the surrounding matrix pulls open the lymphatic valves creating a gap for the interstitial fluid to drain into the lumen. The model predicts that after a certain number of valve cycles (close to open to close) the system relaxes to a steady state, in which the lymphatic valve stays open.

Contents

List of Figures

List of Tables

List of Publications

1. C.W Heppell, G. Richardson, and T. Roose. A model for fluid drainage by the lymphatic system. *Bull Math Biol* 2012 Nov;75(1):49-81.

2. C.W Heppell, T.Roose, and G. Richardson. A Model for Interstitial Drainage through a Sliding Lymphatic Valve. *Bull Math Biol* 2013 *Submitted*.

Declaration of Authorship

I, **Charles William Heppell**, declare that this thesis entitled **Modelling the Fluid Drainage Through Primary Lymphatic Valves** and the work presented in it are both my own, and have been generated by me as the result of my own research. I confirm that:

- this work was done wholly or mainly while in candidature for a research degree at this University;
- if any part of this thesis has previously been submitted for a degree or any other qualification at this University or any other institution, this has been clearly stated;
- where I have consulted the published work of others, this is always clearly attributed;
- where I have quoted from the work of others, the source is always given. With the exception of such quotations this thesis is entirely my own work;
- I have acknowledged all main sources of help;
- where the thesis is based on work done by myself jointly with others, I have made clear exactly what was done by others and what I have contributed myself;
- parts of this work have been published.

Signed: Date:

Acknowledgements

First and foremost I would like to thank my supervisors; Professor Tiina Roose and Dr Giles Richardson for their constant guidance, limitless patience and their constructive support throughout the compilation of this thesis. They were never short of brilliant ideas and insightful comments. Their advice and support not only in the academic matters, but also in the personal ones had given me the strength to continue until now. To Tiina, for her guidance on all things biology related and her tireless efforts to make my work resemble something like the English language. And to Giles, for always having spare time to discuss new methods even if its at the end of the day, i.e. all things mathematics related. Suffice to say that I could not have imagined having better supervisors and mentors for my PhD study. I have enjoyed working with them immensely, and have learned to appreciate the intricate workings of mathematical models.

Besides my supervisors, I would also like to thank Dr Marvin Jones and the rest of the staff in the mathematics department for making my stay enjoyable and welcome during an experience I will never forget. I would like to express my utmost gratitude to the School of Mathematics of the University of Southampton for giving me the opportunity to study applied mathematics at PhD level and the funding of my research EPSRC. Not only was I given the honour to carry out research in the applied department but I was also given the opportunity to travel to various places to present my work.

I am incredibly grateful for the support provided throughout my education by my parents, Madeleine and Paul Heppell, and to my twin brother, James, for his competitive nature, always driving me to do my best. Finally, I would like to give praise to my other half, Jin Heppell, who provided me with affection and moral support throughout my PhD study.

Chapter 1

Introduction to the Lymphatic System

This thesis is arranged as follows: this chapter provides a general introduction to the entire lymphatic system, in particular, the primary lymphatic system. Then we discuss previous models of the lymphatic system and derive two model hypotheses for primary lymphatic drainage, which will be the main focus of this thesis.

In Chapter 2 we develop the model of primary lymphatic drainage of hypothesis 1. We present our findings and compare them to the experimental literature. We conclude by comparing our model to previous models of primary lymphatic drainage.

In Chapter 3 we develop the model of lymphatic drainage of hypothesis 2. And in Chapter 4 we numerically solve the model. Again, we conclude by comparing results to previous models of primary lymphatic drainage.

Finally, in Chapter 5 we provide a summary of the work done in this thesis and conclude by considering which model surpasses the other. We also address possible future work.

1.1 Background to the Lymphatic System

The structure and importance of the lymphatic system is similar to the circulatory system [21, 94]. However, the lymphatic system is not as well understood as its counterpart. The lymphatics have been recognised both as a drainage system and as immunological control system for over a century now [110]. However, the mode of operation and mechanisms of this complex system have evaded a detailed analysis. This is primarily due to a failure to comprehend the full importance of the lymphatic system. Considerable progress in understanding the lymphatic system has been made in the last 20 years at the microcirculatory level [3, 47, 110]. Interest in the lymphatic system has grown in the biomedical research community as a result of its importance in cancer growth and metastasis [32, 93, 120].

Every day 2-4 litres of fluid are pushed into the interstitium by the pressure difference between the interior of blood capillaries and their surroundings [76, 136]. The lymphatic system, a network of capillaries adjacent to blood capillaries, drains this interstitial fluid and returns it to the blood circulation. This system in vertebrates is a network of conduits with clear fluid inside called lymph. The lymphatic system also includes the lymphoid tissue through which the lymph travels. These structures dedicated to the circulation and production of lymphocytes include: the spleen, lymphatic nodes, thymus gland and bone marrow [102].

If the exudate from blood capillaries is not drained efficiently by the lymphatic system then an abnormal accumulation of interstitial fluid causes the tissue to deform [122]. Edema, an abnormal accumulation of fluid in the interstitium, is the common outcome if the lymphatic system is damaged or becomes compromised. In addition to regulating the tissue fluid balance, the lymphatics serve as a major transport route for immune cells and interstitial macromolecules [128]. Cells and particles that flow in the lymphatic system experience lower flow rates and smaller shear stresses than they would in the blood circulation [1]. This is due to the high

permeability of the lymphatics [111]. There is little, if any, exclusion of interstitial molecules from the primary lymphatics. This is because of the nature of the one way valve system that allows the fluid and proteins to enter the lymphatic system but not leave it. Mediated immune responses occur in lymphatic nodes, which are part of the lymphatic system where mature lymphocytes reside. Lymph travels through many of these nodes before returning to the bloodstream. The lymph is cleaned by the removal of foreign materials and microorganisms (bacteria) in lymphatic nodes. For these reasons many studies have investigated drug delivery into the lymphatics [38, 45, 46, 57, 62, 132]

In the lymphatics there are two types of valve systems, both provide unidirectional flow. One at the level of the primary lymphatics, overlapping endothelial cells line the lymphatic capillaries and act as the primary valves; they open to drain interstitial and close to prevent back flow. The interstitial fluid first enters the lymphatic system through the primary lymphatic valves [105]. The other unidirectional valve system occurs in the lumen of the collecting lymphatics. These valves open to drain lymph through the capillary network to the blood circulation. The structure and mechanism of the secondary valve system is well recognized [70, 83, 131], and will only be briefly summarized in this introductory chapter.

1.2 History of the Lymphatic System

Hippocrates was one of the first persons to mention the lymphatic system, back in the fifth century BC. In his work "On Joints", he briefly mentioned lymphatic nodes. Which we now know plays an important role in mediating immune responses. The first mention of lymphatic vessels was in 3^{rd} century BC by Herophilus, a Greek anatomist living in Alexandria. He incorrectly concluded that the "absorptive veins of the lymphatics", by which he meant the lacteals, drained

into the hepatic portal veins, and thus into the liver. Next, Rufus of Ephesus, a Roman physician, identified the axillary, inguinal and mesenteric lymph nodes as well as the thymus gland during the first to second century AD [35]. Findings of Ruphus and Herophilus were further propagated by the Greek physician Galen, who described the lacteals and mesenteric lymph nodes in his dissection of apes and pigs in the second century A.D [35]. In the sixth century AD Procopius discovered a disease that he claimed "attacks the lymphatic glands" around the body. This disease was known as the Plague of Justinian (a disease supposed to be identical to the plague known as the Black Death), which had its origin in the east, and made its first appearance in Europe 543 AD, at Constantinople. Dr Musgrave discovered a disease in the ninth century AD called elephantiasis that was due to a migratory inflammation of the lymphatic system. According to Dr. Musgrave, this disease may affect many organs of the body, more often the legs. Eustachius was the first to discover the thoracic duct in a horse, around 1563. In 1622, Gaspare Aselli, an Italian physician, discovered the "milky veins" in the intestines of dogs. This is documented as the first historical discovery of the lymphatic vessels. In 1746, William Hunter thoroughly analyzed the function and the role of lymph ducts. Manual lymphatic drainage was introduced in the 1930s by a German doctor, Emil Vodder, for the treatment of immune disorders such as chronic sinusitis. While treating chronic colds he noticed that many of his patients had swollen lymph nodes. Although at the time the lymphatic system was poorly understood by the medical profession, Dr Vodder developed careful hand movements to aid lymph movement. Many scientists have studied the lymphatic system and have tried to model the system, mathematically. More recently, in 2002, Swartz modelled the lymphatic system in a mouse's tail [124]. In 2003, Mendoza modelled the mechanics of primary lymphatic valves and concluded that the overlap between neighbouring lymphatic endothelial cells in primary lymphatics

may serve as the primary valve system required for unidirectional transport from the interstitium into the lymphatic system [85]. The reason that the lymphatic system is becoming studied more in recent years is that it is now believed to play an important role in the development of diseases, such as certain types of cancer [66, 82, 86]. If we improve our understanding of the lymphatic system, we can improve our techniques in the methods that we use to cure these diseases.

1.3 Lymphatic Organs

An accumulation of lymphiod tissue can be found all around the body. For example, the tonsils (found in the back of the throat and nasal cavity) are an accumulation of lymphoid tissue. Below we describe the major primary and secondary lymphatic organs.

1.3.1 Primary Lymphatic Organs

Bone Marrow

Bone marrow is the flexible tissue found in the hollow interior of bones. There are two types of bone marrow: red marrow (consisting mainly of hematopoietic tissue) and yellow marrow (consisting mainly of fat cells). In adults, marrow in large bones produces new blood cells. Bone marrow contributes around 4 percent of our total body weight [122].

Stem cells in the bone marrow grow into immature B cells and T cells (lymphocytes). These cells are a group of white blood cells that are responsible for specific immune responses. B and T cells mature in primary lymphatic organs (thymus gland and the bone marrow). After maturity they migrate via the blood circulation to secondary lymphatic organs (lymph nodes and the spleen). Upon activation by specific antigens, B cells proliferate and differentiate into antibody–

secreting plasma cells. B cells also process and present antigens to helper T cells. B cells mature in the bone marrow. The T in "T cells", refers to the thymus gland, which is where they mature. This group of lymphocytes includes three subclasses: cytotoxic T cells, helper T cells and suppressor T cells. Immature T cells migrate from the bone marrow to the thymus gland. Upon activation by specific antigens, cytotoxic T cells directly attack cells bearing the same type of antigen. Helper T cells help to activate B cells and T cells, and suppressor T cells inhibit cytotoxic T cells and antibody production, i.e. turning off an immune response [122].

Thymus Gland

The thymus gland is colonized by immature T cells. It is a soft structure consisting of two lobes. It is located in the thorax, which is behind the sternum. At birth it weighs about 15 grams and by puberty weighs approximately 30 to 40 grams. It atrophies in old age and weighs about 15 grams again. The cortex has a sponge–like texture and consists of a network of epithelial reticular cells bound together by desmosome. Dense granules in the cytoplasm of these cells secrete hormones that promote the differentiation of T cells. Epithelial reticular cells envelop groups of T cells in the process of mitotic division and maturation. They also surround all blood vessels in the cortex, providing a blood–thymus barrier that prevents antigens in the blood from making contact with developing T cells. T cells in various stages of differentiation and maturation reside in the spaces between the reticular cells of the cortex. T cells develop into mature T cells here and are released into the blood circulation. These mature cells travel via the blood to the lymph nodes, where they reside and are responsible for cell mediated immune responses [122].

1.3.2 Secondary Lymphatic Organs

Lymphatic Nodes

All lymph passes through at least one lymphatic node before returning to the blood circulation [39, 48, 81]. There are hundreds of lymphatic nodes in an adult and they vary in size from 1 mm to 10 mm in diameter. White blood cells incubate and proliferate in these nodes. Lymphatic nodes consist of connective tissue with various types of white blood cells, most numerous being the lymphocytes. A lymph node is an organized collection of lymphoid tissue, through which lymph passes on its way to return to the blood circulation. Afferent lymphatic vessels carry in lymph, which percolates through the substance of lymphatic nodes, and is drained out by efferent lymphatic vessels. Lymphatic nodes are particularly numerous in the mediastinum in the chest, neck, pelvis, axilla (armpit) and inguinal (groin) region [1]. They are spherical in shape and are covered by a capsule of dense connective tissue. Lymphatic nodes filter the lymph by removing foreign material and micro–organisms (bacteria). Antibody–mediated and cell–mediated immune responses occur in these nodes [8, 122].

Spleen

The spleen is the largest of the lymphatic organs, about 12 cm long. It is located in the upper left portion of the abdominal cavity, just beneath the diaphragm and adjacent to the 10^{th} rib. Its shape resembles a large lymphatic node. The main function of the spleen is to filter the blood, as lymphatic nodes filter lymph. Antigens in the blood activate B and T cells residing in the spleen, triggering immune responses [122].

1.4 Lymphatics Development

Lymphatic tissues begin to form by the end of the fifth week of embryonic development [95]. They emerge from lymphatic sacs that arise from developing veins. The first lymphatic sacs to appear are the paired jugular sacs at the junction of the internal jugular and subclavian veins [103]. From the jugular lymphatic sacs, lymphatic capillary plexuses spread to the thorax, upper limbs, neck and head. Some of these plexuses grow and form lymphatic vessels in their respective regions. Each jugular lymphatic sac retains at least one connection with its jugular vein [41]. The next lymphatic sac to appear is the unpaired retroperitoneal lymphatic sac at the root of the mesentery of the intestine. It evolves from the primitive vena–cava and mesonephric veins. Capillary plexuses and lymphatic vessels spread from the retroperitoneal lymphatic sacs to the abdominal viscera and the diaphragm [18, 36]. This sac establishes connections with the cisterna chyli, but loses its connections with neighbouring veins. The last of the lymphatic sacs to form are the paired posterior lymphatic sacs, which mature from iliac veins [29]. The posterior lymphatic sacs produce capillary plexuses and lymphatic vessels on the abdominal wall, pelvic region, and lower limbs. The posterior lymphatic sacs join the cisterna chyli and lose their connections with adjacent veins. Lymphatic endothelial cells accumulate along the lymph vessels and sacs, and as connective tissue invades the sacs, the cells are caught in the developing mesh. Their rapid proliferation then forms the typical postnatal cortical nodules and medullary cords. The cortical nodules are small nodules of microscopically normal tissue. Medullary cords are the portions of the lymph node that contain lymphatic tissue [112]. Most of these sacs become lymphatic nodes.

1.5 Damaged Lymphatics

If the lymphatic system becomes damaged or has malformations, abundant accumulation of lymph is often observed and this can cause swelling in the tissue [24], usually affecting the lower limbs, although the face, neck and abdomen may also become affected. Also, the immune response system becomes weaker, i.e. more susceptible to foreign particles [50, 87]

1.5.1 Edema

Edema or oedema, formerly known as dropsy or hydropsy syndrome, is an abnormal accumulation of fluid beneath the skin. Many factors contribute to the formation of edema. We have summarised them into five key factors below [67],

1. An increase in hydrostatic pressure inside blood vessels.

2. A reduction in osmotic/oncotic pressure within blood vessels.

3. An increase in the blood vessel wall's permeability (as in inflammation).

4. An obstruction of fluid clearance via the secondary lymphatics.

5. Changes in the water retaining properties of the tissues themselves.

1.5.2 Lymphedema

Lymphedema, also known as lymphatic obstruction, is a condition of localized fluid retention and tissue swelling caused by a compromised lymphatic system [84]. There are two types of lymphedema: primary lymphedema and secondary lymphedema. It may be inherited (primary) or caused by an injury to the lymphatic system (secondary). It is most frequently seen after lymph node dissection, surgery, radiation therapy or the treatment of cancer, most notably breast cancer

[101, 127]. This condition might not even develop until months or years after therapy has concluded. Lymphedema may also be caused by accidents, certain diseases, or problems that may inhibit the lymphatic system from functioning properly. In tropical areas of the world, a common cause of secondary lymphedema is filariasis, a parasitic infection. While the exact cause of primary lymphedema is still unknown, it generally occurs due to poorly–developed or missing lymphatic nodes in the body. Secondary lymphedema affects both men and women. In women, it is most prevalent in the upper limbs after breast cancer surgery and lymphatic node dissection, occurring in the arm on the side of the body, where the surgery was performed. In men, lower–limb secondary lymphedema is most common, occurring in one or both legs [59, 60]. Head and neck lymphedema can be caused by surgery or radiation therapy for tongue or throat cancer.

The symptoms of lymphedema may include: a heavy swollen limb or localized fluid accumulation in other body areas, discoloration of the skin overlying the lymphedema, all accompanied by severe fatigue. When the lymphatic impairment becomes so great that the lymph exceeds the lymphatic system's ability to drain it, an abnormal amount of fluid collects in the tissues of the affected area. If left untreated, this stagnant, fluid will cause tissue to deform. This interferes with immune responses and provides a rich culture medium for bacterial growth.

Whether primary or secondary, lymphedema develops in stages, from mild to severe. Methods of staging are numerous and inconsistent. They range from three to as many as eight stages [107]. Here are the most common stages.

Stage 0 (latent)- The lymphatic capillaries have sustained some damage that is not yet apparent. Transport capacity is still sufficient for the amount of lymph being drained. Lymphedema is not present.

Stage 1 (spontaneously reversible)- When pressed by the fingertips, the affected area indents and holds the indentation. Usually upon waking in the morn-

ing, the limb or affected area is normal or almost normal in size.

Stage 2 (spontaneously irreversible)- The tissue is now "spongy". When pressed by the fingertips, the tissue bounces back without any indentation. The limbs are now hardened and increased in size.

Stage 3 (lymphostatic elephantiasis)- The swelling is irreversible and usually the limbs or affected area are very large. The tissue is hard and unresponsive; This generally occurs only in the legs.

Lymphedema can also be categorized by its severity:

Grade 1 (mild lymphedema)- Lymphedema involves the distal parts such as, your forearm, your hand and your lower leg or foot. The difference in circumference is less than 4 cm, and other tissue changes are not yet present.

Grade 2 (moderate lymphedema)- Lymphedema involves an entire limb or corresponding quadrant of the trunk. Difference in circumference is more than 4 cm but less than 6 cm.

Grade 3a (severe lymphedema)- Lymphedema is present in one limb and its associated trunk quadrant. The difference in circumference is greater than 6 cm. Significant skin alterations are present. Additionally the patient may experience repeated attacks of erysipelas.

Grade 3b (massive lymphedema)- The same symptoms as Grade 3a except that two or more extremities are affected.

Grade 4 (gigantic lymphedema)- Also known as elephantiasis. In this stage of lymphedema, the affected extremities are huge due to an almost complete blockage of the lymphatic channels.

1.6 Lymphatic Drainage

There are two lymphatic valve systems in the lymphatics, primary and secondary that drain interstitial fluid. They are distinguished by their valves. Primary valves are at the level of the initial lymphatic endothelium and secondary valves are positioned in the lumen of secondary lymphatic vessels. Micro–spheres ($0.3\mu m$ in diameter) deposited in the immediate proximity of an initial lymphatic channel readily enter into the primary lymphatics. Once inside the lymphatic channel they are not able to return back into the interstitial space without rupture of the lymphatic wall because of the unidirectional feature of the valve [104]. The secondary valve system provides unidirectional transport of lymph to the blood circulation via lymphatic nodes. The structure and mechanics of the secondary valve system is well recognized. Unlike the cardiovascular system, the lymphatic system is not a closed loop and has no central pump (i.e., heart). Lymph movement through secondary lymphatic vessels occurs due to peristalsis, valves, compression during contraction of adjacent skeletal muscles and arterial pulsation [4, 51, 91, 135]. A drawing from Leak [72] of a short segment of a lymphatic capillary was reconstructed from election micrographs, see Figure 1.1.

As the blood travels from the branching arteries down to the smallest capillaries, plasma fluid and proteins are forced out of the capillaries and into the interstitial space. Most of the exudate actually gets reabsorbed into the post–capillary venules, but because of the osmotic forces resulting from protein extravasation, there is a small net fluid flux out of the vasculature into the interstitium [125]. This excess fluid builds up in the interstitium and forces itself to convect through the tissue and to be drained by the lymphatics. The primary lymphatic system is freely permeable to macromolecules and thus serves as a primary role in maintaining osmotic and hydrostatic pressures within the interstitial space. The protein composition of the lymph is nearly equivalent to that of the interstitial

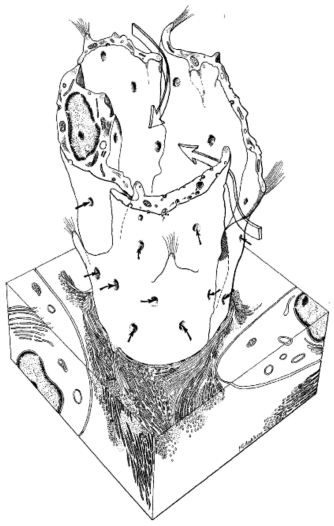

Figure 1.1: Figure from Leak [72]. A diagram of a short segment of a lymphatic capillary that was reconstructed from collated electron micrographs.

fluid, which in turn, is similar to, but usually less concentrated than, that of blood plasma.

1.6.1 Primary Lymphatics

Blood capillaries supply nutrients and important metabolites to all tissues in the body [30, 92, 123]. The exchange of respective constituents between the blood and the tissues is not direct, it travels through an intermediary called interstitial space [115, 138]. The interstitial space occupies the spaces between the cells and acts as their immediate environment. As blood capillaries and surrounding cells continually add and remove substances from the interstitial space, its composition will be constantly changing. Interstitial fluid forms at the arterial end of blood capillaries because of the high pressure inside these capillaries. Some of the exudate from blood capillaries, which amounts to 10 to 20 percent of interstitial fluid, enters the lymphatic capillaries as lymph [117]. About three litres of excess interstitial fluid is produced daily by the filtration of the blood plasma. Thus, lymph, when formed, is a watery clear liquid with a similar composition to the

interstitial fluid [113].

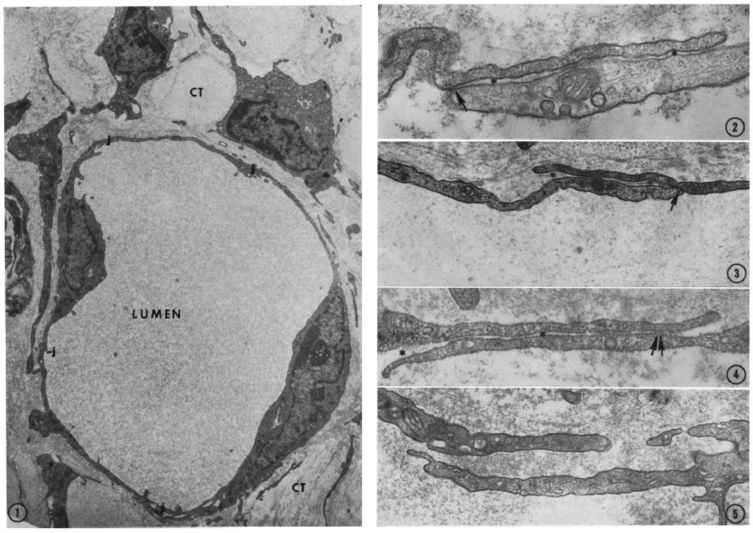

(a) (b)

Figure 1.2: Both images (a) and (b) are micrographs from Leak [72]. (a) Cross section of a lymphatic capillary (in a guinea pig); CT and J refer to connective tissue elements and intracellular junctions. $\times$ 7000. (b) A micrograph that illustrates the overlap of lymphatic endothelial cells. Fig. 2, $\times$ 89,500; Fig. 3, $\times$ 21,000; Fig. 4, $\times$ 39,000; Fig. 5, $\times$28,000.

Lymphatic capillaries are tiny thin–walled structures (around 20μm in diameter) that are closed at one end and are located in the spaces between cells throughout the body. The main purpose of these capillaries is to drain excess interstitial fluid from around the cells ready to be filtered and returned to the blood circulation. Figure 1.3 shows a cross–sectional drawing of the primary lymphatics, while Figure 1.2a and 1.2b, images from Leak [72], illustrate the circular nature of a lymphatic capillary and the short lymphatic endothelial cell overlap. Lymphatic capillaries are slightly larger in diameter than blood capillaries and they have a unique structure that allows interstitial fluid to drain into them, but not out. The ends of the endothelial cells that make up the wall of a lymphatic capillary overlap [16, 23, 111] and are the primary lymphatic valves. Swartz [126] proposed that the lymphatic valves open in response to different pressures between the lymphatic lumen and the surrounding interstitial space. The lymphatic

lumen fluid pressure will start to increase due to the incoming fluid from the interstitium and eventually become comparable to that in the interstitial space, which would result in the cells adhering more closely and the lymph not being able to escape back into the interstitium. Another theory of how the primary lymphatic valve system functions is that the lymphatic valves open in response to interstitial deformations [20, 22, 55]. Attached to lymphatic valves are anchoring filaments that contain elastic fibres. They extend out from lymphatic capillaries, creating a normal force to the wall. These anchoring filaments maintain the firm attachment of the capillary network to their surrounding matrix. Thus when the interstitial space surrounding lymphatic capillaries deform, it must have an affect on lymphatic drainage [27, 52, 77].

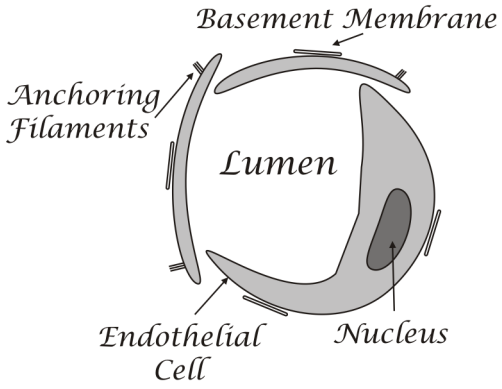

Figure 1.3: Cross–sectional view of the initial lymphatics [8].

1.6.2 Secondary Lymphatics

There are five main categories of conduits in the lymphatic system: the capillaries, the collecting vessels, the lymph nodes, the trunks and the ducts [19]. Their sizes range from 10 μm to 2 mm in diameter. An illustration of fluid flow through the secondary lymphatics is shown in Figure 1.4. Fluid travels from one segment to another, illustrated by the arrows in Figure 1.4, by contractions of the surrounding

skeletal muscles and the unidirectional feature of secondary valve system. All of the five conduits have secondary valves that keep the flow unidirectional [134]. Once in the lymphatic lumen the fluid is drained down the collecting vessels and into lymphatic nodes. Then the lymph drains into larger lymphatic vessels called lymphatic trunks, which, in turn, lead into the lymphatic ducts. The lymphatic trunks are the largest structures that drain lymph from the final set of lymph nodes into the ducts. Finally, the ducts return the lymph back into the bloodstream via the subclavian vein, completing the circuit of fluid transport. There are two types of lymph ducts: the right lymphatic duct and the thoracic duct (aka the left lymphatic duct). The right lymphatic duct drains lymph from the right arm, the right side of the head and the neck, and the lower lobe of the left lung into the right subclavian vein. All other sections of the body are drained by the thoracic duct. The right lymphatic duct stems from the subclavian and bronchomediastinal trunks and rarely extends beyond a centimeter at most. It lies in front of the scalenus anterior muscle. The thoracic duct drains the lymph into the blood circulation at the left subclavian vein. It starts in the upper abdomen at a small sac named the cisterna chyli. The morphology of the thoracic and right lymphatic ducts conforms to other large lymphatic vessels, although the walls are often thicker. Both ducts are guarded at their central ends by valves that stop the back flow of blood.

The term, "lymphatic trunk", is often used loosely, being properly defined as those named structures that drain the major regions of the body and that form the larger tributaries of the ducts. The walls of the lymphatic trunks are also thin, although thicker than their tributaries. The trilaminar structure is usually evident by light microscopy and the valves are plentiful [1, 26].

Lymphatic capillaries lack a definitive basal lamina around their wall [90, 69]. This is a structural feature that serves as a major criterion for the identification

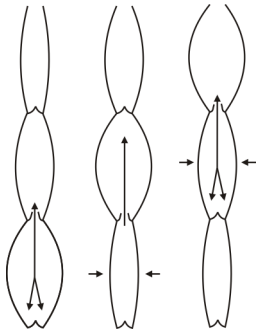

Figure 1.4: Shows the expansion and contraction of the secondary lymphatics. Fluid travels from one segment to another by contractions of the surrounding skeletal muscles and the unidirectional feature of secondary valve system. The arrows in the lumen illustrate the fluid movement, while the arrows outside illustrate tissue dilation.

of these capillaries at the electron microscopic level. The short segments of a basal lamina around the wall are presumed to represent the transitional region between lymphatic capillaries and the larger lymphatic collecting conduits that contain a continuous basal lamina. Segments of newly formed or regenerated blood capillaries also lack a continuous basal lamina, and they are likewise very permeable to large molecules.

1.7 Previous Models of the Lymphatic System

Despite the importance of the lymphatic system, relatively few people have attempted to model it. Below are brief descriptions of a few models for the flow through collecting lymphatics followed by models of the flow though the primary lymphatics.

In the work by Macdonald et. al [78], the flow in collecting lymphatic vessels is modelled. They measure the static and dynamic mechanical properties of excised bovine collecting lymphatics and develop a one–dimensional computational model of the coupled fluid flow/wall motion. The computational model is able to reproduce the pumping behaviour of the real vessel.

Reddy and Patel [99] developed a mathematical model of the fluid flow through terminal lymphatics. Their computer simulation results concluded that fluid absorption and flow through the terminal lymphatics occur due to suction mechanisms of the adjacent contractile lymphatic segments and due to periodic fluctuations in the interstitial fluid pressure.

Swartz and Boardman [124] have investigated normal lymphatic functions in a mouse tail skin and used it in various capacities for multi level studies of lymphatic function, physiology, and biology. The technique they used to image lymphatic flow is called microlymphangiography. It involves injecting fluid tracer intermediately into the tail tip. As the fluid tracer travels into the lymphatics, it reveals the functional vessels through which it flows. Also, an injection of fluid tracer at the tail tip allows transport only in the proximal direction, first within the tissue interstitium and then within the lymphatic network. Their work was initially used to characterize and quantify flow velocities within the lymphatic network, then went onto evaluating mechanical events at the interstitial lymphatic interface. They developed a theoretical model to describe the balance between lymphatic uptake, fluid flow, and fluid pressure in the tail. By measuring transient and spatial distributions of interstitial fluid pressure with micropipettes, they validated the model and it was estimated that there are three key bulk parameters of tissue fluid balance: lymphatic conductance, hydraulic conductivity and extracellular matrix elasticity. The extracellular matrix is the extracellular part of a tissue that usually provides structural support to the cells in addition to performing various other important functions. Their unique model provided the first in situ measurements of these parameters. They also modified their model to study the changes in these fluid transport properties during altered conditions such as chronic lymphedema [124].

Another paper by Swartz et. al [126], aimed to test their hypothesis that bulk

tissue fluid movement can be evaluated in situ and described by a linear biphasic theory which integrates the regulatory function of the lymphatics with the mechanical stresses of the tissue. They accomplished this by developing an experimental and theoretical model using the skin of a mouse's tail. The model produced here was based on a previously developed model to describe fluid movement in solid tumours with capillary re–absorption (Netti et al [89]). They expanded on this model by focusing on the role of the lymphatics in controlling this mechanical relationship. The results shown in their paper validated their hypothesis. This model is useful for examining potential treatments for edema and lymphatic disorders as well as substances which may alter the lymphatic drainage.

Reddy et al [100] developed an in vivo model for evaluating interstitial convection of injected macromolecules and nanoparticles. Fluorescently labelled macromolecules and particles are injected into a mouse tail tip. The relative convection coefficients are determined from spatial and temporal interstitial concentration profiles. In their sensitivity analysis, they compare the effects of size, shape, and charge on interstitial convection.

Dixon et al [31] measured lymphocyte velocity, lymphatic contraction, and shear stress in phasically contracting lymphatics in situ. They used a high speed video system to capture multiple contraction cycles. Ikomi et al [56] examined the protein transport, and the transport of leukocytes in prenodal lymph vessels in the skin with and without massage. A comparison is made under similar circumstances in a region of the skin where the microanatomy of the lymphatic network has previously been delineated.

Mendoza and Schmid–Schönbein [85] proposed a model for primary lymphatic valves at the junctions between lymphatic endothelial cells. The model consists of two overlapping endothelial extensions at a cell junction in the initial lymphatics. One cell extension is firmly attached to the adjacent connective tissue while the

other cell extension is not attached to the interstitial collagen. It is free to bend into the lumen of the lymphatics. This analytical model illustrates the mechanics of the valve's movement, the model also provides analysis of the mechanisms underlying fluid collection in the initial lymphatics and lymph transport in the microcirculation.

Galie and Spilker [42] utilizes a finite element model to characterize the transendothelial transport through overlapping endothelial cells in primary lymphatics during the uptake of interstitial fluid. They produced a computational model which is built upon the analytic model created by Mendoza and Schmid–Schönbein [85]. Their goal was to investigate how adding more sophisticated biomechanics affects the model's prediction of fluid uptake. One of the outcomes they found was that the cell deflection was less in the computational model than in the analytical model at each point along the endothelial cell. The main differences in the cell deflection was that the computational model used a porous medium to represent the interstitial space and they used both components of the velocity, whereas in the analytical case they did not use a porous medium to represent the interstitial space and they only used the velocity tangent to the attached endothelial cell.

1.8 Lymphatic Drainage Model Hypotheses

It is still unclear how primary lymphatic valves truly operate due to the complexity of the system and the scarcity of research in this field. Previous models of the drainage of the primary lymphatic valve system need further investigation to add more physiological detail, which has a significant affect to primary lymphatic drainage. For example, to include the curved nature of primary lymphatic valves, a short lymphatic endothelial cell overlap, resistance to flow from the interstitium and through the blood capillaries and the regular deformation of surrounding

tissues. Primary lymphatic valves are presumed to open to drain interstitial fluid and close to prevent back flow. This opening could for instance be driven by the pressure difference between the interior and exterior of the lymphatic capillaries [42, 49, 78, 85, 99], or open in response to the surrounding interstitial space deforming [5, 6, 17, 65, 98]. Below two hypotheses of how the primary lymphatic valve opens and closes are discussed, with predictions of the fluid flux into the lymphatic system from both hypotheses, see Figure 1.6 and Figure 1.8. These two hypotheses are the focus of this thesis, and are evaluated in Chapters 2, 3 and 4.

1.8.1 Hypothesis 1: Fluid drainage Through a Bending Lymphatic Valve

The focus of this section is to introduce to the reader a model of primary lymphatic drainage. We start with the exudate from blood capillaries (the first resistance to fluid flow), then the flow through the interstitial space (another resistance to flow), opening of the lymphatic valve and the drainage into the lymphatic lumen (the last resistance to fluid flow). These stages of lymphatic drainage are displayed in Figure 1.5. This approach to modelling lymphatic drainage, similar to primary lymphatic valve models in [42, 49, 85, 99], is limited to the analysis of junctions formed by overlapping endothelial cells around lymphatic capillaries. Studying the mechanics of these valves will help our understanding of the interstitial fluid flow rates into lymphatic capillaries. The interstitial fluid is assumed to be Newtonian and inertial forces are neglected since the Reynolds number for the flow is small [42, 85, 110].

We formulate a model that consists of the interstitium (modelled as a porous medium), the blood capillary wall (modelled as a permeable membrane that produces a linear resistance to flow) and a geometrically nonlinear elastic primary lymphatic valve. The lymphatic valve is modelled in two states, closed and open.

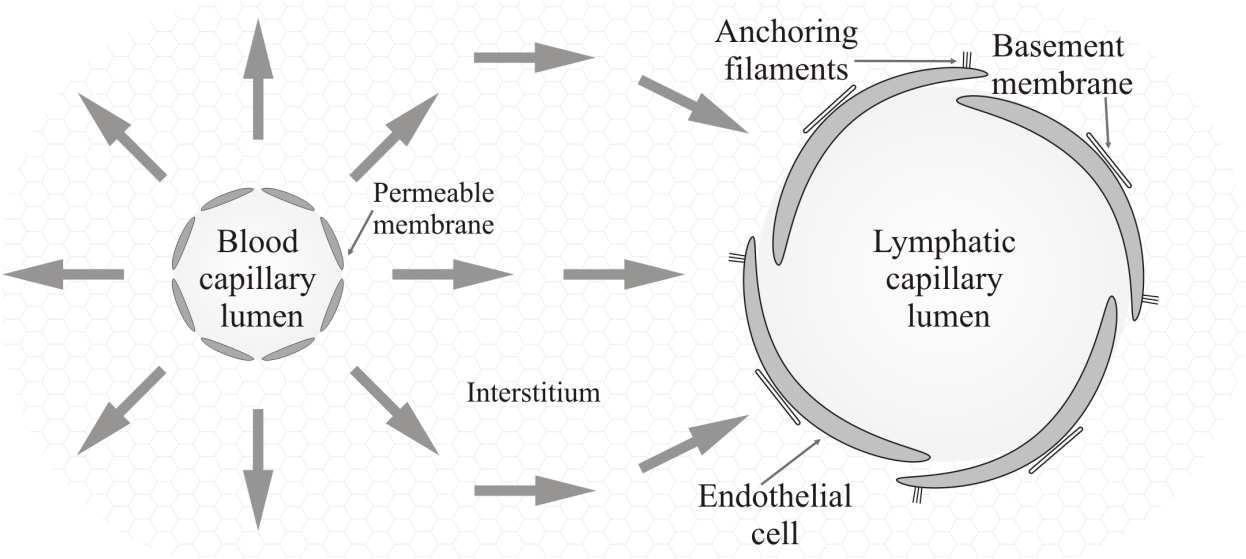

Figure 1.5: A cross sectional view of a tissue where lymphatic drainage occurs. Fluid travels from the blood capillary through the interstitial space into the lymphatics as shown by the arrows in the above drawing. The overlapping lymphatic endothelial cells make up the primary valve system.

When a lymphatic valve is closed, no interstitial fluid enters or exits via the primary lymphatic valves. When a lymphatic valve is open, interstitial fluid drains into the lumen of the lymphatics. The fluid that resides in the lymphatic capillary lumen is thought to drain through the collecting lymphatics by expansions and compressions of skeletal muscle around secondary lymphatic vessels [122].

Most of our attention was to the mechanism of the primary lymphatic valves. We were motivated by anatomical studies of Leak [73], to consider a lymphatic valve formed by endothelial cells that span a quarter of the circumference of the capillary, anchored at one end and with a relatively small region of overlap with the next endothelial cell. Assuming that the valve is unstressed when straight, but under stress in its usual curved configuration leads to the predictions (that we shall elucidate further in Chapter 2) that the lymphatic valve opens when the pressure difference between the exterior (P_l) and interior (P_0) of the lymphatic lumen exceeds a certain critical pressure P_{crit}, and that the minimum resistance of an open lymphatic valve is constant and proportional to P_{crit}. In other words

either the volumetric fluid flow rate per unit length into the lymphatic capillary is zero or proportional to the pressure difference $P_l - P_0 = P_{crit}$. Once this critical pressure difference has been reached it takes little extra pressure difference to open the valve further and allow appreciably more flow. In other words the major resistance to extra flow is nearly all due to the resistance of the interstitial space. Our reason for believing this to be true is the small overlap between the valve and the endothelial wall which is incapable of providing much resistance to flow through it. Mathematically this statement when combined with the linear fluid flow through the interstitium and the blood capillary wall, can be formulated in terms of the following piecewise linear relation between the volumetric fluid flow rate per unit length Q between the blood capillary and the lymphatic capillary,

$$Q = \begin{cases} 0 & \text{if} \quad \widehat{P} < P_0 + P_{crit} \\ \Lambda(\widehat{P} - (P_0 + P_{crit})) & \text{if} \quad \widehat{P} > P_0 + P_{crit}. \end{cases}$$

Here Λ is a geometric constant taking into account the specific arrangement of lymphatic capillaries with respect to blood capillaries and $\widehat{P}$ is the lumen fluid pressure in the blood capillary. The predicted flux Q is plotted in Figure 1.6.

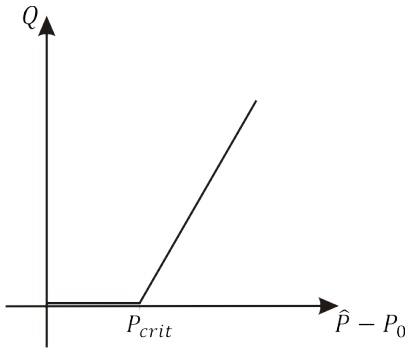

Figure 1.6: The predicted piecewise linear fluid flux per unit length through the interstitial space and the initial lymphatics as a function of the pressure difference between the blood and lymphatic lumen $\widehat{P} - P_0$.

This work is presented in Chapter 2, and published in [49].

1.8.2 Hypothesis 2: Fluid Drainage Through a Sliding Lymphatic Valve

The models in [42, 49, 85, 99] for the mechanism of primary lymphatic valves have lymphatic valves open in response to pressure differences between the interstitium and the lymphatic lumen. In [49], for example, a single lymphatic valve is treated as a geometrically nonlinear elastic beam that is deformed by the pressure differences between the interstitium and the lymphatic lumen. However, the model did not include the frequent expansions and contractions of the interstitium (that contains lymphatic capillaries) throughout the body. These changes in the tissue's matrix are likely to affect lymphatic drainage because anchoring filaments attached to the lymphatic valves are believed to maintain firm attachment between the lymphatic capillary wall and the surrounding interstitium [20, 22, 27, 74, 77]. Hence when the interstitium deforms these anchoring filaments get pulled, creating normal tensions inside the capillary wall. Lymphatic anchoring filaments are presumed to increase the lumenal volume when the interstitium is undergoing swelling [55, 99, 122]. The effects of tissue expansions on interstitial drainage has not been previously included in models of the primary lymphatic system.

In this Hypothesis we propose a 'sliding door' theory of how lymphatic valves drain interstitial fluid that is different to the premise of hypothesis 1. This theory incorporates regular tissue deformations, which occur when the lymphatic system is unable to drain the excess interstitial fluid. This model is based upon the premise that when the interstitial space around the lymphatic capillary expands it pulls open the lymphatic valves. This creates a gap for the interstitial fluid to drain into the lumen. We predict a smooth transition from a closed to open lymphatic valve in this model. In Figure 1.7, we demonstrate the opening of the lymphatic valve in this 'sliding door' fashion. The thick arrows in both drawings Figures 1.7a and 1.7b indicate the deflection of the interstitial space, while

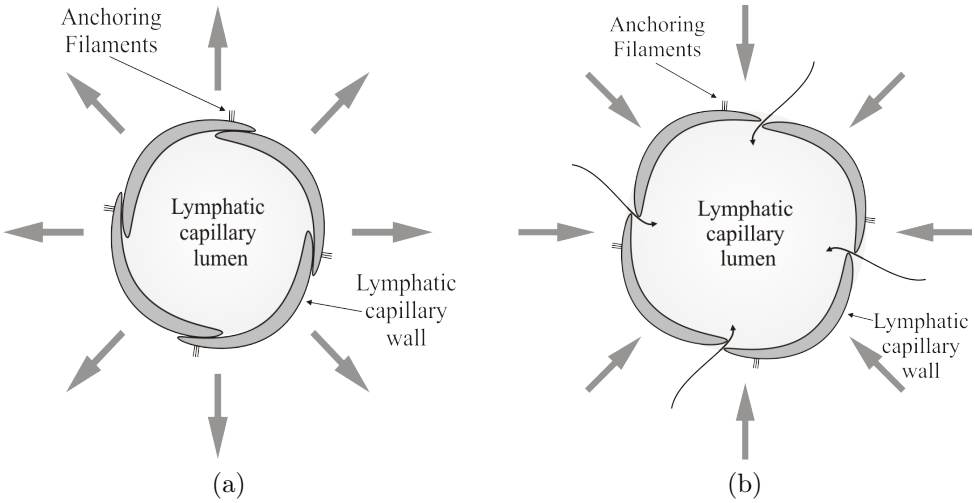

Figure 1.7: Two cross sectional drawings of a lymphatic capillary. The lymphatic valve cycles from closed (a) to open (b) by the expansion of the surrounding interstitium. The thick arrows in (a) and (b) indicate the direction of the tissue deformation, while the thin arrows in (b) indicate fluid motion.

the thin arrows indicate the fluid movement. Around a lymphatic capillary we presume there are four valves. We are unaware of any previous analysis of this 'sliding door' hypothesis of primary lymphatic drainage. Rossi et al [106] hypothesized that interstitial fluid drainage is accommodated by the act of pulling apart interendothelial junctions on the lymphatic capillary wall. Based on their results they speculated that lymphatic anchoring filaments do help in the drainage of interstitial fluid. The predicted flux Q is plotted in Figure 1.8.

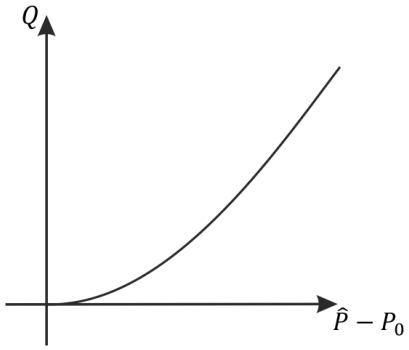

Figure 1.8: The predicted non–linear fluid flux per unit length through the interstitial space and the initial lymphatics as a function of the pressure difference between the blood and lymphatic lumen $\widehat{P} - P_0$.

Chapter 2

Model of Hypothesis 1: Fluid drainage Through a Bending Lymphatic Valve

2.1 Introduction

In this chapter we formulate and solve a model for lymphatic drainage, that was discussed in section 1.8.1 (hypothesis 1). Firstly, we derive and solve the interstitial fluid flow (i.e. for a Darcy flow through a porous medium). This results in one second order partial differential equation for the fluid flow through the interstitium. Due to the complex geometric nature in this problem we use a conformal mapping approach to determine all the geometrical parameters. Then we formulate and solve a model for the mechanism of the lymphatic valve (based upon the hypothesis that the overlapping lymphatic endothelial cells act as unidirectional valves). In order to do this we use geometrically non linear beam theory to model the deflection of the lymphatic valve. This results in a third order ordinary differential equation. Finally we couple the model for the interstitial fluid

flow with the model for the deflection of the lymphatic valve to give the reader a complete picture of lymphatic drainage from the vascular capillaries, through the interstitium and into the lymphatic system. At the end of this chapter we draw our conclusions and compare our results to similar studies by others.

2.2 Modelling the Interstitial Fluid Flow

The model formulated in this chapter demonstrates how the drainage of fluid from tissues occurs. In our treatment of the fluid flow we concentrate on the regions across which we expect the major pressure drops to occur. There are three: (I) when the fluid moves through the wall of the blood capillary into the interstitium, (II) when the fluid passes through the interstitial space, and (III) when the fluid travels into the lumen of the lymphatic capillary.

Pressure variation in the capillary lumen occurs over relatively long length scales in the z–direction (out of the the plane shown in Figure 2.1). This suggests that a two dimensional analysis restricted to the x-y plane is sufficient in order to provide a good understanding of the functioning of the initial lymphatic valves.

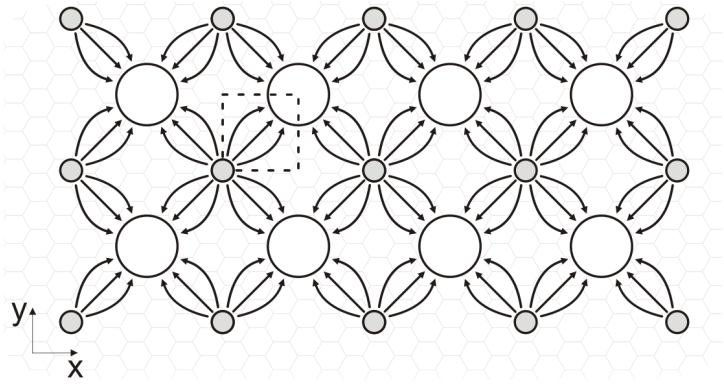

Figure 2.1: An idealised drawing of a cross–sectional view of lymphatic and blood capillaries. The white and gray circles correspond to lymphatic and blood capillaries, respectively. The arrows indicate the fluid's movement across the interstitial space filling the regions between the lymphatic and blood capillaries. The dotted square represents a periodic tile that we model the fluid flow from a single blood capillary to a single lymphatic capillary, 117 $\mu m \times 117$ μm.

In order to further simplify the modelling we assume that the lymphatic and blood capillaries are arranged in a square lattice, as displayed in Figure 2.1. The symmetry of this lattice means we need only consider a representative tile as illustrated by the dotted square in Figure 2.1. We take an average distance between blood and lymphatic capillaries to be 150μm [72], so that the periodic tile has sides of length $\sqrt{(150\mu m)^2/2} \approx 117\mu$m. The symmetry of the pattern ensures that the pressure gradients normal to the walls of the tile are zero. Figure 2.2 provides a detailed schematic of this tile. We assume that lymphatic valves occur quarterly around the circumferential lining of lymphatic capillaries (see, for example [72]).

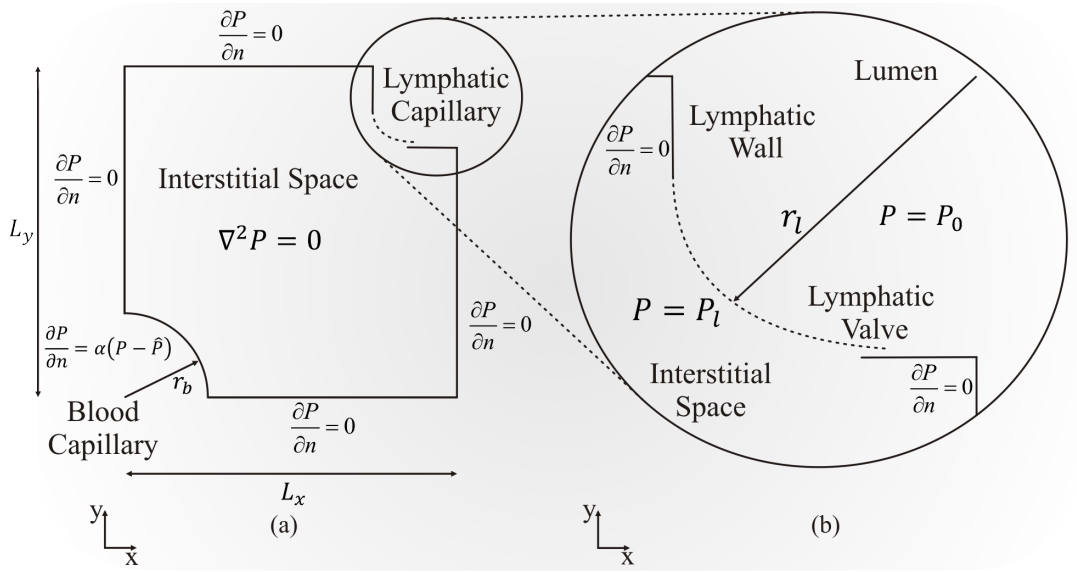

Figure 2.2: (a) Successive blow ups of the periodic tile in Figure 2.1 and around the lymphatic capillary. (b) Magnification of the lymphatic capillary from the first figure (a), delivering a more detailed view.

Blood capillaries are the smallest vessels in the body's circulatory system and typically measure $5 - 10$ μm in diameter. Furthermore, they are small compared to the separation between blood and lymphatic capillaries (150μm). So we can assume that the flow in the immediate vicinity of the blood capillary is radially symmetric about the centre of the blood capillary and can be approximated by

the solution to Laplace's equation, $P = \overline{\chi} + \overline{\gamma}\ln(r)$, for arbitrary constants $\overline{\chi}$ and $\overline{\gamma}$, where $r = (x^2 + y^2)^{\frac{1}{2}}$. Without loss of generality we can rewrite this in the form,

$$P \approx \widehat{P} + \chi + \gamma \ln\left(\frac{r}{r_b}\right), \tag{2.2.1}$$

where χ and γ are constants and r_b is the radius of the blood capillary. We discuss the local form of the solution further in section 2.2.4.

2.2.1 Model Development for the Fluid Flow

In this section we introduce a model of the fluid flow through the interstitial space and into the lymphatic capillary. We focus on the three areas of high resistance to flow that were mentioned in the previous section.

The first of these regions occurs as the fluid passes through the permeable wall of the blood capillary. This wall has a very low permeability, preventing excessive leakage of fluid, and can be modelled by a boundary condition on the wall, of the form $\mathbf{n} \cdot \mathbf{u}_B = -\beta(P - \widehat{P})$, where β ($\mu\text{m}^2 s\ \text{kg}^{-1}$) describes the semipermeable membrane of blood capillaries (the permeability of the blood capillary wall divided by the product of the viscosity of the lymph and the thickness of blood capillary wall), $\mathbf{n}$ is the normal vector to the blood capillary wall pointing in the direction of the interstitial space, $\mathbf{u}_B$ (μms^{-1}) is the fluid velocity in the blood capillary and P (Pa) and $\widehat{P}$ (Pa) are the fluid pressures in the interstitium and in the blood capillary lumen, respectively.

The next major source of resistance to flow is from the interstitial space, which is modelled as a porous medium. Darcy's Law, together with incompressibility of the fluid, characterizes the interstitial flow, such that the fluid velocity ($\mathbf{u}$) satisfies,

$$\mathbf{u} = -\frac{\kappa}{\mu}\nabla P, \tag{2.2.2}$$

$$\nabla \cdot \mathbf{u} = 0, \tag{2.2.3}$$

where P (Pa) is the interstitial fluid pressure, κ (μm^2) is the permeability of the interstitium and μ (kgm^{-1}s^{-1}) is the viscosity of the fluid. Since $\mathbf{n} \cdot \mathbf{u}_B = \mathbf{n}.\mathbf{u}$ on the blood capillary wall, we can rearrange the boundary condition in terms of the interstitial fluid pressure, giving

$$\left.\frac{\partial P}{\partial n}\right|_{r=r_b} = \alpha(P\,|_{r=r_b} - \widehat{P}), \tag{2.2.4}$$

where $\alpha = \mu\beta/\kappa$ (μm^{-1}), r is the radial distance from the centre of the blood capillary and r_b is the radius of the blood capillary. On the edge of the periodic tile we impose the symmetry boundary conditions

$$\frac{\partial P}{\partial n} = 0. \tag{2.2.5}$$

The final boundary condition required to close the interstitial fluid flow problem is provided by assuming a spatially independent pressure on the edge of the lymphatic capillary wall,

$$P\,|_{\widehat{r}=r_l} = P_l, \tag{2.2.6}$$

where $\widehat{r}$ is the radial distance from the center of the lymphatic capillary and r_l is the radius of the lymphatic capillary[1]. The boundary conditions on the periodic tile are shown in Figure 2.2a.

The final major source of resistance to flow occurs in the initial lymphatics

[1]The assumption of a spatially independent pressure is not unrealistic since the capillary is much smaller than the separation between it and the blood capillary and there are a number of valves lying along its circumference

formed by the overlapping endothelial cells, see Figure 2.2b. The lymphatic valve is comprised of endothelial cells that can only deflect into the lumen of the capillary. We assume that the four fluid pressures P_0 (lumen fluid pressure) , P_l, $\widehat{P}$ and P_{crit} are all functions of time only. The lymphatic valve cycles from closed to open and repeats on a time scale of around 3 seconds [110] due to the pressure fluctuation in the secondary lymphatics, i.e. drainage of fluid into the collecting lymphatics. In section 2.3, we formulate and solve a model for the deflection of the lymphatic valve.

2.2.2 Parameter Values

Measurement from Butler et al [14] for the value of the interstitial permeability was 7.6×10^{-3} μm^2, which is consistent with measurements from Levick [76] who recorded many values of the interstitial permeability in different tissues of the body, a range between 1×10^{-2} μm^2 to 1×10^{-6} μm^2. Therefore, in this chapter we take the value of κ to be of the order 7.6×10^{-3} μm^2.

We take the average distance between blood and lymphatic capillaries to be 150μm [72]. Therefore our periodic tile has approximate dimensions of 117μm$\times 117\mu$m ($L_x = L_y = 117\mu$m).

The parameter values used in §2.2.1 are shown in the table below.

Parameter	Value	Units	Description	Source
β	1.7×10^4	$\mu\text{m}^2\text{skg}^{-1}$	The permeability of the blood capillary wall ($1 \times 10^{-5}\mu$ m^2) divided by the product of the viscosity of the lymph ($1.5 \times 10^{-3}\text{kgm}^{-1}\text{s}^{-1}$) and the thickness of blood capillary wall (0.4μm)	[31, 76]
κ	7.6×10^{-3}	μm^2	Permeability of the interstitium	[14, 76]
μ	1.5×10^{-3}	$\text{kgm}^{-1}\text{s}^{-1}$	Viscosity of the lymph	[31]
L_x, L_y	117	μm	Side lengths of the periodic tile (see Figure 2.1 and 2.2)	[72]

Table 2.1: Summary of dimensional parameters used in this chapter along with their reference

2.2.3 A Conformal Mapping Approach for the Interstitial Fluid Flux

Problem formulation

The purpose of this section is to find an expression for the fluid flux per unit length through the interstitium. With a closed lymphatic valve there is no fluid flow into the lymphatic capillary ($\partial P/\partial n = 0$ on the exterior of the lymphatic valve) and therefore no fluid flow through the blood capillary wall since our model does not include tissue expansion. A very trivial solution to this is for the fluid flow through the interstitium to be $P = \widehat{P}$, making $\partial P/\partial n = 0$ on the wall of the blood capillary. For the rest of this section we investigate an open lymphatic valve. Darcy's law, $\mathbf{u} = -\frac{\kappa}{\mu}\nabla P$, characterizes the fluid flow in the interstitium. Assuming the fluid is incompressible, $\nabla \cdot \mathbf{u} = 0$, and κ/μ is constant, reveals Laplace's equation when we take the divergence of Darcy's Law,

$$\nabla^2 P = 0. \tag{2.2.7}$$

Figure 2.3 displays the complex domain in which Laplace's equation is to be solved as well as all the boundary conditions. The periodic tile now has non–circular boundaries for the capillaries because polygonal boundaries are sufficient in representing the morphology of capillaries and in addition this simplifies the analysis later on. Since Laplace's equation holds under conformal mapping, we use a transformation technique to simplify our domain.

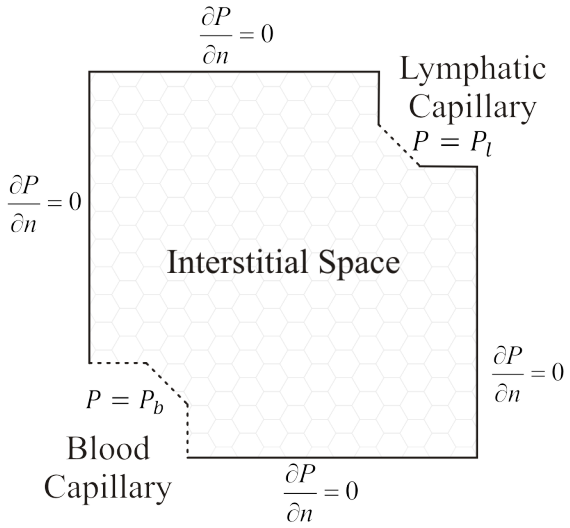

Figure 2.3: A cross–sectional view of the interstitium.

The dotted lines in Figure 2.3 are where we impose a constant pressure. The pressure profile near the blood capillary will be calculated in section 2.2.4. It demonstrates a constant pressure of the form $P_b = (\widehat{P}\pi\alpha r_b + 2\xi P_l)/(\pi\alpha r_b + 2\xi)$ on the blood capillary wall, where ζ is a dimensionless geometric factor.

Conformal Mapping

The conformal map used in this chapter is the Schwarz–Christoffel's transformation. We describe the Schwarz–Christoffel's transformation in detail since we believe it is useful to understand how the transformation works and how we interpret the transformation for our model. Schwarz–Christoffel's transformation is a conformal map of the upper half–plane onto the interior of a polygon. Proof of

the Schwarz–Christoffel's Formula is shown in appendix A.

Mapping to the periodic tile from the upper half plane can be accomplished by using the Schwarz–Christoffel's transformation formula. Solving Darcy's law in the upper half plane is less challenging than inside the polygonal area. However, we can still simplify the new domain further, a square or a rectangle would suffice since we could engineer it to have only one boundary condition on each side. Therefore, the two maps that we will investigate are: a transformation from a rectangle to the upper half plane, Figure 2.5, and another transformation from the upper half plane to the periodic tile, Figure 2.4 (the original domain,).

The method behind the Schwarz–Christoffel's transformation is that a conformal transformation f may have a derivative that can be expressed as

$$f' = \prod_m f_m,$$

for certain functions f_m.

We assume that a polygon has vertices $q_1, ..., q_n$ and interior angles $\vartheta_1\pi, ..., \vartheta_n\pi$ in counterclockwise order and let f be any conformal map from the upper half–plane to the interior of the polygon with $f(\pm\infty) = q_n$. Then the Schwarz–Christoffel's formula for a half plane is

$$f(z) = A + C\int^z \prod_{m=1}^{n-1}(\zeta - z_m)^{\vartheta_m - 1}d\zeta, \tag{2.2.8}$$

for some complex constants A and C, where $q_m = f(z_m)$. Derivation of this formula uses the method of the Schwarz reflection principle [33]. The exponents in the integrand in equation (2.2.8) induce the correct angles in the image of the half plane, regardless of where the pre–vertices lie on the polygon. In order to map to a given target, we determine the locations of the pre–vertices by enforcing

conditions involving the side lengths,

$$\frac{\left|\int_{z_m}^{z_{m+1}} f'(\zeta)d\zeta\right|}{\left|\int_{z_1}^{z_2} f'(\zeta)d\zeta\right|} = \frac{|q_{m+1} - q_m|}{|q_2 - q_1|}, \tag{2.2.9}$$

where $m = 2, ..., n-2$ [33]. This formula produces simultaneous equations where one can confidently solve if good starting values are known.

The Schwarz–Christoffel mapping integral below maps from the upper half plane to the polygon (the original domain):

$$\Phi = f(z) = \int_0^z \frac{(\zeta - c)^{\frac{1}{4}}(\zeta - d)^{\frac{1}{4}}(\zeta + k)^{\frac{1}{4}}(\zeta + l)^{\frac{1}{4}}}{(\zeta - a)^{\frac{1}{2}}(\zeta - b)^{\frac{1}{2}}(\zeta - e)^{\frac{1}{2}}(\zeta + h)^{\frac{1}{2}}(\zeta + p)^{\frac{1}{2}}} d\zeta, \tag{2.2.10}$$

with $a = 0$ μm, $b = 0.1$ μm, $c = 0.1006$ μm, $d = 0.1023$ μm, $e = 0.103$ μm, $h = -0.148$ μm, $k = -0.151$ μm, $l = -0.156$ μm, $p = -0.159$ μm being the prevertices on the real axis, obtained by solving equations (2.2.9) and (2.2.10). Only the ratio between each prevertex not the magnitude creates our desired domain. Using the conditions on the side lengths, equation (2.2.9), the prevertices are comfortably determined. Figure 2.4 shows to where each prevertex transforms in our polygon.

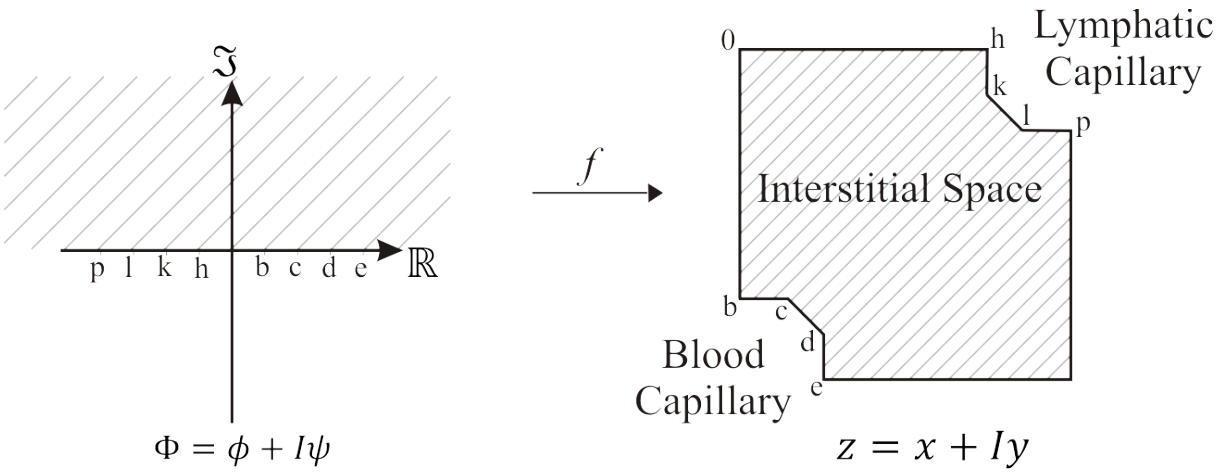

Figure 2.4: The Schwarz–Christoffel's transformation from the upper half plane to the polygon.

For the transformation from a rectangle to the upper half plane needs the inversion of the Schwarz–Christoffel's formula (2.2.8). To decipher the inverse of this formula is difficult, because in general no formula exists [33]. The two main strategies for inversion are, Newton iteration on the forward map $f(z) - q = 0$, and a numerical solution of the initial value problem,

$$\frac{dz}{dq} = \frac{1}{f'(z)}, \qquad z(q_0) = z_0. \tag{2.2.11}$$

The Newton iteration method is attractive because $f'(z)$ is known. However, in practice one may need a rather good starting guess to avoid divergence. Solving the initial value problem, on the other hand, is more reliable, but considerably slower [33].

By using Jacobian elliptic functions we can invert the Schwarz–Christoffel's formula for the transformation from the upper half plane to a rectangle, in this case, the Jacobian elliptic sine function. The Schwarz–Christoffel's formula for a map to a rectangle is,

$$\begin{aligned} w = g(\Phi) &= \overline{A} + \overline{C} \int^{\Phi} \prod_{m=1}^{4} (\zeta - \Phi_m)^{-\frac{1}{2}} d\zeta, \\ &= \overline{A} + \overline{C} \int^{\Phi} \frac{d\zeta}{\sqrt{(\zeta - b)(\zeta - e)(\zeta - k)(\zeta - l)}}. \end{aligned} \tag{2.2.12}$$

For the sake of argument we assume the complex constants to be, $\overline{A} = 0$ and $\overline{C} = 1$, because we have no preference where and how large the rectangle is in the complex v–plane. If we had a symmetrical polygon (the diameter of the blood and lymphatic capillaries are the same i.e. $b = -k$ and $e = -l$), the inverse of equation (2.2.12) would become simple because we can change the variable of the mapping function by $\zeta = \sin\theta$, which results directly to the Jacobi elliptic sine function. However, the sizes of the blood and lymphatic capillaries are different,

so a different approach is required. To acquire the inverse, we need to integrate equation (2.2.12) before inverting. Integrating equation (2.2.12) gives

$$w = \frac{2(l-b)\sqrt{\frac{(b-k)(\Phi-l)}{(b-l)(\Phi-k)}}(\Phi-k)^2\sqrt{\frac{(k-l)(\Phi-e)}{(e-l)(\Phi-k)}}\sqrt{\frac{(k-l)(\Phi-b)}{(b-l)(\Phi-k)}}\text{EllipticF}\left(\sqrt{\frac{(b-k)(\Phi-l)}{(b-l)(\Phi-k)}},\sqrt{\frac{(k-e)(l-b)}{(l-e)(k-b)}}\right)}{(b-k)(k-l)\sqrt{(\Phi-b)(\Phi-e)(\Phi-k)(\Phi-l)}}, \tag{2.2.13}$$

which simplifies to

$$w = \begin{cases} \frac{2}{\sqrt{b-k}\sqrt{e-l}}\text{EllipticF}\left(\sqrt{\frac{(b-k)(\Phi-l)}{(b-l)(\Phi-k)}},\sqrt{\frac{(e-k)(b-l)}{(e-l)(b-k)}}\right) & \text{if} \quad l<\Phi<k, \\ \frac{-2}{\sqrt{b-k}\sqrt{e-l}}\text{EllipticF}\left(\sqrt{\frac{(b-k)(\Phi-l)}{(b-l)(\Phi-k)}},\sqrt{\frac{(e-k)(b-l)}{(e-l)(b-k)}}\right) & \text{if} \quad l>\Phi>k. \end{cases} \tag{2.2.14}$$

This inverts to

$$\Phi = \begin{cases} \frac{l-k\frac{b-l}{b-k}\text{JacobiS}\left(\frac{\sqrt{b-k}\sqrt{e-l}}{2}w,\sqrt{\frac{(e-k)(b-l)}{(e-l)(b-k)}}\right)^2}{1-\frac{b-l}{b-k}\text{JacobiS}\left(\frac{\sqrt{b-k}\sqrt{e-l}}{2}w,\sqrt{\frac{(e-k)(b-l)}{(e-l)(b-k)}}\right)^2} & \text{if} \quad l<\Phi<k, \\ \frac{l-k\frac{b-l}{b-k}\text{JacobiS}\left(-\frac{\sqrt{b-k}\sqrt{e-l}}{2}w,\sqrt{\frac{(e-k)(b-l)}{(e-l)(b-k)}}\right)^2}{1-\frac{b-l}{b-k}\text{JacobiS}\left(-\frac{\sqrt{b-k}\sqrt{e-l}}{2}w,\sqrt{\frac{(e-k)(b-l)}{(e-l)(b-k)}}\right)^2} & \text{if} \quad l>\Phi>k, \end{cases} \tag{2.2.15}$$

where w are points in the rectangle. Therefore, we now have a map to our polygon from a rectangle via the upper half plane. Figure 2.5 shows to where each prevertex transforms in the upper half plane. The vertices on the rectangle are $w_1 = 0$ μm, $w_2 = 100.06$ μm, $w_3 = 30.26\imath$ μm, $w_4 = 100.06 + 30.26\imath$ μm map to l, e, k, b, respectively.

Solving Laplace's equation inside the rectangle to acquire the stream–lines of the flow has become trivial because we have assumed that the pressure is approximately constant on the wall of the blood capillary. Using separation of variables on Laplace's equation leads to,

$$P = \frac{P_l - P_b}{w_2}u + P_b. \tag{2.2.16}$$

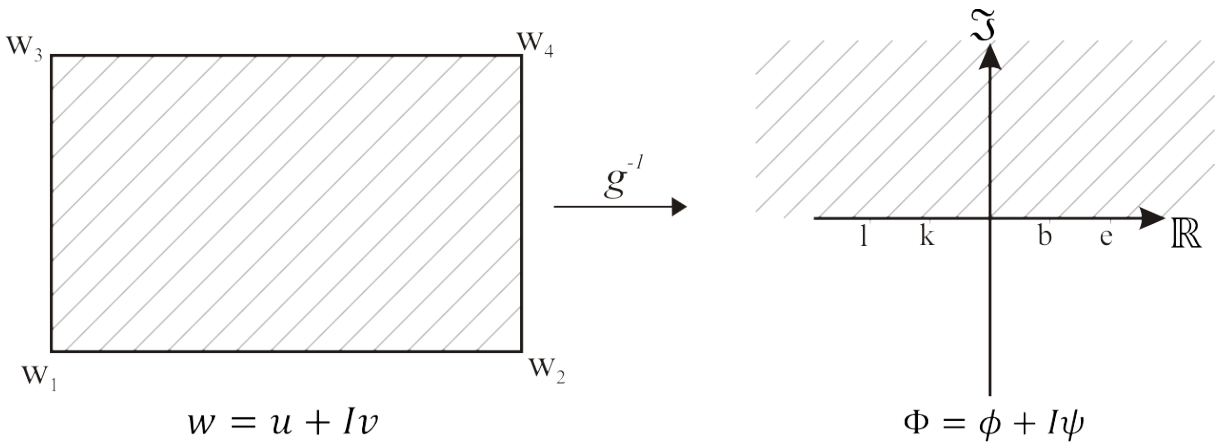

Figure 2.5: The Schwarz–Christoffel's transformation from a rectangle to the upper half plane.

The instantaneous discharge rate through the interstitium, Q, is

$$Q = \xi \frac{k}{\mu}(P_b - P_l), \tag{2.2.17}$$

where ξ corresponds to the height divided by the length of the rectangle in Figure 2.5 which represents the interstitial space ($zeta = 0.302$).

Figure 2.6 graphically demonstrates the Schwarz–Christoffel's transformation from a rectangle to the upper half plane. The stream–lines in each region are plotted in Maple.

An initial glance at the solution concurs that the Schwarz–Christoffel's mapping technique was a success in predicting the fluid flow. The accuracy of our analytical solution is compared to a numerical solution from a finite element package, Comsol Multiphysics. Figure 2.7 compares the numerics to the analytics and we can see they are very similar. We have plotted the numerical solution on its own to give the reader a basic visual interpretation between the two solutions.

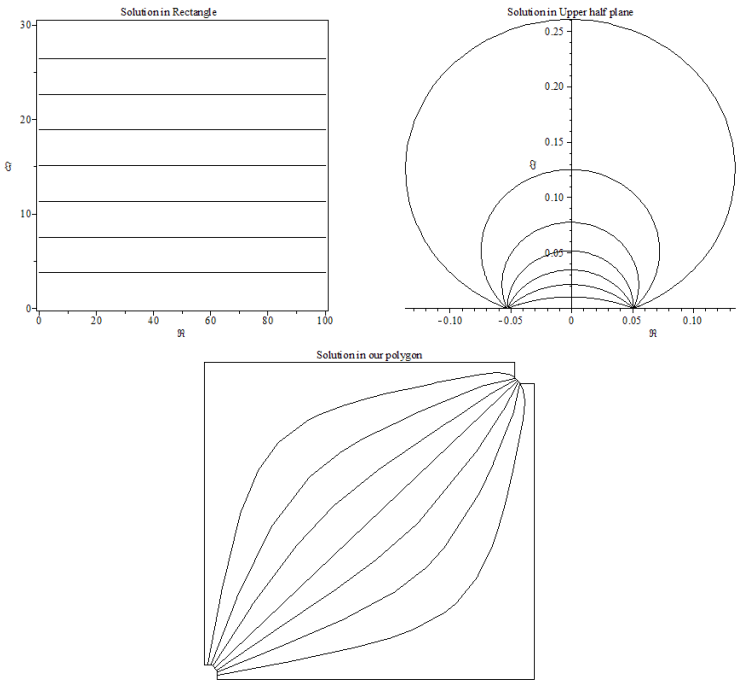

Figure 2.6: Solution of Darcy's Law in the rectangle mapped to our polygon via the upper half plane by the Schwarz–Christoffel integral equations.

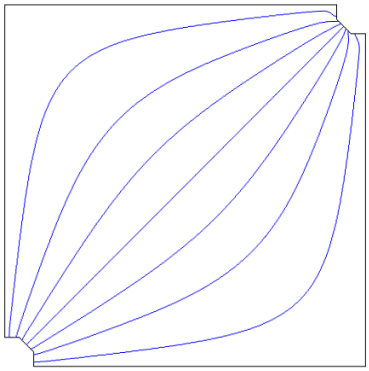

Figure 2.7: (1) Stream–lines of the fluid flow in the interstitium plotted in Comsol.

2.2.4 Model Solution for the Interstitial Fluid Flow

We seek a solution to the problem discussed in section 2.2.1. This involves solving for a Darcy flow (2.2.2)-(2.2.3) in the interstitial space. In this section, we derive the volumetric fluid flow rate per unit length through the interstitium as a function

of the pressure difference between the exterior of the blood capillary and the lymphatic capillary.

Here we investigate the flow in the interstitium by solving Laplace's equation for pressure

$$\nabla^2 P = 0, \tag{2.2.18}$$

which arises as a consequence of (2.2.2) and (2.2.3), and applying appropriate boundary conditions on the edges of the blood and lymphatic capillaries and on the boundary of the periodic tile (see Figure 2.2).

In general when solving for the Darcy flux through the interstitium the pressures on the exterior of the blood and lymphatic capillaries must be known. Since the blood capillary is small in comparison to its separation from the adjacent lymphatic capillary, we can assume the flow in its immediate vicinity is approximately radially symmetric, so that the pressure takes the form

$$P \sim \widehat{P} + \chi + \gamma \ln\left(\frac{r}{r_b}\right), \tag{2.2.19}$$

where χ and γ are constants that are related by the pressure boundary condition (2.2.4) on $r = (x^2 + y^2)^{\frac{1}{2}} = r_b$ (the blood capillary wall). This takes the form

$$\left.\frac{dP}{dr}\right|_{r=r_b} = \alpha\left(P|_{r=r_b} - \widehat{P}\right), \tag{2.2.20}$$

where $\alpha = \mu\beta/\kappa$ (see equation 2.2.4) and results in the relation $\chi = \gamma/\alpha r_b$. In turn we can relate γ to the total fluid flux per unit length flowing out the blood capillary,

$$\begin{aligned} Q_I = \int \mathbf{n}\cdot\mathbf{u}\, ds &= -\frac{k}{\mu}\int_0^{\frac{\pi}{2}} r\left.\frac{\partial P}{\partial r}\right|_{r=r_b} d\theta, \\ &= -\frac{k\gamma\pi}{2\mu}, \end{aligned} \tag{2.2.21}$$

From which it follows that $\gamma = -2\mu Q_I/k\pi$ so that the pressure near the blood capillary takes the form,

$$P \sim P_b - \frac{2\mu Q_I}{k\pi} \ln\left(\frac{r}{r_b}\right) \quad \text{as} \quad r \to r_b, \tag{2.2.22}$$

where $P_b = \widehat{P} - 2\mu Q_I/\alpha k\pi r_b$.

The linearity of Darcy's Law, for the fluid flow through the interstitium, implies that the total fluid flux from the blood capillary to the lymphatic capillary is linearly related to the pressure difference between the walls of these two vessels by an equation of the form

$$Q_I = \xi \frac{k}{\mu}(P_b - P_l), \tag{2.2.23}$$

where ξ is a dimensionless geometric factor, P_b is the pressure on the outer edge of the blood capillary, k is the permeability of the interstitium and μ is the viscosity of the interstitial fluid. The method for calculating ξ from the solution to equation (2.2.18) with the boundary conditions, $P\,|_{r=r_b} = P_b$, $P\,|_{\widehat{r}=r_l}$ and $\partial P/\partial n = 0$ on the boundary of the periodic tile, is presented in section 2.2.3. Where the circular boundaries of the vessels were replaced by polygons and conformal transformation techniques were used to find the approximate solution.

2.3 Modelling the Deflection of the Lymphatic Valve

The model formulated in this section demonstrates how the mechanics of the lymphatic valve affects lymphatic drainage. The model couples fluid flow effects to elastic effects in the primary lymphatics. Mendoza and Schmid–Schönbein (MSS) [85] investigated an analogous problem for the drainage of fluid into the initial

lymphatics, considering the case where the curvature of the wall of the lymphatic capillary is neglected, and the case where the lymphatic valve is modelled by a linear elastic beam. Their flat beam model for a primary valve is unrealistic since given any fluid pressure on the exterior of the valve will open it. Here, we will formulate the problem in which the curvature of the wall of the lymphatic capillary is significant, and make use of nonlinear beam theory to model the lymphatic valve. Thus the beam is pre–stressed, so the interstitial fluid pressure has to overcome the elastic forces of the beam to enter the lumen. We believe these changes are important in achieving more realistic results because the geometrical structure of lymphatic capillaries is cylindrical, not planar and there are only 4-5 lymphatic endothelial cells per circumference [71, 73].

2.3.1 Model Development for the Deflection of the Lymphatic Valve

In this section we outline how to model potentially large deflections of the lymphatic valve by using a nonlinear beam equation. The lymphatic valve has two states as described in the Introduction, closed and open. We model the lymphatic valve as a beam that is clamped at one end and closes onto a rigid substrate (see Figure 2.8). Inertial forces can be neglected for this problem [31, 76].

The main differences between this model of the lymphatic valve and the model created by Mendoza and Schmid–Schönbein [85] is that we take into account the curvature of the lymphatic capillary wall and make use of geometrically nonlinear beam theory [122] (rather than linear beam theory) to model the relatively large deflections of the lymphatic valve, which we assume tries to be straight.

We describe the valve deformation using arc length s along the beam and the angle $\theta(s)$ between the beam and the x–axis, as shown in Figure 2.8, and assume the beam to be inextensible, so that the arc–length is conserved by the deformation

[54]. The transverse displacement is given parametrically by $x = x(s)$, $y = y(s)$, where

$$\frac{\mathrm{d}x}{\mathrm{d}s} = \cos\theta, \qquad \frac{\mathrm{d}y}{\mathrm{d}s} = \sin\theta. \tag{2.3.1}$$

The nonlinear beam equation that models the deflection of the lymphatic valve, is derived in Appendix B, is

$$\frac{\mathrm{d}^3\theta}{\mathrm{d}s^3} + \frac{1}{2}\left(\frac{\mathrm{d}\theta}{\mathrm{d}s}\right)^3 = \frac{P_l - P_0}{D}, \tag{2.3.2}$$

where D ($\mathrm{kg}\mu\mathrm{m}^2\mathrm{s}^{-2}$) is the flexural rigidity of the valve. Here D is given in terms of the Young's modulus (E), the Poisson ratio (ν) and the beam thickness (ι) by $D = E\iota^3/12(1-\nu^2)$.

Equation (2.3.2) is the Euler–Bernoulli beam equation for large deformations in terms of angle and arc–length, which we solve together with the two first order ordinary differential equations (2.3.1) for $x(s)$ and $y(s)$ between $s = 0$ (the anchored end of the valve) and $s = s_f$ (the far end of the valve).

In its closed state the valve takes one of two configurations, which we denote as Case 1 and Case 2, and is illustrated in Figure 2.8a and 2.8b. In Case 1 the valve is shut so firmly that a portion of the flap between s_1 and s_f is pushed flat onto the underlying substrate. In Case 2 the valve is less firmly shut and only the end of the flap $s = s_f$ impacts on the substrate. Case 1 corresponds to having all of the overlapping portion of lymphatic valve in contact with the anchored end of another lymphatic endothelial cell (the capillary wall). In Case 2 only the end of the lymphatic valve is in contact with an anchored end of another lymphatic endothelial cell.

Finally we look at a configuration modelling the instantaneous open state after a sudden decrease in lymphatic lumen pressure. In practice this state always rapidly relaxes as the lymphatic valve equilibrates to a state that is only just open

(at the bifurcation point) since the resistance provided by a fully open lymphatic valve is negligible in comparison to that of the interstitium. In Figure 2.8c below, the lymphatic valve has deflected into the lumen and has lost contact with the anchored end of the other lymphatic endothelial cell (the capillary wall), resulting in fluid flow into the lumen of the lymphatics, Case 3. The three figures below are sketches of possible valve geometries.

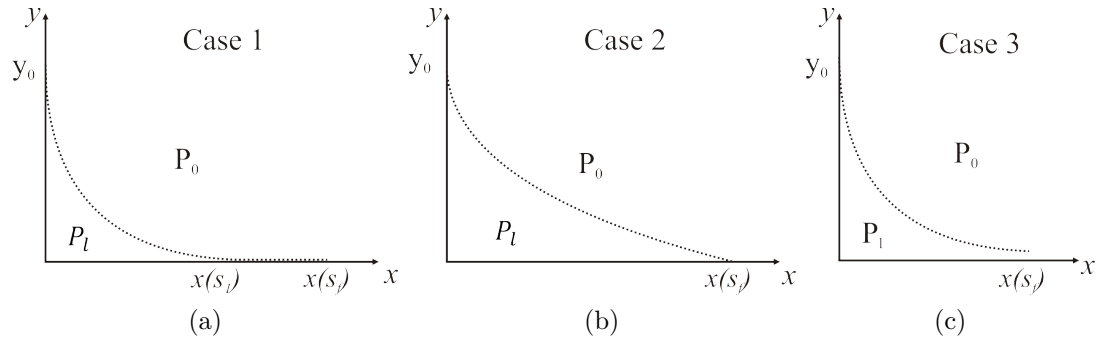

Figure 2.8: (a) Case 1 models the lymphatic valve when the fluid pressure in the lumen is far greater than the interstitial fluid pressure; the valve is firmly closed. (b) Case 2 models the lymphatic valve when just the end of the valve is in contact with the capillary wall. (c) Case 3 models the lymphatic valve when it is open, allowing fluid to enter lymphatic lumen, therefore, $\partial P/\partial n < 0$ and $P_l - P_0 \geq P_{crit}$.

Since we define the anchored end of the valve to lie on $s = 0$, s_1 has the property that $\sqrt{y_0^2 + x^2(s_1)} \leq s_1 \leq s_f$. $x(s_1)$ is where the beam makes first contact with the capillary wall. The value of y_0 has been deduced from prior research of the geometry of the initial lymphatics, i.e. the valve length, the diameter of the lymphatic capillary and assuming valves occur quarterly around lymphatic capillaries [71, 73]. We take y_0 to be of the order 3 μm.

In Case 1, a portion of the beam is forced onto the underlying substrate (which here lies on the x-axis) between $x(s_1)$ and $x(s_f)$. Since s_1 is unknown we have a free boundary value problem and the closed state of the valve implies no flow such that $\partial P/\partial n = 0$ on the exterior of the lymphatic valve and $P_l - P_0 < P_{crit}$. As the pressure drop across the initial lymphatics ($P_l - P_0$) increases, the distance between $x(s_1)$ and $x(s_f)$ decreases until only one point remains in contact with the

substrate $s = s_f$, which is described by Case 2. In Case 2 the lymphatic valve is still closed preventing back flow of fluid into the interstitium, so that $\partial P/\partial n = 0$ on the exterior of the lymphatic valve and $P_l - P_0 \leq P_{crit}$.

To solve Case 1, six boundary conditions are required. By inspecting Figure 2.8 Case 1, we have an initial deflection of $-\pi/2$ (since the lymphatic capillary is cylindrical), an initial height of y_0 and a starting value for x, say $x(0) = 0$. At the 'moving' boundary, $s = s_1$, we assume no bending moment and y equals zero since the lymphatic valve is in contact with the capillary wall. To determine the value of s_1, we require one more boundary condition. Assuming the angle θ is zero at the free boundary and $\theta < 0$ when $s < s_1$ will be sufficient to close the problem. Thus, the boundary conditions are,

$$\begin{aligned} \theta(0) = -\tfrac{\pi}{2}, \quad & \tfrac{d\theta}{ds}(s_1) = 0, \\ y(0) = y_0, \quad & y(s_1) = 0, \\ x(0) = 0, \quad & \theta(s_1) = 0. \end{aligned}$$

To solve Case 2, only five boundary conditions are required since $s_1 = s_f$. The boundary conditions are almost identical to those in Case 1 with the exception that the angle at the end of the beam is unknown and the end boundary s_f is known. The boundary conditions in Case 2 are thus

$$\begin{aligned} \theta(0) = -\tfrac{\pi}{2}, \quad & \tfrac{d\theta}{ds}(s_f) = 0, \\ y(0) = y_0, \quad & y(s_f) = 0, \\ x(0) = 0. & \end{aligned}$$

In Case 3 the pressure drop across the initial lymphatics has risen to the critical pressure value and lifted the beam off the underlying substrate. Five boundary conditions are required in this case to close the problem. At the fixed end of the beam ($s = 0$), the boundary conditions are the same as in Case 1 and Case 2, which are, an initial deflection of $-\pi/2$, an initial height of 3 μm and

an initial value for x, $x(0) = 0$. The boundary conditions are different at the free end of the beam ($s = s_f$) to Case 1 and Case 2 because the lymphatic valve has lost contact with the capillary wall. However, we still assume no bending moment applied to the boundary $s = s_f$. The last condition arises from the loss in contact between the lymphatic valve and the underlying substrate. When there is a flux through the initial lymphatics the normal force (N) acting on the end of the lymphatic valve from the underlying substrate vanishes. To be consistent with the other boundary conditions we relate the normal force N to the angle θ, $N = -D\ d^2\theta/ds^2$. Physically this condition means the shear force is zero at the end of the beam. Thus, the boundary conditions in Case 3 are,

$$\begin{aligned} \theta(0) &= -\tfrac{\pi}{2}, \quad & \tfrac{d\theta}{ds}(s_f) &= 0, \\ y(0) &= y_0, \quad & \tfrac{d^2\theta}{ds^2}(s_f) &= 0, \\ x(0) &= 0. \end{aligned}$$

It is reassuring to confirm that the nonlinear beam theory reduces to the linear beam theory in MSS's paper [85] for cases where deflections are small. For small θ, we can simplify the geometric relations in equation (2.3.1) to the lowest order, to give, $x = s$, $\frac{dy}{dx} = \theta$, and thus the Euler–Bernoulli beam equation for small deflections becomes (as in MSS's model),

$$\frac{\mathrm{d}^4 y}{\mathrm{d}x^4} = \frac{P_l - P_0}{D}. \tag{2.3.3}$$

2.3.2 Parameter Values

The parameter values used in §2.3.1 are shown in Table 2.2.

Parameter	Value	Units	Description	Source
E	1000	$\mathrm{kgm^{-1}s^{-2}}$	Young's modulus for lymphatic endothelial cells	[129]
s_f	6	μm	Length of the lymphatic valve	[73]
y_0	3	μm	Initial height of the lymphatic valve in our geometry	[71, 72]
ι	0.4	μm	Thickness of lymphatic endothelial cells	[73]
ν	0.5	–	Poisson ratio	[78]

Table 2.2: Summary of dimensional parameters used in this chapter along with their reference.

In Mendoza's and Schmid–Schönbein's model, a Young's modulus of $1,000$ Pa was used for a lymphatic endothelial cell; this was obtained by experimental measurements by Theret et al [129]. In our model of the lymphatic valve we also use the results from Theret et al [129] for the Young's modulus of a lymphatic endothelial cell. Thus we can directly compare our results with MSS's model.

The structure of lymphatic capillaries is relatively well understood. The studies by Leak [73] on lymphatic capillaries described their irregular shapes and large diameters, which are created by circumferentially oriented, overlapping endothelial cells. Lymphatic capillaries have measured diameters of around 20 μm; the largest diameter measured is nearly 60 μm [73]. In this model we consider a lymphatic capillary diameter of 20 μm. The endothelial cells that make up the lymphatic valve are presumed to be of the order of 6 μm long in this work with an overlapping portion of 0.7 μm to 2 μm [71, 72]. Using these values and assuming that the lymphatic valves occur quarterly around the capillary wall lets us choose the value of y_0, the initial height of the lymphatic valve, see Figure 2.8. The thickness of the endothelial cells near the lymphatic valve is of the order 0.1 μm to 0.7 μm from values shown by Leak [71, 72]. We take an average thickness of

lymphatic endothelial cells of the order 0.4 μm.

2.4 Solution to the Model of Hypothesis 1

We seek a solution to the problem discussed in section 2.3.1. This involves solving the nonlinear beam equation (2.3.2) conjoint with the transverse displacements equation (2.3.1), for all three cases. In this section, we model the deflection of the lymphatic valve by using the Euler Bernoulli beam equation, and we use this to relate the pressure inside the lymphatic capillary to that immediately outside it. Finally we combine the results of interstitial fluid flow and valve mechanics to arrive at an algebraic relation for the fluid flux in terms of the pressure difference between the interior of the blood capillary and the lymphatic capillary.

Cases 1 and 2 model a closed lymphatic valve while Case 3 models an open lymphatic valve. The Euler Bernoulli beam equation describes the relationship between the beam's deflection and the applied load. In our case the applied load per unit area is the pressure difference between the lymphatic capillary lumen and the exterior of the lymphatic valve. The nonlinear beam equation and the equations for the Cartesian $x-y$ positions of the lymphatic valve are,

$$\frac{\mathrm{d}^3\theta}{\mathrm{d}s^3} + \frac{1}{2}\left(\frac{\mathrm{d}\theta}{\mathrm{d}s}\right)^3 = \frac{P_l - P_0}{D}, \tag{2.4.1}$$

$$\frac{\mathrm{d}x}{\mathrm{d}s} = \cos\theta, \qquad \frac{\mathrm{d}y}{\mathrm{d}s} = \sin\theta, \tag{2.4.2}$$

where P_l and P_0 are the pressures on the exterior of the lymphatic capillary and in the lumen of the lymphatic capillary, respectively. Solving the nonlinear beam equation analytically is challenging, because of the cubic term. This will result in incomplete elliptic integrals of the first and third kind. We choose instead a numerical method.

Solving equations (2.4.1) and (2.4.2) numerically is accomplished by using a boundary value problem solver, bvp4c, in Matlab for all three cases described in section 2.3. Bvp4c is a finite difference solver that implements shooting and Runge Kutta methods. The boundary conditions for each case are shown in the table below.

Case 1		Case 2		Case 3	
$\theta(0) = -\frac{\pi}{2}$	$\frac{d\theta}{ds}(s_1) = 0$	$\theta(0) = -\frac{\pi}{2}$	$\frac{d\theta}{ds}(s_f) = 0$	$\theta(0) = -\frac{\pi}{2}$	$\frac{d\theta}{ds}(s_f) = 0$
$y(0) = y_0$	$y(s_1) = 0$	$y(0) = y_0$	$y(s_f) = 0$	$y(0) = y_0$	$\frac{d^2\theta}{ds^2}(s_f) = 0$
$x(0) = 0$	$\theta(s_1) = 0$	$x(0) = 0$		$x(0) = 0$	

Table 2.3: The boundary conditions for Cases 1, 2 and 3.

The initial height of the beam, y_0, is assumed to be of the order 3 μm. Figure 2.9 displays plots from Matlab of the geometric shape of a closed and open valve. Also these plots demonstrate the position of the valve for when the pressure difference is varied.

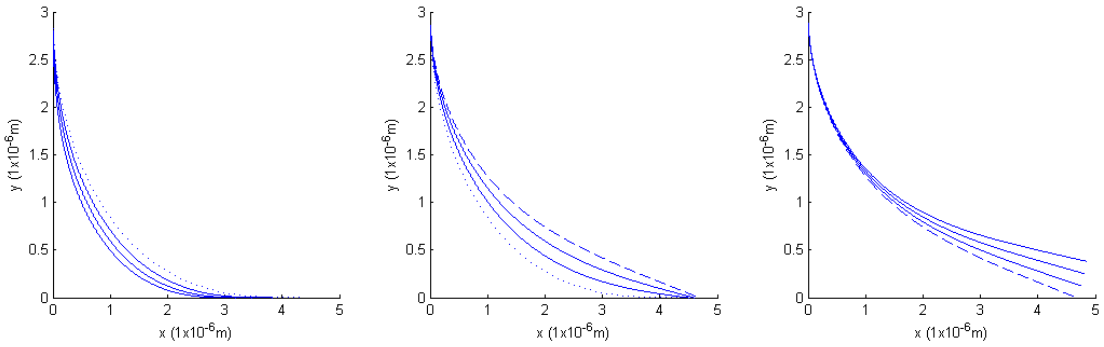

(a) Case 1 (b) Case 2 (c) Case 3

Figure 2.9: In the three plots above we show valve positions for successively increasing pressure drops, $P_l - P_0$. Plots (a) and (b) show a closed valve in cases 1 and 2 respectively. Plots (c) show an open valve, case 3. (a) The dotted line has a pressure drop of -0.134 Pa. The other positions of the lymphatic valve decrease in steps (of the pressure) of 0.192 Pa. (b) The dotted line is identical to that in (a). Here we have increased the pressure drop by a step of 0.137 Pa for the each position of the lymphatic valve. (c) The dashed line is identical to that in (b). The positions plotted are for increases in the pressure in steps of 0.007 Pa.

In Figure 2.9a, Case 1 is plotted. To visualize each deflection of the lymphatic valve we have varied the pressure drop $(P_l - P_0)$ by a step of 0.192 Pa. The dotted line in Case 1 corresponds to a pressure drop of -0.134 Pa. In practice the pressure drop does not vary much from the critical pressure drop which will be revealed shortly. In this scenario the lymphatic valve is firmly closed and the fluid pressure drop is less than the critical fluid pressure. As the pressure drop increases, the valve contact with the capillary wall decreases, as demonstrated in Figure 2.9a. This results in the value of $x(s_1)$ increasing until it equals the value of $x(s_f)$. When $x(s_1)$ merges into $x(s_f)$ only the end of the lymphatic valve is in contact with the capillary wall (Case 2).

In Figure 2.9b, Case 2 is plotted as the dashed curve. In Case 2, the lymphatic valve is still closed but only the end of the valve contacts the capillary wall. When the pressure drop exceeds 0.277 Pa the valve opens (Case 3).

In Figure 2.9c, the solution to Case 3 is plotted. As the pressure drop rises above the critical pressure value of 0.277 Pa, the lymphatic valve deflects further from the capillary wall, resulting in a larger gap for the fluid to convect into the lumen of the lymphatic capillary. In practice this open valve configuration is unrealistic since the fluid flow will cause the pressure to (almost) equalize between the two sides of the lymphatic valve. In reality the pressure drop for an open valve must remain close to the critical value of 0.277 Pa.

Figure 2.10 shows the valve deflection when the pressure drop equals the critical fluid pressure of 0.277 Pa (dashed line). Since we have assumed that the lymphatic valve is very flexible, i.e. having a low Young's modulus, the low value of the critical fluid pressure is reasonable. In MSS's model, they varied the pressure drop by 0.1 Pa, 0.25 Pa, 0.5 Pa and 1 Pa to see how the deflection of the lymphatic valve changed.

To summarize, the fluid flux per unit length through the initial lymphatics

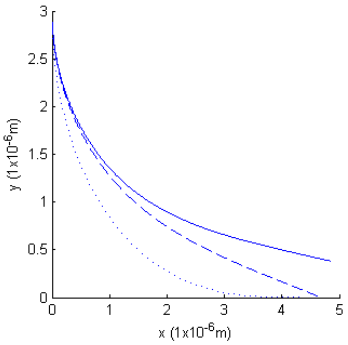

Figure 2.10: The lymphatic valve's deflection in each case on a single graph. Case 1 is the dotted line with a pressure drop of -0.134 Pa, Case 2 is the dashed line with a pressure drop of 0.277 Pa and Case 3 is the solid line with a pressure drop of 0.300 Pa.

(Q_L) is

$$\begin{aligned} P_l < P_0 + P_{crit} \quad &\Rightarrow \qquad Q_L = 0, \\ \text{if } Q_L > 0 \quad &\Rightarrow \quad P_l = P_0 + P_{crit}. \end{aligned}$$

Amalgamating this result with that for the interstitial fluid flow (2.2.23) leads to the follow critical state model,

$$\begin{array}{llll} \text{if} \quad \widehat{P} < P_0 + P_{crit} & \text{then} & Q = 0 & \text{closed valve} \\ \text{if} \quad \widehat{P} > P_0 + P_{crit} & \text{then} & Q = \frac{\xi\alpha\pi r_b}{\alpha\pi r_b + 2\xi}\frac{k}{\mu}(\widehat{P} - (P_0 + P_{crit})) & \text{open valve.} \end{array}$$

We note that if we took a different geometry we would obtain the same result, but with a modified dimensionless interstitial domain shape coefficient ξ.

A comparison of our model and the resulting flow rates to MSS's model of the lymphatic valve [85] is shown in Figure 2.11. Figure 2.11a and 2.11b show the geometric interpretation of the lymphatic valve in each model while Figure 2.11c displays a plot of the fluid flux per unit length through the initial lymphatics against the pressure difference $P_l - P_0$.

In comparing the two models depicted in Figure 2.11a and Figure 2.11b we can appreciate why the flux plots in Figure 2.11c are different. At first glance we notice the geometric interpretation of the lymphatic valve is significantly different

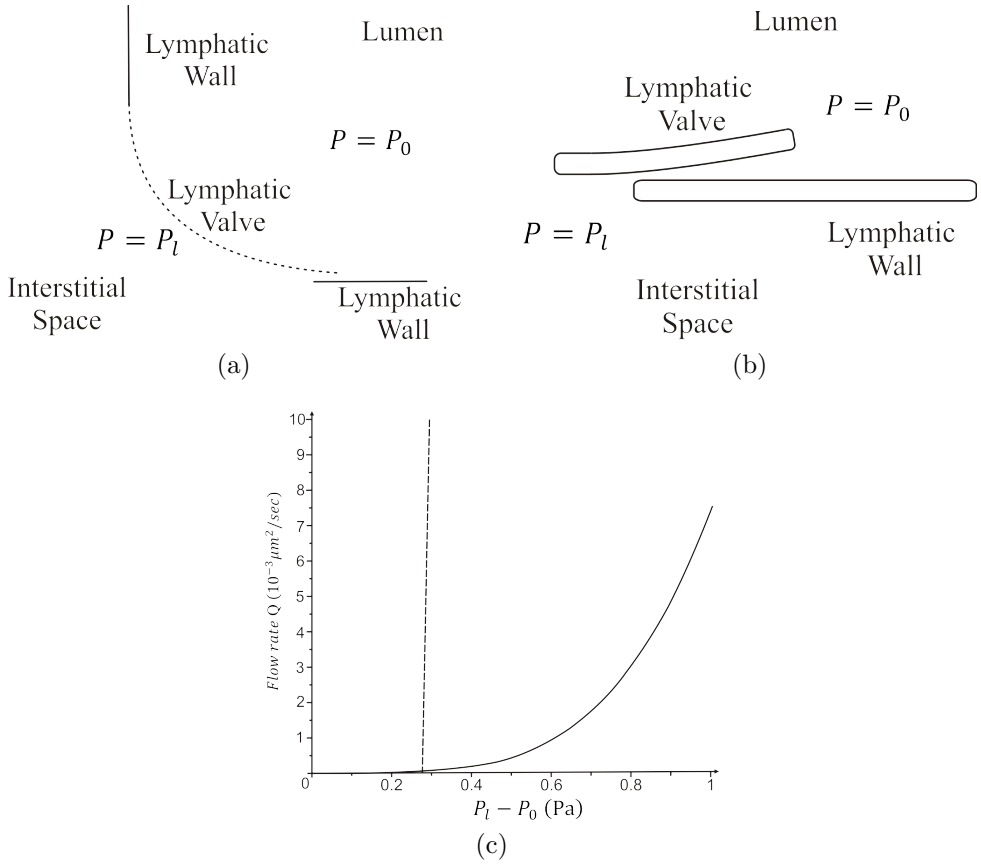

Figure 2.11: (a) Displaying the geometry of the lymphatic valve in our model. (b) Displaying the geometry of the lymphatic valve in Mendoza's and Schmid–Schönbein's model [85]. (c) Displaying plots of the fluid flux per unit length through the initial lymphatics in our model (dashed line) and in Mendoza's and Schmid–Schönbein's model (solid line) [85].

in each model. This results in two major differences between the models that influences the fluid flow. Firstly, the lymphatic endothelial cells' overlap is small (as seen in the anatomical literature [73]) in our model compared to MSS's model. With a small overlap in these cells the resistance to fluid flow between the valve and the capillary wall becomes negligible. While in MSS's model the large overlap of lymphatic endothelial cells results in a geometry in which one dimension is considerably smaller than another (lubrication theory). The fluid must pass through this channel created by the endothelial cells in order to enter the lymphatic lumen and the channel produces a non–negligible resistance to the flow. The consider-

ably different lengths in the overlap of lymphatic endothelial cells give rise to different gradients in the fluid flux, see Figure 2.11. If we were to modify MSS's model to have a small lymphatic endothelial cell overlap, the pressure gradient vs fluid flux graph in Figure 2.11c would still be significantly different from the one based on our model. The MSS's flat valve assumption implies that any positive pressure gradient opens the valve. In our model the pressure gradient has to overcome the elastic forces of the valve to allow entry into the lumen, which compares better to the physiological details of primary lymphatic valves. Secondly, we notice that the curvature of the lymphatic valve is different in each model. In our model (Figure 2.11a) the curvature of the lymphatic valve is large compared to that in MSS's model (Figure 2.11b). As a result, in our model we use nonlinear beam theory rather than linear beam theory. Realistically lymphatic capillaries are surrounded by the interstitium, which has an influence on the fluid flow. In our model we have included the resistance from interstitial space, while MSS's model does not include it. The improvements we have made to MSS's model in trying to make it more realistic has resulted in a slightly larger fluid flux through the initial lymphatics around $10 \times 10^{-3} \mu\text{m}^2/s$ in comparison to MSS's fluid flux of around $7.5 \times 10^{-3} \mu\text{m}^2/s$. To further validate our result for the fluid flux through the initial lymphatics we have compared it with other experimental data. This will be further discussed in the next section.

2.5 Conclusion

This chapter has briefly outlined the fluid drainage problem that arises from the exuded fluid from blood capillaries. Around 20% of the body's mass is assumed to be interstitial fluid that is in constant slow motion [76]. Thus understanding the mechanics of the lymphatic system is essential in understanding how our

bodies drain interstitial fluid. Special attention was given to the behaviour of the overlapped endothelial cells around lymphatic capillaries that were assumed to act as a unidirectional valve system.

An introduction of the lymphatic system was provided in the first chapter for the reader to gain the required background knowledge of this complex system to understand how and why the model was developed. The model covers the three key areas of resistance to fluid flow in tissues where lymphatic drainage occurs. These are: the permeable membrane around blood capillaries, the resistance of the interstitium and that of the overlapped endothelial cells that form the lymphatic valve. We showed that to a good approximation the complex model that we formulated to describe the 2-D fluid flow through the interstitium, the blood capillary membrane and the nonlinear elastic behaviour of lymphatic valves can be approximated by the following simple critical state model for the fluid flux per unit length Q in terms of the pressure difference between blood and lymphatic capillaries $\widehat{P} - P_0$. This takes the form

$$Q = \begin{cases} 0 & \text{if} \quad \widehat{P} < P_0 + P_{crit}, \\ \frac{\xi \alpha \pi r_b}{\alpha \pi r_b + 2\xi} \frac{k}{\mu} (\widehat{P} - (P_0 + P_{crit})) & \text{if} \quad \widehat{P} > P_0 + P_{crit}, \end{cases} \tag{2.5.1}$$

where P_{crit} is a critical fluid pressure difference that needs to be exceeded before the lymphatic valve opens, ξ is a dimensionless parameter that describes the effect the geometry has on the fluid flux, k is the permeability of the interstitium and μ is the viscosity of the interstitial fluid.

The results in this chapter were compared with the results obtained in MSS's model [85]. The value of the fluid flux per unit length in our model and in MSS's model were very similar. This was due to us assuming that the flow through the open valve causes the pressure difference on either side of the valve $(P_l - P_0)$ to equalize at the critical opening pressure. In effect we assume that the intersti-

tium always provides significantly more resistance to flow than that of an open lymphatic valve. This is one of the reasons why we have such a sharp transition in the flow rate in Figure 2.11c. For an open lymphatic valve the fluid flux per unit length was $10 \times 10^{-3} \mu\text{m}^2/s$ in our model and $7.5 \times 10^{-3} \mu\text{m}^2/s$ in MSS's model, see Figure 2.11c. The most significant differences between these models that resulted in different flow rates was the geometric view of the lymphatic valve and the fact that Mendoza and Schmid–Schönbein did not take into account the resistance to flow from the interstitium. In MSS's model a flat valve was considered, which we believe to be biologically unrealistic because lymphatic capillaries are cylindrical. The geometry Mendoza and Schmid–Schönbein used to model the lymphatic valve is shown in Figure 2.11(b). In our model of the lymphatic valve we had a significant curvature in the valve that caused it to spring shut sharply in contrast to that of MMS (see Figure 2.11(a)). In addition Mendoza and Schmid–Schönbein assumed the endothelial cell overlap is large compared with the valve length. MSS's model had the fluid experience a long narrow gap when entering the lymphatic capillary, which results in a high resistance to flow. In our model, we assumed a small overlap and a heavily curved endothelial cell, which from the anatomical data [71, 73, 116] we believe to be more realistic than the more flaccid valve behaviour in MSS's model [85]. It is this that gives the sharp transition between a closed and open valve. Also we note that changing the stiffness (Young's modulus) of the lymphatic valve in our model would only change the critical fluid pressure P_{crit}. However, in MSS's model it would change the gradient of the fluid flux.

Two benchmark problems are discussed to validate the assumptions made in our model compared to those made in MSS. These benchmark problems investigate how manipulating each model in a certain way influences the fluid flow. Firstly, our model could be used to describe an intervention in which a synthetic

chemical that affects the permeability of the interstitial space is injected into the tissue. This is turn would directly affect lymphatic drainage, through the interstitium. Tissue permeability is not included in MSS's model. The effects of the interstitium to the resistance to fluid flow could be applied to MSS's model. However we still believe, on the basis of anatomical differences [73], that the resistance the valve is providing due to the elastic force required to open it (as in our model) is much larger than the drag it exerts on the fluid flowing through it (as in MSS's model). Secondly, if we inject different synthetic chemicals that just change the elastic properties of lymphatic endothelial cells, it would also influence the resistance to fluid flow. Changing the elastic properties of lymphatic endothelial cells in our model would affect the critical pressure at which the valve opens but not the slope of the subsequent flow rate as a function of pressure. In our model multiplying D (the flexural rigidity of the valve) by a factor Γ results in the value of P_{crit} being scaled by the same factor Γ. Scaling D in MSS's model by a factor Γ results in a change in the fluid flux by a factor $1/\Gamma^3$.

Mendoza and Schmid–Schönbein estimated the total length of endothelial junctions in the initial lymphatics to convert the fluid flux per unit length into the volumetric flow rate, thus comparing results with other work was achievable. Converting the fluid flux per unit length in our model gives us the volumetric flow rate of $4.4 \times 10^{-11} \mathrm{m}^3\mathrm{s}^{-1}$. We also realize that the qualitative features of the model presented in this study are little changed by changes to the lymphatic capillary and interstitial geometries because the fluid flow up until the lymphatic valve is described by a linear model. Thus changing the geometry will only affect P_{crit} and ξ.

Validating the model presented in this chapter was made difficult by the magnitude of variation of the geometrical and physical parameters of lymphatic capillaries and in the environment surrounding these capillaries. Several papers have

investigated the volumetric flow rate through the lumen of lymphatic capillaries in different animals [31, 78, 124, 126]. Although these papers focus on the lymph flow inside the capillary, it should still provide a crude comparison for the fluid flux into lymphatic capillaries. In the study by Dixon et al [31], the volumetric flow rate through the collecting lymphatics was measured in situ by tracking the movements of lymphocytes in the lymphatic system of a rat. This method found the volumetric flow rate to be of the order $1.9 \times 10^{-11}\mathrm{m}^3\mathrm{s}^{-1}$, which was a couple of magnitudes lower than the study by Macdonald et al [78]. Macdonald's et al computational model was designed to reproduce the pumping behaviour of the collecting lymphatics in bovine mesenteric vessels. The method found volumetric flow rates through the collecting lymphatics of around the order of $1.5\times10^{-8}\mathrm{m}^3\mathrm{s}^{-1}$. Swartz et al [126] measured the volumetric flow rate through the collecting lymphatics of the skin in a mouse's tail to be $4.2\times10^{-12}\mathrm{m}^3\mathrm{s}^{-1}$. However, more recently they measured a larger value of the volumetric flow rate through the collecting lymphatics, around the order of $1.7\times10^{-10}\mathrm{m}^3\mathrm{s}^{-1}$ [124], which seems to agree more with the other cited experimental data. An alternate source of validation is the study by Levick on the flow through the interstitium for a rabbit knee synovium and a bovine femoral condylar cartilage [76]. Levick measured volumetric flow rates of the order $3 \times 10^{-7}\mathrm{m}^3\mathrm{s}^{-1}$ in the rabbit knee synovium and $3 \times 10^{-10}\mathrm{m}^3\mathrm{s}^{-1}$ in the bovine femoral condylar cartilage. To finish with a study by Ikomi et al [56] on the fluid uptake into initial lymphatics of a rabbit's hindleg found a volumetric flow rate of the order $2.7 \times 10^{-11}\mathrm{m}^3\mathrm{s}^{-1}$. On average, the volumetric flow rate through the lumen of lymphatic capillaries is similar in magnitude to the volumetric flow rate into lymphatic capillaries, which is to be expected according to our model. Thus we conclude that our model provides results of comparable magnitude to that of experimental data. In addition we have identified potential experiments to further validate the model.

Chapter 3

Model of Hypothesis 2: Fluid Drainage Through a Sliding Lymphatic Valve

3.1 Introduction

In this chapter we propose a 'sliding door' theory of how the primary lymphatics drain interstitial fluid; this is different to the premise modelled in Chapter 2, that lymphatic valves deflect into the lumen in response to a pressure difference between the interstitium and the lumen. The theory in this chapter incorporates regular tissue deformations that occur when the exudate of blood capillaries fills up all the pores of the surrounding interstitial space. This model is based upon the premise that when the interstitial space surrounding lymphatic capillaries expands, it pulls open their valves in a sliding fashion. This creates a gap in the lymphatic capillary wall for the interstitial fluid to drain into the lumen. In Chapter 1 we illustrated the hypothesised valve opening mechanism in Figure 1.7.

To our knowledge there is no previous analysis of this sliding door mecha-

nism in the primary lymphatics. The only hypothesis found in the literature was by Rossi et. al [106], where they hypothesized that interstitial fluid drainage is accommodated by the act of pulling apart interendothelial junctions on the lymphatic capillary wall. Based on their results they speculated that lymphatic anchoring filaments help in the drainage of interstitial fluid.

We begin this model by defining an idealized tissue that contains a periodic array of blood and lymphatic capillaries separated by the interstitium. Then we go on to describe the fluid flow from the blood capillary (through the interstitium) to the lymphatic capillary, and the tissue deformation using the theory of poroelasticity.

3.2 Model Development

Here we develop a model for lymphatic drainage of a tissue comprising a periodic array of blood and lymphatic capillaries (as illustrated in Figure 3.1). We treat the interstitial space lying between the blood and lymphatic capillaries as a linear poroelastic medium. Blood enters the interstitium from blood capillaries in response to the pressure difference between the blood and the interstitial fluid (the resistance of the blood capillary membrane to this flow is considered to be linearly proportional to the flow rate). Drainage of fluid from the interstitium takes place through lymphatic valves in the wall of the lymphatic capillary that open in response to the local deformation of the interstitium (i.e. they only open once the circumference of the lymphatic capillary has exceeded a critical size).

The model geometry is designed to be consistent with the literature. Measurements by Leak [72] found the radii of lymphatic capillaries to be of the order of 10×10^{-6}m, i.e. slightly larger than an average blood capillary [13]. Measurements by Geleff et al and Sauter et al [44, 109] found distances between blood and

lymphatic capillaries of the order of 10^{-4}m. Lymphatic capillaries are known to follow blood capillaries in close proximity around the entire body [15, 71]. This motivates us to consider an idealized periodic geometry, displayed in Figure 3.1 (arrows indicate the fluid movement), in which blood and lymphatic capillaries are distributed uniformly through a tissue. Choosing such a periodic array allows us to characterize the behaviour of the entire tissue by a single periodic tile (represented by the dotted square in Figure 3.1). This single periodic tile contains the fluid flow from one blood capillary to one lymphatic capillary.

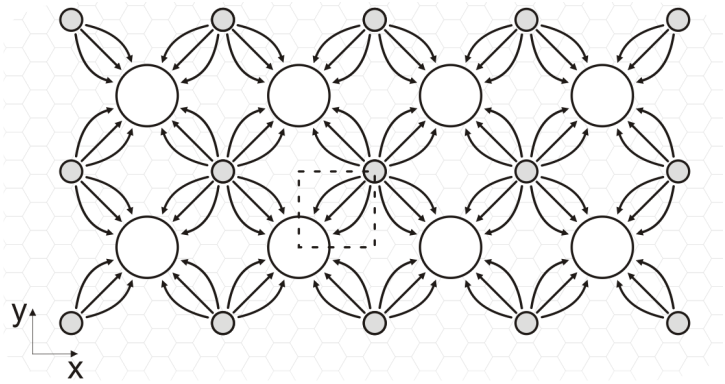

Figure 3.1: A cross sectional view of an idealized tissue with blood (grey) and lymphatic (white) capillaries surrounded by the interstitium. The arrows indicate the fluid's movement. The dotted box is a periodic tile used to model the fluid flow.

Valve Mechanics

The primary lymphatic valve system controls the rate at which interstitial fluid drains into the lymphatics. We model this valve as a sliding door that opens and closes in response to the expansions and contractions of the surrounding interstitium, respectively. That is, we take the valve to be closed if its circumference, $C(t)$, is less than or equal to a critical value C_{crit}, and open if it exceeds this value. Thus,

$$\begin{aligned} &\text{if} \quad C(t) < C_{crit} \quad \text{then} \quad \text{valve closed,} \\ &\text{if} \quad C(t) > C_{crit} \quad \text{then} \quad \text{valve open.} \end{aligned} \tag{3.2.1}$$

3.2.1 Governing Equations

Here we model the coupled interstitial fluid flow and deformations by Biot's equations of poroelasticity [11] (these describe the flow of a Newtonian fluid through a deformable linear elastic porous medium). This approach has been adopted previously in biological tissues, and validated against experiments, in [53, 126]. A comprehensive review of the theory is provided in [12].

The Fluid Equations

In the Biot model, the fluid flux relative to the solid ($\mathbf{Q}_f$) is related to the fluid pore pressure gradient (∇P) by Darcy's law,

$$\mathbf{Q}_f = -K\nabla P, \tag{3.2.2}$$

where K ($\mathrm{m^3skg^{-1}}$) is the interstitial hydraulic conductivity. Here we assume that K is constant (i.e. independent of tissue deformation), an assumption that is only valid when tissue deformations remain small. We can write the fluid flux $\mathbf{Q}_f$ in terms of the difference in velocities of the fluid ($\mathbf{v}^f$) and solid ($\partial\mathbf{u}/\partial t$) by,

$$\mathbf{Q}_f = \phi\left(\mathbf{v}^f - \frac{\partial \mathbf{u}}{\partial t}\right), \tag{3.2.3}$$

where ϕ is the fluid volume fraction.

Both the interstitial fluid and the solid material making up the matrix are assumed to be separately incompressible. The assumption that the solid matrix is incompressible does not however imply that the interstitium as a whole is in-

compressible since it can be compressed by allowing fluid to flow out of its pores. Conservation of fluid and solid volumes gives,

$$\frac{\partial \phi}{\partial t} + \nabla \cdot (\phi \mathbf{v}^f) = 0, \tag{3.2.4}$$

$$-\frac{\partial \phi}{\partial t} + \nabla \cdot \left((1-\phi) \frac{\partial \mathbf{u}}{\partial t} \right) = 0. \tag{3.2.5}$$

The addition of (3.2.4) and (3.2.5) results in the relation,

$$\nabla \cdot \left[\phi \left(\mathbf{v}^f - \frac{\partial \mathbf{u}}{\partial t} \right) \right] = -\nabla \cdot \left(\frac{\partial \mathbf{u}}{\partial t} \right). \tag{3.2.6}$$

On subtracting for the factor $\phi(\mathbf{v}^f - \partial \mathbf{u}/\partial t)$ for $-K\nabla P$, using equations (3.2.2)-(3.2.3), in the above we obtain the following equations for the conservation of fluid. Furthermore, since the geometry we consider is 2-d we need only consider plane–strain and pressure variation within the plane,

$$\mathbf{u} = (u_1(x,y,t), u_2(x,y,t), 0) \quad \text{and} \quad P = P(x,y,t), \tag{3.2.7}$$

$$\nabla \cdot (K \nabla P) = \nabla \cdot \left(\frac{\partial \mathbf{u}}{\partial t} \right). \tag{3.2.8}$$

Solid Governing Equations

In Biot's model, the elastic stress strain relation is linear, but crucially depends upon the fluid pore pressure [11]. It thus takes the form,

$$\sigma_{ij} = 2\mu \epsilon_{ij} + \lambda \delta_{ij} \epsilon_{kk} - P \delta_{ij}, \tag{3.2.9}$$

$$\epsilon_{ij} = \epsilon_{ji} = \frac{1}{2} \left(\frac{\partial u_i}{\partial x_j} + \frac{\partial u_j}{\partial x_i} \right), \tag{3.2.10}$$

where σ_{ij} is the stress tensor, ϵ_{ij} is the strain tensor, u_i is the tissue displacement, δ_{ij} is the Kronecker delta tensor and λ (Pa) and μ (Pa) are the first and second

drained Lam*é* parameters.

These drained Lam*é* parameters are calculated by subjecting a material volume of the porous medium to an external load and measuring the resulting strains while allowing the fluid contained within the volume to freely drain out of it (or enter it) at constant fluid pressure P. Generally parameters in problems where the movement of fluid and solid needs to be calculated independently are calculated under drained conditions.

Neglecting inertial forces and any external body forces in the solid leads to a force balance equation of the form,

$$\frac{\partial \sigma_{ij}}{\partial x_j} = 0. \tag{3.2.11}$$

Substituting the stress strain relationship (3.2.9) into (3.2.11) under the assumption of plane strain, (3.2.7), yields two equations for the displacements u_1 and u_2 in terms of pressure gradient, i.e.,

$$(2\mu+\lambda)\frac{\partial^2 u_1}{\partial x_1^2} + \lambda\frac{\partial^2 u_2}{\partial x_1 \partial x_2} - \frac{\partial P}{\partial x_1} + \mu\left(\frac{\partial^2 u_1}{\partial x_2^2} + \frac{\partial^2 u_2}{\partial x_1 \partial x_2}\right) = 0, \tag{3.2.12}$$

$$\mu\left(\frac{\partial^2 u_1}{\partial x_1 \partial x_2} + \frac{\partial^2 u_2}{\partial x_1^2}\right) + (2\mu+\lambda)\frac{\partial^2 u_2}{\partial x_1^2} + \lambda\frac{\partial^2 u_1}{\partial x_2 \partial x_1} - \frac{\partial P}{\partial x_2} = 0, \tag{3.2.13}$$

where u_i is the tissue displacement.

The three equations (3.2.8), (3.2.12) and (3.2.13), for three unknown variables (u_1, u_2 and P), are the governing poroelastic equations that model the interstitial deformation and the interstitial fluid flow.

3.2.2 Boundary Conditions

The periodicity of the geometry illustrated in Figure 3.1 allows us to reduce the problem to that on a single periodic tile containing one blood and one lymphatic

capillary, see Figure 3.2. The arrows in Figure 3.2 indicate the fluid movement.

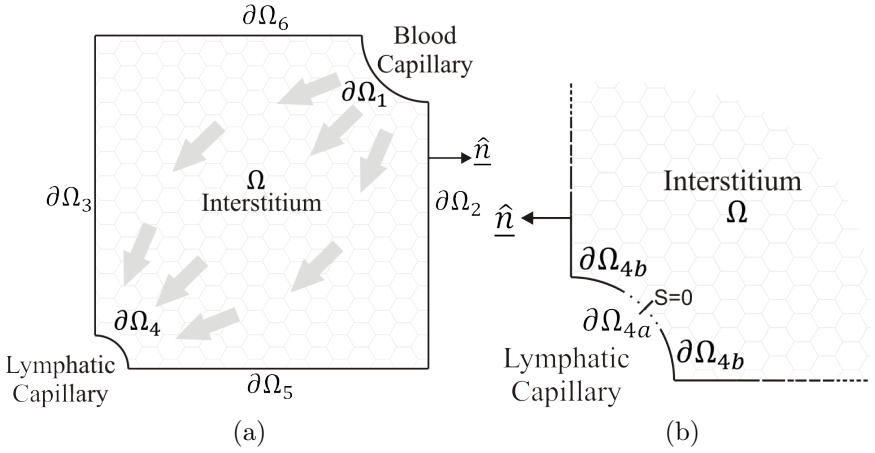

Figure 3.2: (a) The single periodic tile, containing one lymphatic and blood capillary separated by the interstitium. (b) A zoom of the lymphatic capillary identifying different parts of the capillary wall. Arrows in (a) indicate fluid motions.

Evaluation of $\partial\Omega_{4a}$ and $\partial\Omega_{4b}$

The lymphatic capillary wall ($\partial\Omega_4$) is split into two parts, which are denoted by $\partial\Omega_{4a}$ and $\partial\Omega_{4b}$ (see Figure 3.2b). Here $\partial\Omega_{4a}$ represents the interface between the lymphatic lumen and the interstitium not covered by lymphatic endothelial cells (through which the interstitial fluid flows), while $\partial\Omega_{4b}$ represents the endothelial cell wall (through which there is no flow). We assume that the open section of the lymphatic capillary valve is located half way along the capillary boundary, as illustrated in Figure 3.2b. $C(t)$ is given by the length of the circumference of the lymphatic capillary

$$C(t) = 4 \int_{\partial\Omega_4} ds, \tag{3.2.14}$$

and

$$\partial\Omega_{4a} \quad \text{is defined by} \quad s \in [-\Delta, \Delta] \quad \text{where} \quad \Delta = \max\left\{0, \frac{C(t) - C_{crit}}{8}\right\}, \tag{3.2.15}$$

$$\partial\Omega_{4b} \quad \text{is defined by} \quad s \in \left[-\frac{C(t)}{8}, -\Delta\right] \quad \text{and} \quad s \in \left[\Delta, \frac{C(t)}{8}\right]. \tag{3.2.16}$$

We note that $\partial\Omega_4$ is the union of $\partial\Omega_{4a}$ and $\partial\Omega_{4b}$, and when the lymphatic valve is closed ($\Delta = 0$) $\partial\Omega_4 = \partial\Omega_{4b}$. With this in mind we calculate the length of the open section of the valve ($L_v(t)$), in the relation,

$$L_v(t) = \frac{C(t) - C_{crit}}{4}, \tag{3.2.17}$$

where C_{crit} is the total length of the endothelial cells forming the valve (thus when $C < C_{crit}$ the valve is closed). We note that using (3.2.17) to determine the length of the open section of the valve uses the fact that the length of the endothelial cell wall ($\partial\Omega_{4b}$) does not change (while undergoing the sliding motion). This assumption however does imply that the endothelial cell wall cannot deflect in the normal direction of the lymphatic capillary.

Fluid Boundary Conditions

The Lymphatic capillary, boundary $\partial\Omega_4$

The opening and closing of the lymphatic valve requires us to formulate two sets of fluid flow boundary conditions on the lymphatic valve.

When the lymphatic valve is closed ($C(t) < C_{crit}$) there is no normal fluid flow through the capillary wall relative to the tissue. Once the surrounding interstitium expands enough to open the lymphatic valve ($C(t) > C_{crit}$), i.e., to slide the neighbouring lymphatic endothelial cells apart, fluid flow into the lumen occurs through the gap between the endothelial cells, i.e., through boundary $\partial\Omega_{4a}$. We model this by imposing continuity of pressure on the open part of the lymphatic valve ($\partial\Omega_{4a}$) while keeping the no flux condition on the remaining part of the

lymphatic wall ($\partial\Omega_{4b}$). Thus

$$P = P^l \quad \text{for} \quad \mathbf{x} \in \partial\Omega_{4a}, \tag{3.2.18}$$

$$\nabla P \cdot \mathbf{n} = 0 \quad \text{for} \quad \mathbf{x} \in \partial\Omega_{4b}, \tag{3.2.19}$$

where P^l is the fluid pressure of the lymphatic lumen and $\mathbf{n}$ is the unit normal vector ($\partial\Omega_4$) pointing into the lumen.

The blood capillary, boundary $\partial\Omega_1$

The blood capillary wall is permeable to fluid flow, but provides a resistance to it. This behaviour is modelled by imposing a linear permeability condition on the wall,

$$K\nabla P \cdot \mathbf{n} = L_p(P - P^b) \quad \text{for} \quad \mathbf{x} \in \partial\Omega_1, \tag{3.2.20}$$

where L_p is the vascular hydraulic permeability and $\mathbf{n}$ is the unit normal vector to $\partial\Omega_1$ pointing into the capillary lumen.

Remaining edges of the periodic tile, boundaries $\partial\Omega_2$, $\partial\Omega_3$, $\partial\Omega_5$ and $\partial\Omega_6$

Due to the periodicity of the geometry the fluid only enters the interstitium through the blood capillary and only exits via the lymphatic capillary (once the valve has opened). Thus there is no fluid flux across the boundaries $\partial\Omega_2$, $\partial\Omega_3$, $\partial\Omega_5$ and $\partial\Omega_6$, namely

$$(\mathbf{v}^f - \frac{\partial \mathbf{u}}{\partial t}) \cdot \mathbf{n} = 0 \quad \text{for} \quad \mathbf{x} \in \partial\Omega_2 \cup \partial\Omega_3 \cup \partial\Omega_5 \cup \partial\Omega_6, \tag{3.2.21}$$

where $\mathbf{n}$ is the unit outward normal vector to each edge. It follows from Darcy's equation (3.2.2) that,

$$\nabla P \cdot \mathbf{n} = 0 \quad \text{for} \quad \mathbf{x} \in \partial\Omega_2 \cup \partial\Omega_3 \cup \partial\Omega_5 \cup \partial\Omega_6. \tag{3.2.22}$$

Solid Boundary Conditions

Here we restrict our attention to uniform dilations (and contractions) of the periodic tile so that it remains square. This assumption disallows buckling of the lymphatic capillary and is reasonable for the small deformations considered in this chapter. Since we are looking for a uniform dilation (or contraction) of the interstitium the edges of the periodic tile have to remain horizontal ($\partial\Omega_2$ and $\partial\Omega_5$) and vertical ($\partial\Omega_3$ and $\partial\Omega_6$).

Edges adjacent to the blood capillary, boundaries $\partial\Omega_2$ and $\partial\Omega_6$

Edges $\partial\Omega_2$ and $\partial\Omega_6$ of the periodic tile are only displaced in the tangential direction, keeping the tile square. Thus without loss of generality we impose zero normal displacement of boundaries $\partial\Omega_2$ and $\partial\Omega_6$. However, we allow boundaries $\partial\Omega_2$ and $\partial\Omega_6$ to deform freely in the tangential direction; which is equivalent to imposing zero tangential shear stress conditions. These two conditions can be formulated as

$$u_1 = 0 \quad \text{and} \quad \sigma_{12} = 0 \quad \text{for} \quad \mathbf{x} \in \partial\Omega_2, \tag{3.2.23}$$

$$u_2 = 0 \quad \text{and} \quad \sigma_{21} = 0 \quad \text{for} \quad \mathbf{x} \in \partial\Omega_6. \tag{3.2.24}$$

Edges adjacent to the lymphatic capillary, boundaries $\partial\Omega_3$ and $\partial\Omega_5$

The symmetry of the problem requires that edges $\partial\Omega_3$ and $\partial\Omega_5$ are allowed to deform freely in the tangential direction, but can be displaced normally only by a prior unknown distance u_c, which we shall calculate. These quantities can be formulated in the form,

$$u_1 = u_c \quad \text{and} \quad \sigma_{12} = 0 \quad \text{on} \quad \mathbf{x} \in \partial\Omega_3, \tag{3.2.25}$$

$$u_2 = u_c \quad \text{and} \quad \sigma_{21} = 0 \quad \text{on} \quad \mathbf{x} \in \partial\Omega_5, \tag{3.2.26}$$

and the challenge now is how to compute u_c.

Assuming that the periodic tile deforms uniformly (remains square), which ensures that the normal displacements on both the edges $\partial\Omega_3$ and $\partial\Omega_5$ are equal, this displacement u_c may then be calculated as follows. Integration of the continuity equation (3.2.8) leads to,

$$\iiint_{\Omega} \nabla \cdot (K \nabla P)\, dV = \iiint_{\Omega} \nabla \cdot \left(\frac{\partial \mathbf{u}}{\partial t} \right)\, dV, \tag{3.2.27}$$

which gives, on use of the divergence theorem (2D plane),

$$\iint_{\partial\Omega} K \nabla P \cdot \mathbf{n}\, dS = \frac{\partial}{\partial t} \iint_{\partial\Omega} \mathbf{u} \cdot \mathbf{n}\, dS, \tag{3.2.28}$$

where $\partial\Omega = \partial\Omega_1 \cup \partial\Omega_2 \cup \partial\Omega_3 \cup \partial\Omega_4 \cup \partial\Omega_5 \cup \partial\Omega_6$. We can rewrite the right hand side of equation (3.2.28) as,

$$\begin{aligned} \frac{\partial}{\partial t} \iint_{\partial\Omega} \mathbf{u} \cdot \mathbf{n}\, dS &= \frac{\partial}{\partial t} \left(\int_{\partial\Omega_3 \cup \partial\Omega_5} \mathbf{u} \cdot \mathbf{n}\, dS + \int_{\partial\Omega_1 \cup \partial\Omega_4} \mathbf{u} \cdot \mathbf{n}\, dS + \int_{\partial\Omega_2 \cup \partial\Omega_6} \mathbf{u} \cdot \mathbf{n}\, dS \right) \\ &= \frac{\partial}{\partial t}(2u_c L(t)) + \frac{\partial}{\partial t} \int_{\partial\Omega_1 \cup \partial\Omega_4} \mathbf{u} \cdot \mathbf{n}\, dS, \end{aligned} \tag{3.2.29}$$

where $L(t)$ is the width of the periodic tile (which is square) minus the radius of the lymphatic capillary. Combining equations (3.2.28) and (3.2.29) together and integrating with respect to time gives the following relationship for the normal tissue displacement on boundaries $\partial\Omega_3$ and $\partial\Omega_5$ of the periodic tile,

$$u_c = \frac{1}{2L(t)} \left(\int_{\partial\Omega_1 \cup \partial\Omega_4} \left[\int K \nabla P \cdot \mathbf{n}\, dt \right]\, dS - \int_{\partial\Omega_1 \cup \partial\Omega_4} \mathbf{u} \cdot \mathbf{n}\, dS \right). \tag{3.2.30}$$

The first integral term on the right hand side of equation (3.2.30) is only over the blood and lymphatic capillary wall boundaries because the other boundaries of

the periodic tile have zero normal component of the pressure gradient. The second integral term on the right hand side of equation (3.2.30) is only over $\partial\Omega_1$ and $\partial\Omega_4$ because the boundaries $\partial\Omega_2$ and $\partial\Omega_6$ have zero normal tissue displacement.

The blood and lymphatic capillary wall, boundaries $\partial\Omega_1$ and $\partial\Omega_4$

The fluid pressure in the lumen of the blood and lymphatic capillaries exert a normal force on their walls. We assume that both capillary walls are not capable of exerting a significant elastic force so that the normal stress exerted by the solid matrix on each wall is balanced by their lumen fluid pressure. Furthermore, since we assume that lymphatic valves are allowed to slide freely, we require the tangential component of the solid stress on the capillary wall to be zero. These two conditions can be formulated as follows,

$$\sigma_{ij}n_j = -P^b n_i \quad \text{for} \quad \mathbf{x} \in \partial\Omega_1, \tag{3.2.31}$$

$$\sigma_{ij}n_j = -P^l n_i \quad \text{for} \quad \mathbf{x} \in \partial\Omega_4, \tag{3.2.32}$$

where P^b and P^l denote the lumen fluid pressure in the blood and lymphatic capillaries, respectively.

Initial conditions

We consider a problem in which the tissue is initially undeformed and at the uniform reference pressure zero, that is

$$P\Big|_{t=0} = u_1\Big|_{t=0} = u_2\Big|_{t=0} = 0 \quad \text{in } \Omega. \tag{3.2.33}$$

We then track the subsequent evolution until the deformation on the lymphatic capillary wall is such that its circumference is $C(t) = C_{crit}$ and the valve starts to slide open. We then use the resulting configuration as the initial condition for a

problem in which the valve is open.

3.2.3 Parameter Values

There are 9 material parameter values in our governing equations and boundary conditions, namely L_p, K, L_i, E, ν, P^l, P^b, C_{crit}, $L_{overlap}$, see table 3.1 for their values. Appropriate values for these are discussed below.

The first and second Lam*é* constants, λ and μ, appear in (3.2.12) and (3.2.13). The elasticity of drained soft tissues $(2\mu + \lambda)$ was measured by Swartz [126] to be in the range of 10^4 Pa to 2×10^4 Pa. The Poisson's ratio (ν) and the Young's Modulus (E) are given in [61] for soft tissue as $\nu = 0.35$ and $E = 10^4$ Pa. This gives $\lambda = 8642$ Pa and $\mu = 3704$ Pa. We note that the Poisson ratio thus calculated is consistent with measurements made in [10, 108]. With these parameter ranges E is in the range 5×10^4 Pa to 1.3×10^5 Pa, which is consistent with the studies by [42, 61].

The interstitial hydraulic conductivity, K (permeability/viscosity) appears in (3.2.8). Levick [76] measured fluid flow through the interstitium and other fibrous matrices to determine values for the interstitial permeability, finding it to be in the range $1.5 \times 10^{-14}\text{m}^2$ to $1.5 \times 10^{-19}\text{m}^2$. We choose the average value of $7.6 \times 10^{-15}\text{m}^2$ [85]. The viscosity of interstitial fluid was measured by Dixon [31] to be 1.5×10^{-3} kgm^{-1}s^{-1}. This leads to a value K of 5.07×10^{-12} m^{3}skg^{-1}. Basser [7] and Swartz's [126] experimentally determined values of the same quantity are in broad agreement at 7.5×10^{-12} m^{3}skg^{-1} and 1.123×10^{-12} m^{3}skg^{-1}, respectively.

The vascular hydraulic permeability of a blood capillary, L_p, was measured in various normal tissues by Jain et al [58], Levick [76], Pusenjak [96], Baxter and Jain [10] and Sarntinoranont et al [108] and estimated to be in the range 2.78×10^{-11} m^{2}skg^{-1} to 1.37×10^{-9} m^{2}skg^{-1}. We take the average value $L_p = 7.0 \times 10^{-10}$ m^{2}skg^{-1}.

The blood capillary pressure (average radius 5μm) is normally in the range 2666 Pa to 4000 Pa [13, 58]. Lymphatic lumen pressures have been measured by Lee [75] to be in the range up to 440 Pa. Lymphatic capillaries normally have a radius in the range of 5 μm to 15 μm [99]. However, more recent studies show that in rare cases lymphatic capillaries can reach a large radius of 30 μm [80, 122]. In this model we assume a lymphatic capillary radius of 10 μm. Therefore $C_{crit} = 4L_{ovlap}+2\pi R_l = 66.8$ μm, where R_l is the radius of the blood capillary and $L_{ovlap} = 1\mu m$ is the length of the lymphatic endothelial cell overlap, ranging from 0.1μm to 2μm [71, 72]. Measurements from Leak [72] show that the distance between lymphatic and blood capillaries can be up to 400 μm apart. However, more recent studies [44, 109] found distances between lymphatic and blood capillaries between 50 μm and 250 μm. In this chapter we assume the distance between lymphatic and blood capillaries is 150 μm.

Parameter	Value	Units	Description	Source
L_p	7.0×10^{-10}	m^2skg^{-1}	The vascular hydraulic permeability.	[10, 58, 108]
K	5.07×10^{-12}	m^3skg^{-1}	Hydraulic conductivity of the interstitium	[10, 58, 108]
L_i	1.17×10^{-4}	m	The initial width of the periodic tile, which is square, minus the radius of the lymphatic capillary. So $L(0) = L_i$.	[44, 109]
ν	0.35		The Poisson ratio	[61, 108, 126]
E	10^4	Pa	The Young's modulus	[61, 126]
P^l	100	Pa	Pressure in lymphatic lumen	[75]
P^b	3333	Pa	Blood capillary pressure	[13]
C_{crit}	66.8	μm	Critical lymphatic circumference	[71, 72]
L_{ovlap}	1	μm	Lymphatic endothelial cell overlap	[71, 72]

Table 3.1: Summary of dimensional parameters used in the model along with their references. Note the values of $E = \mu(3\lambda+2\mu)/(\lambda+\mu)$ and $\nu = \lambda/(2(\lambda+\mu))$ above correspond to $\lambda = 8642$ and $\mu = 3704$.

3.2.4 Nondimensionalization

We nondimensionalize the model to determine which key combination of parameters in the governing equations and boundary conditions are of most importance.

A reasonable length scale for the problem is L_i, the initial width of the periodic tile minus the radius of the lymphatic capillary. With this in mind, we scale the governing equations and boundary conditions by

$$P = (2\mu + \lambda)\overline{P}, \quad \sigma_{ij} = (2\mu + \lambda)\overline{\sigma}_{ij}, \quad \mathbf{u} = L\overline{\mathbf{u}}, \quad t = \frac{L^2}{K(2\mu + \lambda)}\overline{t}. \quad (3.2.34)$$

Dimensionless Model

The dimensionless governing equations are (after dropping the bars),

$$\frac{\partial}{\partial t}\left(\frac{\partial u_1}{\partial x_1} + \frac{\partial u_2}{\partial x_2}\right) = \frac{\partial^2 P}{\partial x_1^2} + \frac{\partial^2 P}{\partial x_2^2}, \quad (3.2.35)$$

$$\frac{\partial^2 u_1}{\partial x_1^2} + \frac{\partial^2 u_2}{\partial x_1 \partial x_2} - \widehat{\mu}\left(\frac{\partial^2 u_2}{\partial x_1 \partial x_2} - \frac{\partial^2 u_1}{\partial x_2^2}\right) = \frac{\partial P}{\partial x_1}, \quad (3.2.36)$$

$$\frac{\partial^2 u_1}{\partial x_1 \partial x_2} + \frac{\partial^2 u_2}{\partial x_2^2} + \widehat{\mu}\left(\frac{\partial^2 u_2}{\partial x_1^2} - \frac{\partial^2 u_1}{\partial x_1 \partial x_2}\right) = \frac{\partial P}{\partial x_2}. \quad (3.2.37)$$

The dimensionless fluid flow boundary conditions on the lymphatic capillary are[1],

$$P = \widehat{P}^l \quad \text{on} \quad \mathbf{x} \in \partial\Omega_{4a}, \quad (3.2.38)$$

$$\nabla P \cdot \mathbf{n} = 0 \quad \text{on} \quad \mathbf{x} \in \partial\Omega_{4b}. \quad (3.2.39)$$

On the blood capillary wall we have,

$$\nabla P \cdot \mathbf{n} = R_b(P - \widehat{P}^b) \quad \text{on} \quad \mathbf{x} \in \partial\Omega_1, \quad (3.2.40)$$

[1]See Table 3.2 for definitions of all the dimensionless parameter groupings.

and on the remaining edges of the periodic tile we have,

$$\nabla P \cdot \mathbf{n} = 0 \quad \text{on} \quad \mathbf{x} \in \partial\Omega_2 \cup \partial\Omega_3 \cup \partial\Omega_5 \cup \partial\Omega_6. \tag{3.2.41}$$

The dimensionless solid boundary conditions are,

$$u_1 = \sigma_{12} = 0 \quad \text{on} \quad \mathbf{x} \in \partial\Omega_2, \tag{3.2.42}$$

$$u_2 = \sigma_{21} = 0 \quad \text{on} \quad \mathbf{x} \in \partial\Omega_6, \tag{3.2.43}$$

$$u_1 = u_c \quad \text{and} \quad \sigma_{12} = 0 \quad \text{on} \quad \mathbf{x} \in \partial\Omega_3, \tag{3.2.44}$$

$$u_2 = u_c \quad \text{and} \quad \sigma_{21} = 0 \quad \text{on} \quad \mathbf{x} \in \partial\Omega_5, \tag{3.2.45}$$

where u_c is calculated by,

$$u_c = \int\limits_{\partial\Omega_1 \cup \partial\Omega_4} \int \nabla P \cdot \mathbf{n} \; dt \; dS - \int\limits_{\partial\Omega_1 \cup \partial\Omega_4} \mathbf{u} \cdot \mathbf{n} \; dS. \tag{3.2.46}$$

On the blood and lymphatic capillary wall we have,

$$\sigma_{ij} n_j = -\widehat{P}^b n_i \quad \text{on} \quad \mathbf{x} \in \partial\Omega_1, \tag{3.2.47}$$

$$\sigma_{ij} n_j = -\widehat{P}^l n_i \quad \text{on} \quad \mathbf{x} \in \partial\Omega_4. \tag{3.2.48}$$

The dimensionless initial conditions are,

$$P\Big|_{t=0} = u_1\Big|_{t=0} = u_2\Big|_{t=0} = 0 \quad \text{in } \Omega. \tag{3.2.49}$$

Table 3.2 shows the definitions and values of all the dimensionless parameters.

Parameter	Definition	Estimated Value
$\widehat{\mu}$	$\frac{\mu}{2\mu+\lambda} = \frac{1-2\nu}{2(1-\nu)}$	0.23
R_b	$\frac{LL_p}{K}$	0.016
$\widehat{P}^b$	$\frac{P^b}{2\mu+\lambda} = \frac{P^b(1+\nu)(1-2\nu)}{E(1-\nu)}$	0.21
$\widehat{P}^l$	$\frac{P^l}{2\mu+\lambda} = \frac{P^l(1+\nu)(1-2\nu)}{E(1-\nu)}$	0.02

Table 3.2: The values of the dimensionless groupings.

3.3 Conclusion

In conclusion we have built a model based on Hypothesis 2. This states that lymphatic drainage occurs when the expansion of the interstitial space surrounding the lymphatic capillaries exceeds a certain amount. We were motivated to consider lymphatic drainage in an idealized 2D periodic geometry, in which blood and lymphatic capillaries were distributed uniformly through the tissue (see Figure 3.1). In contrast to earlier studies [42, 85, 99], in which lymphatic valves are presumed to open in response to fluid pressure differences between the interstitium and lymphatic lumen, here we considered valves comprised of overlapping lymphatic endothelial cells that slide apart (and open) in response to interstitial deformations. We assume that no buckling occurs in both the blood and lymphatic capillaries. The model treated solid matrix deformations in conjunction with three significant sources of resistance to fluid flow. The latter are: the permeable membrane around the blood capillaries, the resistance of the interstitium and that of the overlapping endothelial cells forming the lymphatic valve.

Chapter 4

Solution to the Model of Hypothesis 2

4.1 Introduction

In this chapter we numerically solve the model of Hypothesis 2 by using the finite element package, Comsol Multiphysics. We begin by formulating the numerical solution to give the reader a better understanding of how and why we solve the model this way. We present our results graphically and draw our conclusions. We also investigate the effects of parameter influence on lymphatic drainage.

4.2 Numerical Model Formulation

Here we describe how we use the finite element package Comsol Multiphysics (CM) to solve the model formulated in Chapter 3 for fluid drainage by the lymphatic system. CM is an engineering, design, and finite element analysis software environment for the modelling and simulation of physics–based problems. CM facilitates all the steps in the modelling process, defining the geometry, meshing, specifying the physics, solving, and visualization.

Here we use the poroelastiticity equations defined in CM and compare them to our equations in Chapter 3, equations (3.2.8) and (3.2.11). Also we interpret the boundary conditions, (3.2.18) to (3.2.32), used in CM in differential form. Then we use CM to model the solid matrix deformations and the interstitial fluid flow.

Solution of Poroelastic Equations using Comsol

The poroelastic module in CM describes the interaction between the fluid motion and the interstitium deformation in a porous medium. Solving the poroelasticity equations in CM involves coupling of its Darcy's law Interface (which describes the fluid flow in a porous medium) with its solid mechanics Interface (which has the equations for structural displacement) via Biot's constitutive equations. Below we describe each of these interfaces.

4.2.1 Darcy's Law Interface

The Darcy's Law Interface, found under the porous media and subsurface flow module, can be used to solve for the fluid movement through interstices in a porous medium. Darcy's law states that the flux of fluid ($\mathbf{v}^f$) is determined by the pressure gradient (∇P), the fluid viscosity ($\overline{\mu}$), and the permeability of the porous medium (κ),

$$\mathbf{v}^f = -\frac{\kappa}{\overline{\mu}}\nabla P. \tag{4.2.1}$$

The Darcy's Law Interface combines Darcy's Law with the fluid continuity equation,

$$\frac{\partial}{\partial t}(\rho\phi) + \nabla \cdot (\rho\phi\mathbf{v}^f) = Q_m, \tag{4.2.2}$$

where ρ is the density of the fluid, ϕ is the porosity of the tissue and Q_m is the mass source term. In our case the mass source term (Q_m) is zero. Porosity is

defined as the fraction of the control volume that is occupied by pores. Thus, porosity can vary from zero for pure solid regions to unity for pure fluids.

4.2.2 Solid Mechanics Interface

The solid mechanics interface, found under the structural mechanics module, can be used to solve (linear) elasticity problems for displacements, strains and stresses in a material.

Following the small displacement assumption, the normal strain components and the shear strain components, ϵ_{ij}, are given from the deformations, u_i, as follows,

$$\epsilon_{ij} = \frac{1}{2}\left(\frac{\partial u_i}{\partial x_j} + \frac{\partial u_j}{\partial x_i}\right). \tag{4.2.3}$$

The stress in a material is described by the symmetric stress tensor (σ_{ij}). The stress strain relationship in CM is written in matrix form as,

$$\sigma_{ij} = D\epsilon_{ij}, \tag{4.2.4}$$

where D is a 3×3 elasticity matrix. This is because of our plain strain assumption ($\epsilon_{13} = \epsilon_{23} = \epsilon_{33} = 0$). D_{ij} is described in terms of the Young's modulus E and the Poisson's ratio ν. The stress and strain components are described in vector form with the three stress and strain components in column vectors defined as,

$$\begin{bmatrix} \sigma_{11} \\ \sigma_{22} \\ \sigma_{12} \end{bmatrix} = \frac{E}{(1+\nu)(1-2\nu)} \begin{bmatrix} 1-\nu & \nu & 0 \\ \nu & 1-\nu & 0 \\ 0 & 0 & \frac{1-2\nu}{2} \end{bmatrix} \begin{bmatrix} \epsilon_{11} \\ \epsilon_{22} \\ \epsilon_{12} \end{bmatrix}. \tag{4.2.5}$$

The equilibrium equations for the structural mechanics module in a 2D geometry

are,

$$\frac{\partial \sigma_{11}}{\partial x_1} + \frac{\partial \sigma_{12}}{\partial x_2} = -F_1, \tag{4.2.6}$$

$$\frac{\partial \sigma_{21}}{\partial x_1} + \frac{\partial \sigma_{22}}{\partial x_2} = -F_2, \tag{4.2.7}$$

where $\mathbf{F} = (F_1, F_2)$ denotes the body forces. In our case the body forces are negligible, and we take $F_1 = F_2 = 0$, so that equations 4.2.6 and 4.2.7 can be expressed in compact form as

$$\frac{\partial \sigma_{ij}}{\partial x_j} = 0. \tag{4.2.8}$$

4.2.3 Poroelasticity Interface

As noted earlier, the Poroelasticity Interface is the combination of the Darcy's Law Interface with the Solid Mechanics Interface. It modifies the fluid continuity equation (4.2.2), to include a time rate of change of strain, from the solid deformation equations, as follows

$$\nabla \cdot (\mathbf{v}^f) = -\alpha_b \frac{\partial}{\partial t}(\nabla \cdot \mathbf{u}), \tag{4.2.9}$$

where $\alpha_b = 1$ is the Biot–Willis coefficient. The Poroelastic module also adds the pore pressure to the stress–strain relationship, equation (4.2.4), so that the governing solid displacement equation is

$$\sigma_{ij} = D\epsilon_{ij} - \alpha_b P \delta_{ij}. \tag{4.2.10}$$

The governing equations (4.2.8) and (4.2.9), with input parameters κ, μ, α_b and D, are numerically solved to determine the Darcy's flux and the deformations of the solid matrix. Combining equations (4.2.1), (4.2.8) and (4.2.9) results in the same governing equations derived in Chapter 3, equations (3.2.8) and (3.2.11).

4.2.4 Boundary Conditions

Here we interpret the boundary conditions used in CM in differential form. Figure 4.1 reproduces our single periodic tile which we use as the domain in CM.

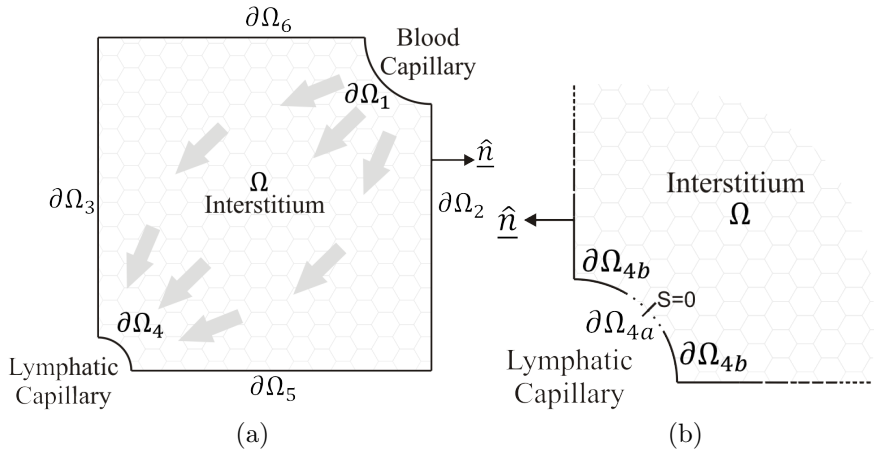

Figure 4.1: Our single periodic tile, displaying interstitial fluid flowing from a blood capillary to a lymphatic capillary. The arrows in (a) indicate the direction of the fluid movement.

We decouple the boundary conditions into fluid and solid conditions (i.e. one from the fluid flow module and two from the structural mechanics module). In the next two subsections we display, in differential form, the boundary conditions.

Fluid boundary conditions

Darcy's Law is evaluated on a given boundary to determine the fluid boundary conditions.

Evaluation of $\partial\Omega_{4a}$ and $\partial\Omega_{4b}$

The lymphatic capillary wall ($\partial\Omega_4$) is split into two parts, which are denoted by $\partial\Omega_{4a}$ and $\partial\Omega_{4b}$, see Figure 4.1. Here boundary $\partial\Omega_{4a}$ represents the interface between the lymphatic lumen and the interstitium not covered by lymphatic endothelial cells (through which interstitial fluid flows) while $\partial\Omega_{4b}$ represents the

endothelial cell wall (through which there is no flow). We assume that the open section of the lymphatic valve is located half way along the capillary boundary, as illustrated in Figure 4.1.

There are two possible ways of evaluating $\partial\Omega_{4a}$ and $\partial\Omega_{4b}$ in CM. One is using length constrictions i.e. fix the length of the boundary $\partial\Omega_{4b}$, and the other is building a function that determines where $\partial\Omega_{4a}$ and $\partial\Omega_{4b}$ lie along the boundary. Using length constrictions in this numerical package is a crude way of evaluating each part of this boundary, so we use the other approach. We introduce two new variables,

$$\theta_s = \frac{\pi C_{crit}}{4C(t)} \tag{4.2.11}$$

$$\theta_f = \frac{\pi(2C(t) - C_{crit})}{4C(t)} \tag{4.2.12}$$

where θ_s and θ_f are the angles from the horizontal to the start of $\partial\Omega_{4a}$ and the end of $\partial\Omega_{4a}$ respectively, to determine where $\partial\Omega_{4a}$ and $\partial\Omega_{4b}$ lie along $\partial\Omega_4$. So, $\theta_s < \partial\Omega_{4a} < \theta_f$ and $\partial\Omega_{4b} > \theta_f \cup \partial\Omega_{4b} < \theta_s$.

Using these angles in CM allows us to use only one boundary condition on the lymphatic capillary and still incorporate the valve mechanics. To determine $C(t)$ we introduce a boundary integral unit with respect to the material coordinates and integrate over $\partial\Omega_4$.

The lymphatic capillary wall, boundary $\partial\Omega_4$

We assume the lymphatic valve is closed when $C(t) < C_{crit}$, and open when $C(t) > C_{crit}$. When the lymphatic valve is closed there is no flow into the lumen and when the valve is open fluid flows into the lumen only through $\partial\Omega_{4a}$.

The boundary condition we use in CM on the lymphatic capillary is

$$\nabla P \cdot \mathbf{n} = (\nabla P \cdot \mathbf{n} + P - P^l) \times \text{if}(\theta_s < \theta < \theta_f, 1, 0), \tag{4.2.13}$$

where θ is the angle from the horizontal. This condition then gives

$$P = P^l \quad \text{on} \quad \mathbf{x} \in \partial\Omega_{4a} \ (\theta_s < \partial\Omega_{4a} < \theta_f), \tag{4.2.14}$$

$$\nabla P \cdot \mathbf{n} = 0 \quad \text{on} \quad \mathbf{x} \in \partial\Omega_{4b} (\partial\Omega_{4b} > \theta_f \cup \partial\Omega_{4b} < \theta_s), \tag{4.2.15}$$

where P^l is the fluid pressure of the lymphatic lumen. These are the same as the boundary conditions derived in Chapter 3 on boundary $\partial\Omega_4$, equations (3.2.18)-(3.2.19).

The blood capillary wall, boundary $\partial\Omega_1$

The blood capillary wall is permeable to fluid but provides a resistance to it. We model this behaviour by using a permeability condition on the wall.

We use the boundary condition Pervious Layer in CM to model the fluid flow through the blood capillary wall. The Pervious Layer feature provides a boundary condition that describes a mass flux through a semi–pervious layer connected to an external fluid source (P^b) at a different pressure. This condition is represented by the following differential equation,

$$\frac{\kappa}{\mu} \nabla P \cdot \mathbf{n} = L_p (P - P^b) \quad \text{on} \quad \mathbf{x} \in \partial\Omega_1, \tag{4.2.16}$$

where $\mathbf{n}$ is the unit outward normal vector to the blood capillary wall. This is the same as the boundary condition derived in Chapter 3 on boundary $\partial\Omega_1$, equations (3.2.20).

Remaining edges of the periodic tile, boundaries $\partial\Omega_2$, $\partial\Omega_3$, $\partial\Omega_5$ and $\partial\Omega_6$

Due to the periodicity of the geometry the fluid only enters the interstitium through the blood capillary and only exits via the lymphatic capillary (once the valve has opened). Thus there is no fluid flux across the boundaries $\partial\Omega_2$, $\partial\Omega_3$, $\partial\Omega_5$ and $\partial\Omega_6$ of the periodic tile.

The No Flow feature in CM defines a condition that there is no fluid flow across a given boundary. This effect is represented with the No Flow boundary condition,

$$\nabla P \cdot \mathbf{n} = 0 \quad \text{on} \quad \mathbf{x} \in \partial\Omega_2 \cup \partial\Omega_3 \cup \partial\Omega_5 \cup \partial\Omega_6, \tag{4.2.17}$$

where $\mathbf{n}$ is the unit outward normal vector to each edge. This is the same as the boundary condition derived in Chapter 3 on boundaries $\partial\Omega_2$, $\partial\Omega_3$, $\partial\Omega_5$ and $\partial\Omega_6$ (equation (3.2.22)).

Solid Boundary Conditions

Here we restrict our attention to uniform dilations (and contractions) of the periodic tile so that it remains square. We note that since we are looking for a uniform dilation or contraction of the interstitium that the edges of the periodic tile have to remain horizontal ($\partial\Omega_2$ and $\partial\Omega_5$) and vertical ($\partial\Omega_3$ and $\partial\Omega_6$).

Edges adjacent to the blood capillary, boundaries $\partial\Omega_2$ and $\partial\Omega_6$

As stated earlier, edges $\partial\Omega_2$ and $\partial\Omega_6$ of the periodic tile have to be displaced tangential to keep the tile square. Thus, without loss of generality we impose zero normal tissue displacement on boundaries $\partial\Omega_2$ and $\partial\Omega_6$. We allow the boundaries $\partial\Omega_2$ and $\partial\Omega_6$ to deform freely in the tangential direction; this is equivalent to imposing zero tangential shear stress along the boundaries.

The Roller feature in CM adds a roller constraint as the boundary condition,

that is, the tissue displacement is zero in the direction perpendicular to the boundary, but the boundary is free to move in the tangential direction. This effect is represented with the Roller condition,

$$u_1 = 0 \quad \text{and} \quad \sigma_{12} = 0 \quad \text{on} \quad \mathbf{x} \in \partial\Omega_2, \tag{4.2.18}$$

$$u_2 = 0 \quad \text{and} \quad \sigma_{21} = 0 \quad \text{on} \quad \mathbf{x} \in \partial\Omega_6. \tag{4.2.19}$$

These are the same as the boundary conditions derived in Chapter 3 on boundaries $\partial\Omega_2$ and $\partial\Omega_6$, equations (3.2.23)-(3.2.24).

Edges adjacent to the lymphatic capillary, boundaries $\partial\Omega_3$ and $\partial\Omega_5$

Keeping the symmetry in this problem, we allow edges $\partial\Omega_3$ and $\partial\Omega_5$ of the periodic tile to deform freely in tangential direction; this is equivalent to imposing zero tangential shear stress along the boundaries. However, we must allow both of these edges to deform normally by a distance u_c, which we shall calculate.

The Prescribed Displacement feature in CM adds a condition where the tissue displacement is prescribed in one direction to the boundary. If a displacement is prescribed in one direction, this leaves the solid free to deform in the other direction. These effects are represented with the Prescribed Displacement condition,

$$u_1 = u_c \quad \text{and} \quad \sigma_{12} = 0 \quad \text{on} \quad \mathbf{x} \in \partial\Omega_3, \tag{4.2.20}$$

$$u_2 = u_c \quad \text{and} \quad \sigma_{21} = 0 \quad \text{on} \quad \mathbf{x} \in \partial\Omega_5, \tag{4.2.21}$$

where u_c is calculated by

$$u_c = \frac{1}{2L(t)} \left(\int\limits_{\partial\Omega_1 \cup \partial\Omega_4} \left[\int K \nabla P \cdot \mathbf{n} \, dt \right] \, dS - \int\limits_{\partial\Omega_1 \cup \partial\Omega_4} \mathbf{u} \cdot \mathbf{n} \, dS \right), \tag{4.2.22}$$

where $L(t)$ is the width of the periodic tile, which is a square, minus the radius

of the lymphatic capillary.

The first integral term on the right hand side of equation (4.2.22) cannot be implemented directly in CM because it is a time dependent integral and the inbuilt time integrals in CM (timeint and timeavg) are only available during the results evaluation. We require access to a continuously evolving time integral on this boundary. So we introduce a new time dependent variable, T_1, as well as defining line integrals over the blood and lymphatic capillaries. We assume that T_1 is defined as the time integral of $K\nabla P \cdot \mathbf{n}$. Using the boundary conditions on the blood and lymphatic capillary wall, T_1 can be defined as

$$\begin{aligned}
\frac{dT_1}{dt} &= K\nabla P \cdot \mathbf{n} \quad \text{on} \quad \mathbf{x} \in \partial\Omega_1, \\
&= R_b(P - P^b) \quad \text{on} \quad \mathbf{x} \in \partial\Omega_1, \qquad (4.2.23) \\
\frac{dT_1}{dt} &= K\nabla P \cdot \mathbf{n} \quad \text{on} \quad \mathbf{x} \in \partial\Omega_4, \\
&= K|(\nabla P \cdot \mathbf{n})\mathbf{n} + (\nabla P \cdot \mathbf{t})\mathbf{t}| \quad \text{on} \quad \mathbf{x} \in \partial\Omega_4, \\
&= K\sqrt{\left(\frac{\partial P}{\partial x_1}\right)^2 + \left(\frac{\partial P}{\partial x_2}\right)^2} \quad \text{on} \quad \mathbf{x} \in \partial\Omega_4, \qquad (4.2.24)
\end{aligned}$$

with initial conditions $T_1(0) = 0$, where $\mathbf{n}$ and $\mathbf{t}$ are the normal and tangential components.

To implement the second integral term on the right hand side of equation (4.2.22) in CM, we just use our newly defined line integrals over the blood and lymphatic capillaries,

$$\begin{aligned}
\int\limits_{\partial\Omega_1 \cup \partial\Omega_4} \mathbf{u} \cdot \mathbf{n} \, dS &= \int\limits_{\partial\Omega_1} |(\mathbf{u} \cdot \mathbf{n})\mathbf{n} + (\mathbf{u} \cdot \mathbf{t})\mathbf{t}| \, dS + \int\limits_{\partial\Omega_4} |(\mathbf{u} \cdot \mathbf{n})\mathbf{n} + (\mathbf{u} \cdot \mathbf{t})\mathbf{t}| \, dS, \\
&= \int\limits_{\partial\Omega_1} \sqrt{u_1^2 + u_2^2} \, dS + \int\limits_{\partial\Omega_4} \sqrt{u_1^2 + u_2^2} \, dS. \qquad (4.2.25)
\end{aligned}$$

Hence conditions (4.2.20), (4.2.21) and (4.2.22) are the same as the boundary

conditions derived in Chapter 3 on boundaries $\partial\Omega_3$ and $\partial\Omega_5$, equations (3.2.25), (3.2.26) and (3.2.30).

Blood and lymphatic capillary, boundaries $\partial\Omega_1$ and $\partial\Omega_4$

The fluid pressure in the lumen of the blood and lymphatic capillaries exerts a normal force on their walls. We assume that both capillary walls are not capable of exerting a significant elastic force so that the normal stress exerted by the solid matrix on each wall is balanced by their lumen fluid pressure. Furthermore, since we assume the valves are allowed to slide freely we require that the tangential component of the solid stress on the capillary wall to be zero.

The Boundary Load feature in CM provides a pressure acting on a boundary that equals the normal stress on the boundary. This is represented with the boundary load condition,

$$\sigma_{ij}n_j = -P^b n_i \quad \text{on} \quad \mathbf{x} \in \partial\Omega_1, \tag{4.2.26}$$

$$\sigma_{ij}n_j = -P^l n_i \quad \text{on} \quad \mathbf{x} \in \partial\Omega_4. \tag{4.2.27}$$

These are the same as the boundary conditions derived in Chapter 3 on boundaries $\partial\Omega_1$ and $\partial\Omega_4$, equations (3.2.31)-(3.2.32).

Dependence of the steady state solution on $\widehat{P}^b$ and $\widehat{P}^l$. We note that the steady state solution satisfies (3.2.39)-(3.2.48) and that these equations are invariant under the transformation

$$P \to P + c, \quad \widehat{P}^b \to \widehat{P}^b + c, \quad \widehat{P}^l \to \widehat{P}^l + c, \quad \mathbf{u} \to \mathbf{u},$$
$$\sigma_{11} \to \sigma_{11} - c, \quad \sigma_{12} \to \sigma_{12}, \quad \sigma_{21} \to \sigma_{21}, \quad \sigma_{22} \to \sigma_{22} - c,$$

where c is an arbitrary constant. Such a transformation leaves the Darcy flow in the tissue $-\nabla P$ and the tissue deformation $\mathbf{u}$ unchanged and thus leads to a

physically identical solution. It is thus clear that the steady state solution does not depend independently on lymphatic lumen pressure $\widehat{P}^b$ and blood capillary pressure $\widehat{P}^l$ (neither of which are invariant under the transformation) but depends solely on the pressure difference $\widehat{P}^b - \widehat{P}^l$ (which is invariant under the transformation).

4.3 Solution and Results

Here we display the numerical solutions for the Darcy flux and the deformations of the solid matrix. We solve the model numerically using the Comsol Multiphysics Finite element package.

We produce plots of the interstitial deformation to demonstrate three key stages of the drainage process. In Figure 4.2, we plot the interstitial deformation at times during the drainage process (the arrows in each plot indicate the direction of the fluid flow). In Figure 4.2a, the lymphatic valve is closed and since the inflowing interstitial fluid cannot escape the interstitium it causes it to deform, resulting in the boundaries of the periodic tile moving outwards. At a later stage in the process (Figure 4.2b), the interstitial expansion about the lymphatic capillary is sufficiently large to cause the lymphatic endothelial cells to slide apart creating a gap for the interstitial fluid to drain into the lymphatic lumen. For sufficiently small gaps, the resistance to drainage is sufficiently large so that the net flow into the interstitium remains positive and the solid matrix keeps expanding. Once the interstitial deformation is large enough (Figure 4.2c), the gap length of the open section of the valve becomes sufficient to lower the resistance to drainage to a level where the drainage rate through the lymphatic valve exceeds the fluid inflow (from the blood capillary), and the solid matrix begins to contract. The gap length here has reached its peak and the interstitium contracts until the lymphatic endothelial

cells slide together again, closing the lymphatic valve.

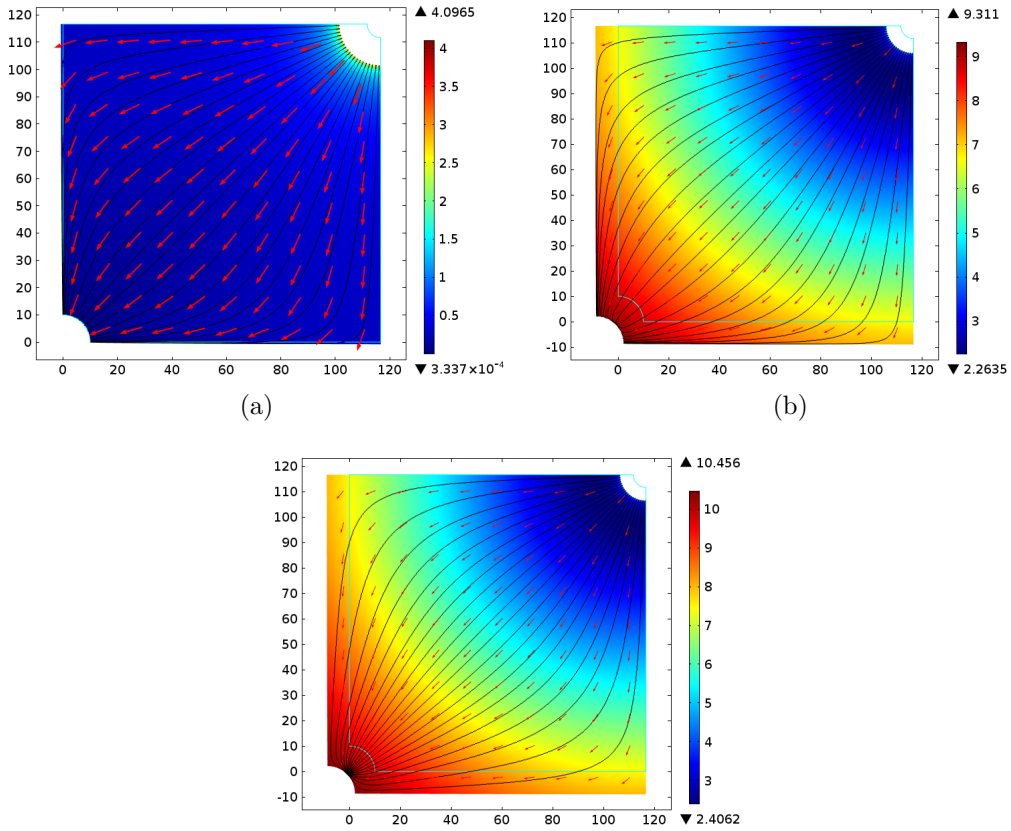

Figure 4.2: These three plots display the solid matrix deformations. The colour map shows the interstitial deformations in μm, the black lines are the streamlines and the arrows show the fluid flow direction. We have marked the undeformed configuration in each plot. (a) The initial deformation of the solid matrix when the lymphatic valve is closed. (b) The deformation of the solid matrix once the lymphatic endothelial cells side apart ($C(t) > C_{crit}$). (c) The maximum expansion of the solid matrix before it starts to contract, i.e. the maximum gap length of the open section of the lymphatic valve.

Figures 4.3a, 4.3b and 4.3c correspond to Figures 4.2a, 4.2b and 4.2c respectively, but have zoomed into the area around the lymphatic capillary. These plots show how the flow in the vicinity of the lymphatic valve changes as the valve opens. Since it is still hard to see the sliding action of the lymphatic valve, we have sketched the three key stages of the lymphatic valve opening in the sliding door fashion in Figure 4.4.

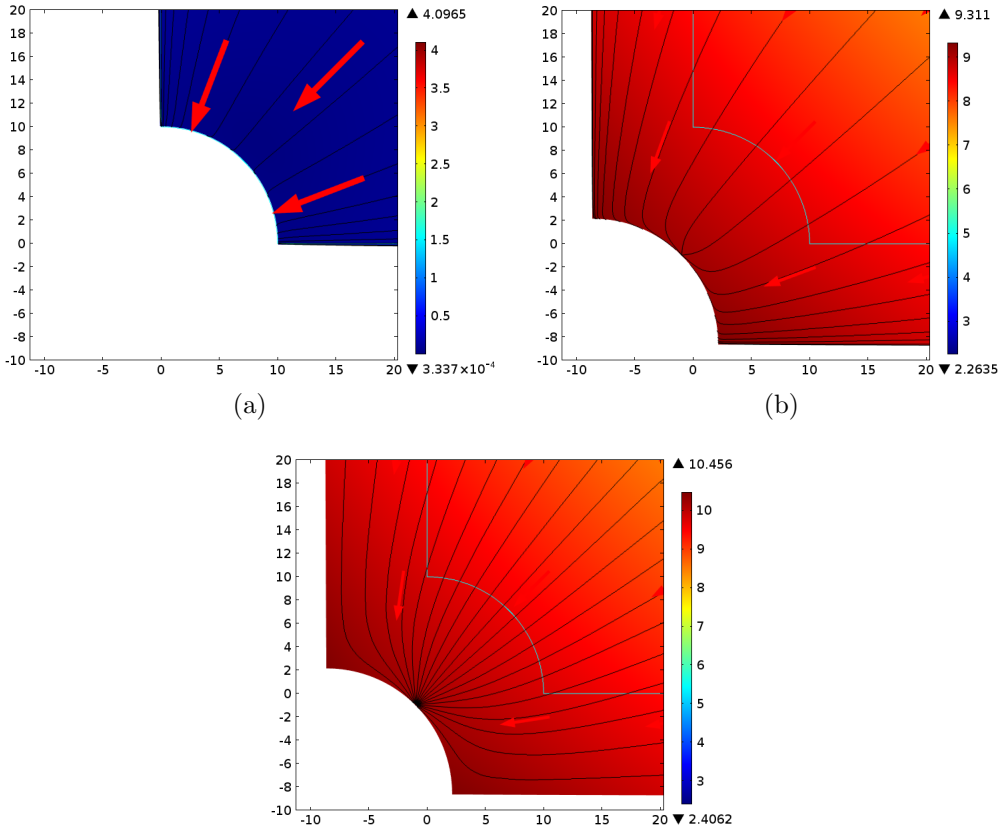

Figure 4.3: These display the solid matrix deformations of the lymphatic capillary. The colour map shows the interstitium deformations in μm, the black lines are the streamlines and the arrows show the fluid flow direction. We have marked the undeformed configuration in each plot. (a) The initial solid matrix deformation of the lymphatic capillary. (b) The solid matrix deformation of the lymphatic capillary once the endothelial cells side apart ($C(t) > C_{crit}$). (c) The maximum expansion of the lymphatic capillary before it starts to contract.

The gap length of the open section of the lymphatic valve is initially zero in Figure 4.5a (i.e. when the valve is closed). It remains closed until enough fluid enters the interstitium to cause an expansion that slides open the valve (this happens at $t = 128$s). The length of this gap increases until the outflow into the lymphatics exceeds the inflow from the blood capillary. Then the gap length decreases until the lymphatic valve closes. In this first cycle the gap length reached a maximum length of 0.045 μm. After two valve cycles the interstitium relaxes into a steady state, where the gap length is constant, 0.01 μm.

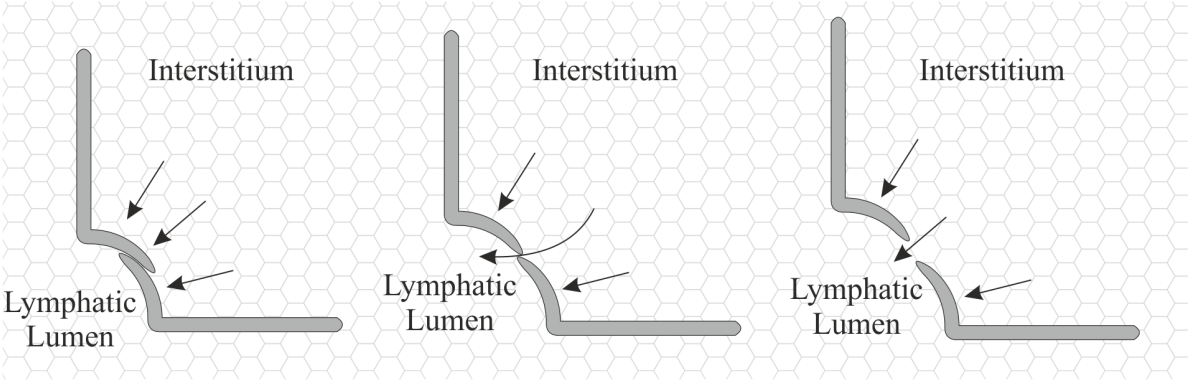

Figure 4.4: A drawing of the three stages described earlier that the lymphatic valve undergoes in draining interstitial fluid.

The Darcy flux into the lymphatic lumen was also calculated (Figure 4.5b). This is initially zero when the valve is closed and first becomes non zero when the valve opens ($t = 128$s). Integrating the velocity around the capillary gives us the Darcy flux into the lumen. It reaches a maximum of $9.74 \times 10^{-11}\text{m}^2/\text{s}$ when the gap length is at its maximum in the first valve cycle. After two valve cycles the interstitium relaxes into a steady state, where the Darcy flux is constant, $0.35 \times 10^{-11}\text{m}^2/\text{s}$. This corresponds to a net Darcy flux per unit length of lymphatic capillary of $1.41 \times 10^{-11}\text{m}^2/\text{s}$, since we hypothesize four valves around the edge of the capillary.

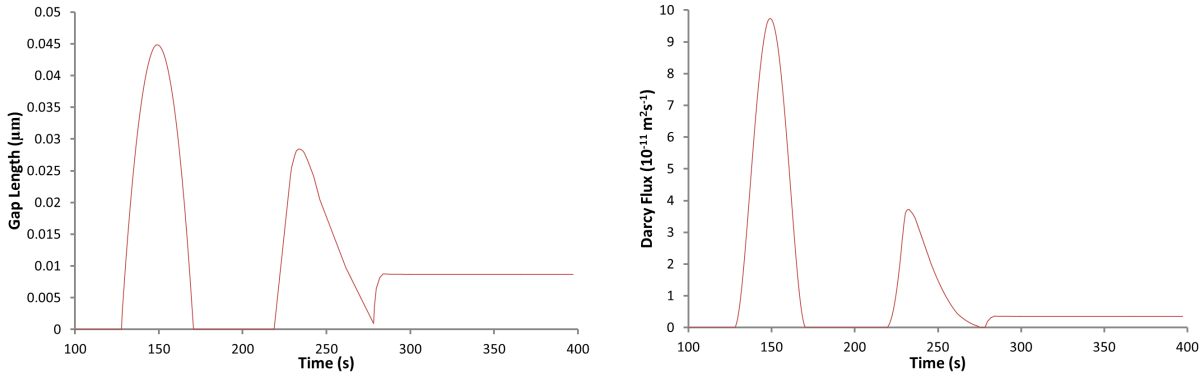

(a) (b)

Figure 4.5: (a) This plot displays how the length of the open section of the lymphatic valve changes over time. (b) This plot displays the Darcy flux into the lymphatic lumen against time.

4.3.1 Parameter Influence

Here we investigate the role of parameter variations on lymphatic drainage by independently varying: (i) Young's modulus, (ii) pressure difference, (iii) vascular permeability, and (iv) initial length of lymphatic endothelial cell overlap in a series of numerical experiments. In Table 4.1 we provide a key that can be used to interpret the results of these experiments which are presented in Figures 4.6-4.9. In all of these figures, as the parameter of interest is varied, we plot the steady state Darcy flux through the tissue (from blood capillary to lymphatic capillary) and the total steady state area of the tissue as a proportion of the undeformed area of the tissue. These quantities are both physiologically important, particularly the latter which gives a measure of tissue swelling, and thus also of oedema.

	Young's modulus E	Pressure Difference $P^b - P^l$	Vascular Permeability L_p	Endothelial cell overlap L_{ovlap}
Figure 4.6	Varying	3233 Pa	7×10^{-10} m^{2}skg^{-1}	1 μm
Figure 4.7	10^4 Pa	Varying	7×10^{-10} m^{2}skg^{-1}	1 μm
Figure 4.8	10^4 Pa	3233 Pa	Varying	1 μm
Figure 4.9	10^4 Pa	3233 Pa	7×10^{-10} m^{2}skg^{-1}	Varying

Table 4.1: A key to the parameter variations in Figures 4.6-4.9 (all other parameters as in Table 3.1).

A brief summary of the results plotted in figures 4.6-4.9 is made below in Table 4.2 which shows how the steady state Darcy flux and the gap length are affected as the model parameters are varied.

		Steady State Darcy Flux	Tissue Expansion
Young's Modulus E	30% ↑	18% ↓	0.158% ↓
	50% ↓	50% ↑	0.819% ↑
Pressure Difference $P^b - P^l$	24% ↑	39% ↑	57% ↑
	69% ↓	90% ↓	85% ↓
Vascular Permeability L_p	43% ↑	46% ↑	1.26% ↑
	96% ↓	55% ↓	1.85% ↓
Overlap Length L_{ovlap}	100% ↑	55% ↓	9.26% ↓
	75% ↓	65% ↑	4.07% ↑

Table 4.2: Quantifying how the model parameters effect the steady state Darcy flux and the gap length of the open section of the lymphatic valve.

Young's Modulus. The Young's modulus is an important measure of the physiological state of a tissue. It is known for example that tissue elasticity decreases with old age [28, 64, 114], pregnancy [63] and obesity [25, 133]. The effects of varying the Young's modulus on the fluid flux into the lymphatic lumen are shown in Figure 4.6. As might be expected increases in stiffness (corresponding to an increase in Young's modulus) lead to significant decreases in the fluid flux through the tissue and a decrease in time to reach steady state. Perhaps somewhat surprisingly increases in Young's modulus result only in very slight decreases in the steady–state tissue area/undeformed area. However this may be explained by noting that a sliding valve opens in response to tissue deformation (rather than pressure difference) and so acts to control tissue dilatation. We have been unable to find physiological evidence, in the literature, that demonstrates a clear negative correlation between edema and the Young's modulus of tissues.

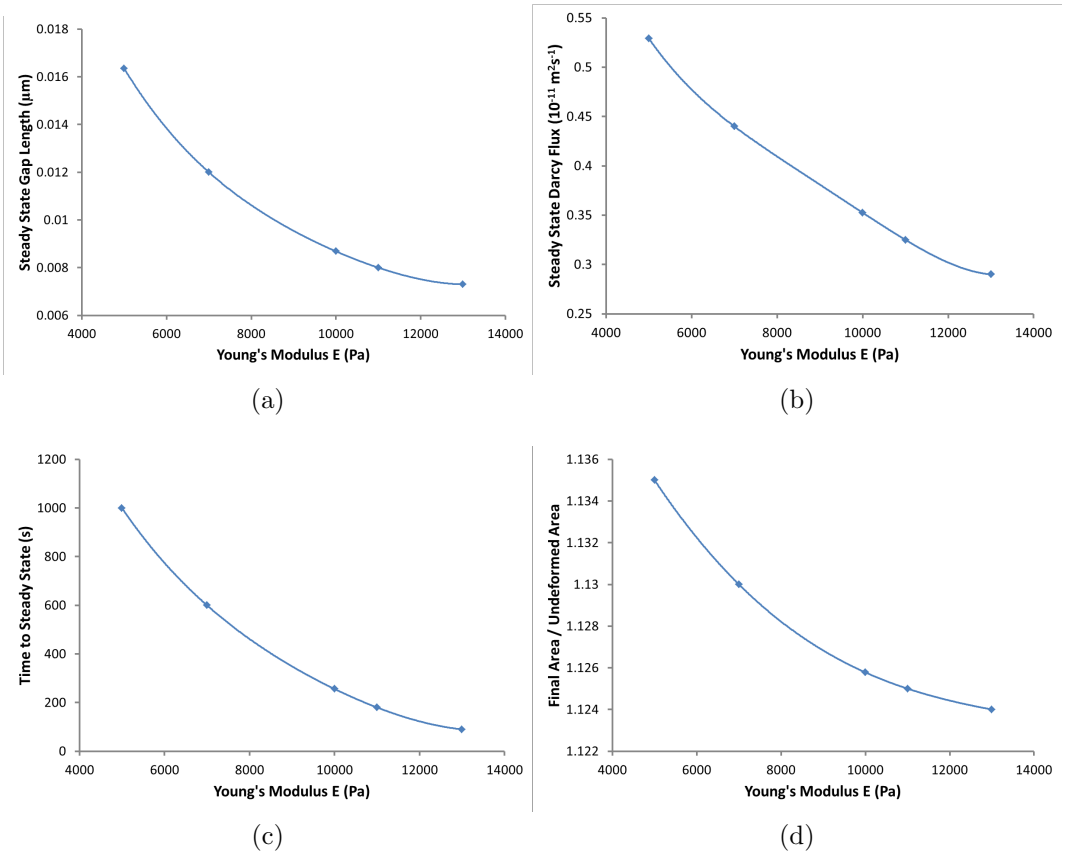

Figure 4.6: Exploring the effects of changes to the Young's modulus on the drainage behaviour. (a) The steady state gap length of the open section of the lymphatic valve. (b) The steady state Darcy flux into the lymphatic lumen. (c) The time it takes to relax to steady state. (d) Final area divided by undeformed area.

Pressure Difference. Increases in blood pressure in hypertensive patients result in increases in the pressure difference, $P^b - P^l$, between the blood capillaries and the lymphatic capillaries. Hypertension occurs more frequently in patients with diabetes compared with patients without the disease [119]. It is also more common in obese patients [97, 118], cancer patients [88] and in pregnancy [79].

The effects of varying the pressure difference, $P^b - P^l$, on the fluid flux into the lymphatic lumen are shown in Figure 4.7. As might be expected physiological increases in the pressure difference result in a significant increase in the Darcy flow through the tissue but also in a significant increase in the steady state dilatation of

the tissue (as measured by the steady–state tissue area/undeformed tissue area). Given that we previously stated that a sliding valve is good at controlling tissue deformation (even as other parameters change) the latter statement may seem slightly surprising. However it must be remembered that the lymphatic valve opens in response to the *local* dilatation about the lymphatic capillary (where the pressure is relatively low) and that an increase in pressure difference causes an increase in the deformation gradient within the tissue in which larger dilatations occur about the blood capillary (where the pressure is high) than about the lymphatic capillary. It is for this reason that even a sliding valve (that opens in response to tissue deformation) is unable to control increases in tissue dilatation brought about by increases in the pressure difference between blood capillaries and the lymphatic capillaries. We therefore conclude (from figure 4.7d and the above argument) that our postulated mechanism for valve opening would lead to hypertensive patients being particularly susceptible to oedema; this conjecture is backed up by clinical observations [43].

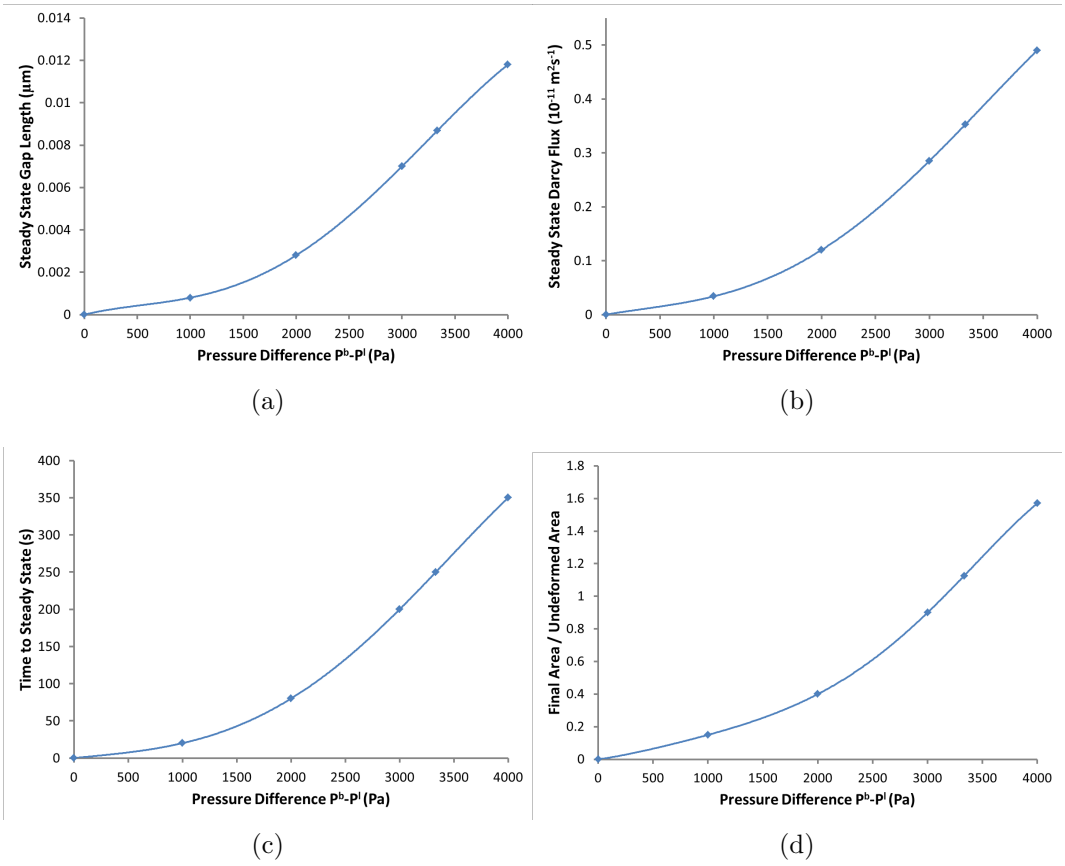

Figure 4.7: Exploring the effects of changes to the lymphatic lumen pressure on the drainage behaviour. (a) The steady state gap length of the open section of the lymphatic valve. (b) The steady state Darcy flux into the lymphatic lumen. (c) The time it takes to relax to steady state. (d) Final area divided by undeformed area.

Vascular Permeability. The effects of varying the vascular permeability on the fluid flux into the lymphatic lumen are shown in Figure 4.8. Of particular note is that physiological increases in vascular permeability result in significant increases in the flow through the tissue (figure 4.8b) but that the same increase in permeability result in only slight increases in tissue deformation (figure 4.8d). Once again, as in the case of the Young's modulus, the small change in tissue deformation with increase in permeability may be attributed to the fact that it is the tissue expansion that is responsible for opening the sliding valve. Clinical studies show that in obesity [37], pregnancy [2, 79] and in the elderly [40, 68], that

vascular permeability increases and furthermore that cases of oedema are common in patients who have a high vascular permeability [9, 121]. This is slightly at odds with the results of our model. However we note that increases in vascular permeability may also be associated with the entry of white blood cells and other large objects into the tissue that can act to block fluid drainage paths and cause swelling. Another possibility, that should perhaps be considered in future, is that real valves may actually be activated by a combination of tissue dilatation and pressure differences across the lining of the lymphatic capillaries.

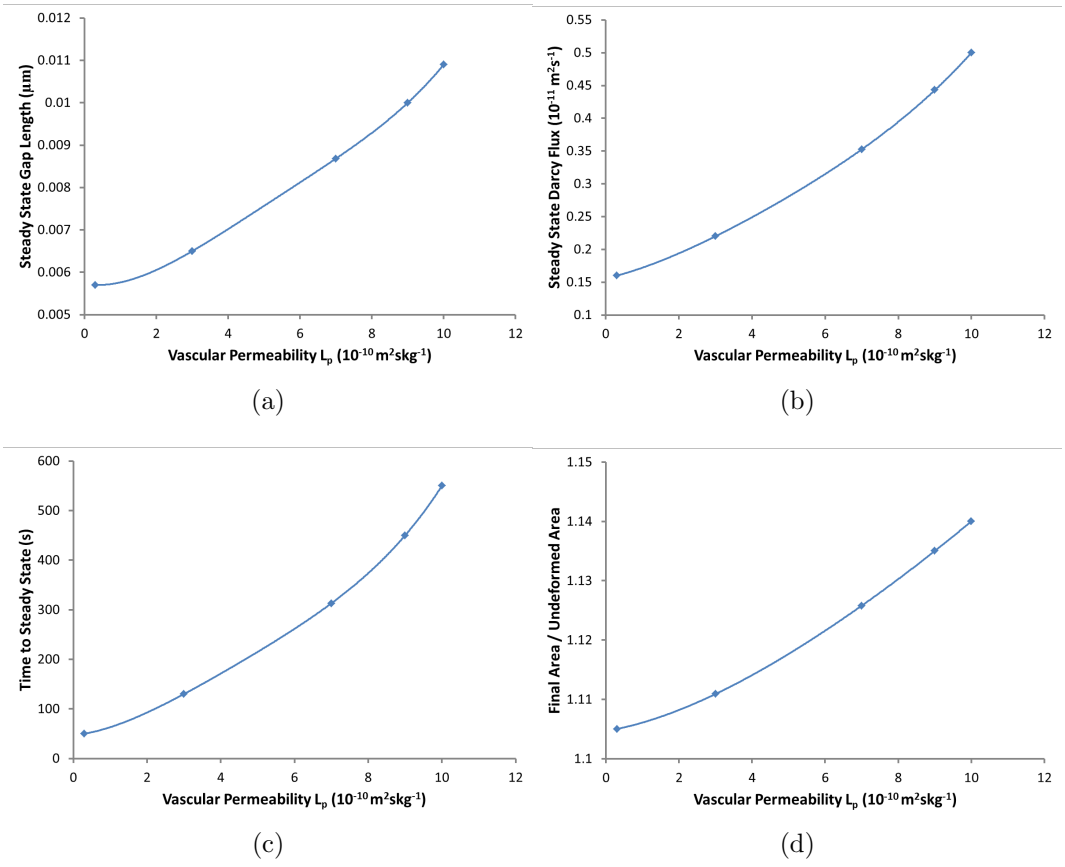

Figure 4.8: Exploring the effects of changes to the hydraulic conductivity on the drainage behaviour. (a) The steady state gap length of the open section of the lymphatic valve. (b) The steady state Darcy flux into the lymphatic lumen. (c) The time it takes to relax to steady state. (d) Final area divided by undeformed area.

Length of the Lymphatic Endothelial Cell Overlap. The effects of varying the length of the lymphatic endothelial cell overlap on the fluid flux into the lymphatic lumen are shown in Figure 4.9. The lymphatic endothelial cell overlap ($C_{crit} - C(0)$) values fluctuate for different lymphatic capillaries throughout the body, most ranging between 0.1μm to 2μm [71, 72]. As shown in figure 4.9(d), increasing this length increases the tissue dilatation; this is because it takes a greater local tissue deformation to slide open the valve. As also might be expected the fluid flux through the tissue (figure 4.9b) also decreases with increases in overlap length.

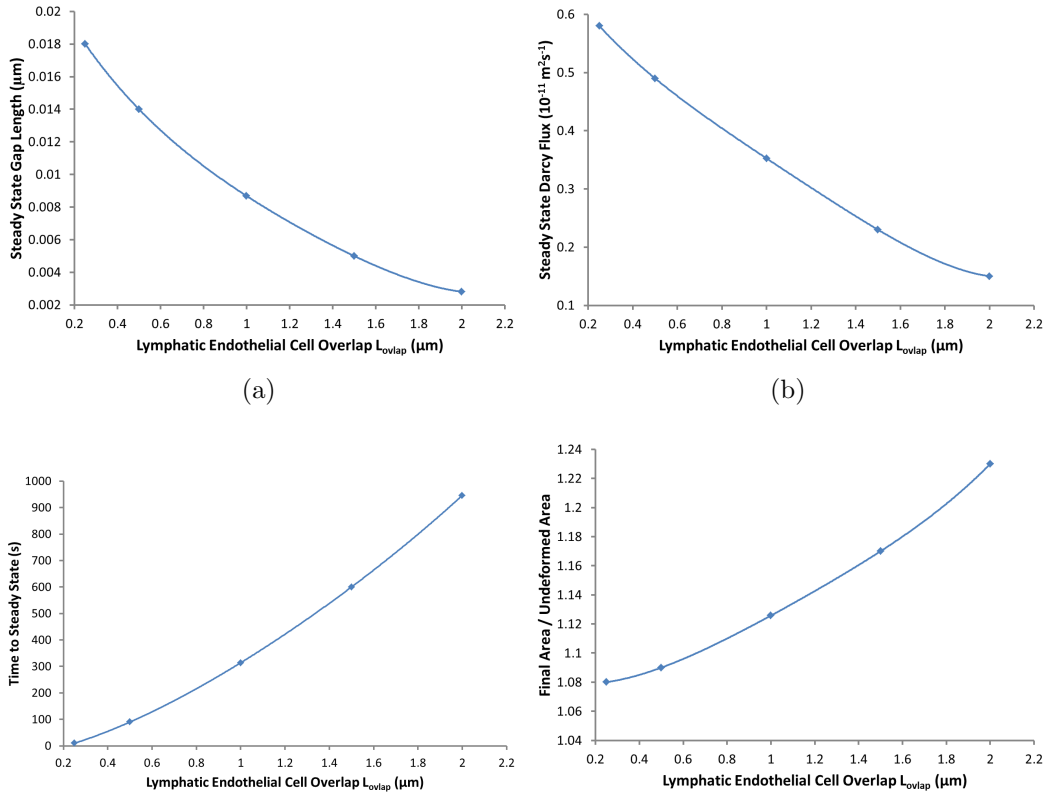

Figure 4.9: Exploring the effects of changes to the overlap length on the drainage behaviour. (a) The steady state gap length of the open section of the lymphatic valve. (b) The steady state Darcy flux into the lymphatic lumen. (c) The time it takes to relax to steady state. (d) Final area divided by undeformed area.

We have been unable to find physiological evidence, in the literature, that

lymphatic endothelial cell overlap length varies in different disease states. However it does vary in different organs, but there seems to be no physiological evidence that it changes in old age, pregnancy and obesity.

4.3.2 Fluctuation to the Lymphatic Lumen Pressure.

The lumen pressure in the primary lymphatic system fluctuates as a consequence of pressure variations in the secondary lymphatic system [34, 130, 137]. In order to model this fluctuation in lymphatic lumen pressure we apply a periodic lymphatic pressure P^l and investigate its effects on primary lymphatic drainage. In particular we take the lymphatic lumen pressure equals 100 Pa for $t < 300$s and $100(1 + \sin(2\pi t/n))$ Pa for $t > 300$s (where the period $n = 2$s) and, as in the previous dynamic simulation, we start the tissue from its undeformed state at $t = 0$. This profile for the lumen pressure has been chosen so that it begins to fluctuate only after the system has relaxed to a steady state. This choice was made because we believe that the magnitude of pressure fluctuations are sufficiently small that they cause only minor perturbations to the steady state. This belief is borne out by the results to the numerical solution plotted in figure 4.10.

Figure 4.10 displays the effects of periodic fluctuations to the lymphatic lumen pressure on the Darcy flux. Figure 4.10a shows the Darcy Flux against time. This graph is identical to Figure 4.5b with the exception that after the system has relaxed to a steady state physiologically small perturbations to the lymphatic lumen pressure are applied. As can be seen this results in only very small perturbations to the Darcy Flux about its steady state value. Figures 4.10b and 4.10d, show blow ups of the Darcy flux as it oscillates about the steady state and of the driving lymphatic lumen pressure.

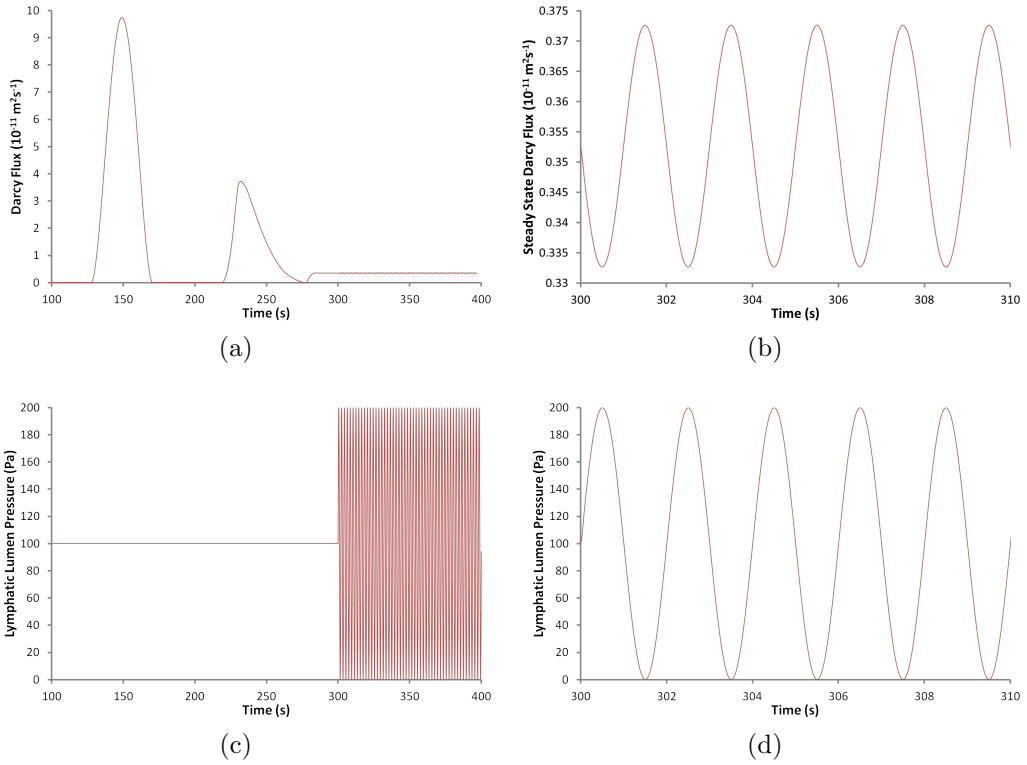

Figure 4.10: Exploring the effects of changes to the lymphatic lumen pressure on the drainage behaviour. (a) The Darcy Flux against time. (b) The steady state Darcy flux into the lymphatic lumen against time. (c,d) The lymphatic lumen pressure against time.

In the following section we discuss our results and compare them with other lymphatic drainage models.

4.4 Discussion

20% of the body's mass is thought to be interstitial fluid [76]. Thus understanding the mechanics of the lymphatic system and its role in interstitial drainage is of significant physiological importance. This work outlined a hypothesis for lymphatic drainage of interstitial fluid that flows into the interstitium from blood capillaries. This hypothesis is based on the conjecture of Rossi [106] that endothelial gap junctions on the lymphatic capillary walls are pulled open when the surround-

ing tissue swells in response to fluid influx. In order to model this we needed to account for interstitial flow and the swelling and deformation of the interstitial matrix as fluid enters it. We modelled the lymphatic valve cycle and concluded that the interstitial deformations relax to a steady state, with a net Darcy flux per unit length of lymphatic capillary of $1.41 \times 10^{-11}\text{m}^2/\text{s}$ and the gap length of the lymphatic valve is 0.01 μm based on our physiological parameter estimates.

Validating our estimated volumetric flow rate through the initial lymphatics against experimental data is not straight forward because of the magnitude of variations in the geometrical and physical parameters of different lymphatic capillaries and in the surrounding environment. Nonetheless, we attempt to compare our results to the experimental literature on initial lymphatic uptake [100, 124, 126] (on mice) and [56] (on rabbits). Ikomi et al [56], measured volumetric flow rates of the order of 1.1 mL/h in the initial lymphatics of a rabbits hindleg. Using a conversion factor of 0.9 calculated in [85], which estimates the length of a single initial lymphatic channel and the total length of endothelial cell junctions in the initial lymphatics of a rabbits hind leg gives a fluid flux of 2.78×10^{-10} m^2/s per initial lymphatic channel. Swartz et al [126] measured volumetric flow rates in the collecting lymphatics of a mouse tail skin vs the infusion pressure of the order of 10^{-8} cm^2/s per mmHg to 10^{-9} cm^2/s per mmHg. Applying an infusion pressure of 30 mmHg (similar to the infusion pressure in our model) gives a fluid flux of 3×10^{-11} m^2/s to 3×10^{-12} m^2/s per initial lymphatic channel. However, more recently they measured a value of the volumetric flow rate through the initial lymphatics, of the order 0.01 mL/min [124]. They assumed 14 initial lymphatic vessels in the tail (plus the assumption of 4 valves per vessel); giving a fluid flux through the initial lymphatics of the order of 4.8×10^{-11} m^2/s per initial lymphatic channel. Reddy et al [100] measured the volumetric flow rates in the initial lymphatics of the order of 1×10^{-8} mL/s through a length of 0.25 mm. Thus con-

verting to fluid flux through the initial lymphatics per μm junction length gives the value of 4×10^{-11} m^2/s for the fluid flux. Thus we conclude that our model provides flow rates that are comparable in magnitude to those in the experiential literature. Our model also utilizes more aspects of the entire lymphatic drainage (e.g. the regular deformations of the surrounding matrix to lymphatic capillaries) than previous models of the primary lymphatic valve system [42, 85, 99].

It is commonly supposed that variations in lymphatic pressure play a significant role in interstitial drainage [34, 130, 137]. The size of such variations is typically around 100 Pa which compares to a mean pressure difference between blood and lymphatic capillaries of around 3000 Pa. Earlier we noted that the steady state solution to the model depends only on lymphatic pressure P^l and blood capillary pressure P^b through their difference $P^b - P^l$. It is thus apparent that fluctuations in the lymphatic lumen pressure provide only a small perturbation to the steady–state solution, and that the physiological state of the tissue is predominantly determined by the mean pressure difference $P^b - P^l$ (as opposed to the relatively small fluctuations in the lymphatic pressure); this is borne out by the time–dependent calculations performed in figure 4.10. This led us to investigate the effects of parameter variations on the steady–state in section 4.3.1. With reference to oedema we found that (I) physiological increases in Young' modulus of the tissue (see figure 4.6) lead to small decreases in tissue swelling but significant decreases in the flow rate through the tissue; (II) physiological increases in the blood–lymphatic pressure difference (see figure 4.7) lead to significant increases in both tissue swelling and flow; (III) physiological increases in the blood capillary permeability (see figure 4.8) lead to relatively small increases in tissue swelling but significant increases in the flow rate through the tissue; and (IV) physiological increases in endothelial cell overlap (see figure 4.9) lead to significant increases in tissue swelling and significant decreases in the flow rate through the tissue. It is

interesting to speculate on the possible advantages of a sliding valve over those of a conventional valve operated by pressure differences between the lymphatic lumen and the surrounding tissue (as described in [49]). It seems to us that the major advantage of the sliding valve system over the pressure operated valve is that it responds directly to tissue swelling. It is therefore better at controlling oedema (than the pressure operated valve) even if the properties of the tissue change over time as, for example, in pregnancy, or with age. This is reflected in the fact that the extra swelling due to decreases in the tissues Youngs' modulus or increases in the blood vessels permeability are both relatively small. However the increase in swelling due to increases in the pressure difference between the blood and lymphatic capillary is much more significant. This is perhaps not that surprising as the valve only responds to local swelling around the lymphatic vessel (where the pressure is relatively low). However increases in the pressure difference cause an increases in the difference between swelling around the blood capillary (where the pressure is relatively high) and that around the lymphatic capillary. The increase in the total tissue swelling observed in our numerics, as the pressure difference between blood and lymphatic capillaries increases, can thus largely be attributed to the increase in swelling around the blood capillary. The model also predicts that the degree of swelling is fairly sensitive to endothelial cell overlap and this suggests that the valve can be modified to give an appropriate level of tissue fluid content.

Chapter 5

Overall Conclusions

In this chapter we briefly discuss and compare the two different approaches that we have taken to modelling primary lymphatic drainage, and indicate the main results.

Conclusions

We began this thesis with a discussion of the lymphatic system. Followed by an explanation of the aims and motivation of this thesis. In particular we sought to model the functioning of primary lymphatic valves in two different ways. By examining the consequences of different hypotheses we hoped to better understand the mechanism of the primary valve system. In order to achieve this, we developed our understanding of the physiological detail surrounding lymphatic capillaries and examined images of electron micrographs of lymphatic capillaries.

In this study, we have presented and applied methods for the design and analysis of lymphatic drainage. Each of the three technical chapters of this thesis was concerned with the modelling of lymphatic drainage. We provided the reader with two approaches to modelling primary lymphatic drainage, in the first approach (Chapter 2) we investigated the opening of primary lymphatic valves in response

to pressure differences between the interstitium and the lymphatic lumen, and in the second approach (Chapters 3 and 4) we investigated interstitial deformations as the main mechanism in the opening (and closing) of primary lymphatic valves.

In Chapter 2, we modelled the fluid flow through tissues where lymphatic drainage occurred. The model incorporated the mechanics of the primary lymphatic valves as well as the fluid flow through the interstitium and that through the walls of blood capillaries. We gave special attention to the mechanics of primary lymphatic valves. In this approach to modelling primary lymphatic drainage, we considered overlapping lymphatic endothelial cells (primary lymphatic valve) deflecting into the lymphatic lumen in response to pressure differences on either side of the valve to drain interstitial fluid. This created a narrow passage for the interstitial fluid to enter the capillary network.

Darcy's Law and nonlinear beam theory are used to model the fluid flux through the tissue and the mechanics of the lymphatic valve, respectively. The linearity of Darcy's Law, for the fluid flow through the interstitium, implied that the total fluid flux from the blood capillary to the lymphatic capillary was linearly related to the pressure difference between the walls of these two vessels multiplied by a dimensionless geometric factor. Conformal transformation techniques were used to find an approximate solution to this dimensionless geometric factor. After solving the geometrically nonlinear beam equation that modelled the deflection of the lymphatic valve, we combined the results with the interstitial fluid flow, which produced a fully working model, published in Bulletin of Mathematical Biology [49], that calculated the fluid flux into the lymphatic lumen.

The second part of this thesis, Chapters 3 and 4, began by explaining the reasons behind the new method of modelling the mechanism of primary lymphatic valves, and then went on to solve the model. Predominantly, mathematical models of the primary lymphatic valve system have been based entirely on the theory

that it is pressure differences between the lymphatic lumen and the interstitium that cause the valve to open and lymphatic drainage to occur. The motivation for this new way of modelling the primary valve system came from the experimental literature. The aim of these chapters was to create a model for lymphatic drainage that incorporated regular tissue deformations. Interstitial deformations occur when blood capillaries leak fluid into the interstitium. This causes the interstitial space around lymphatic capillaries to expand and pull open (via anchoring filaments attached on the capillary wall) the primary lymphatic valves. The model predicts a smooth transition between a closed and an open lymphatic valve, and after a couple of valve cycles, relaxes to a steady state, where there is a constant flow into the capillary.

In both models we produced graphs that illustrate how the pressure difference (blood capillary lumen pressure minus lymphatic capillary lumen pressure) effect the fluid flux into the lymphatics system. Due to the significant differences in both models their pressure–flux graphs had evident discrepancies. The pressure–flux graph in Hypothesis 1, shown in Figure 5.1a, has a piecewise linear relation between the pressure difference and the fluid flux. The fluid flux remains zero until the pressure difference increases enough to overcome the elastic forces of the primary lymphatic valve (P_{crit}), then the flux increases linearly. The pressure–flux graph in Hypothesis 2, shown in Figure 5.1b, has a non–linear relation between the pressure difference and the fluid flux. As the pressure difference increases the surrounding interstitial space expands making the gap length of the open section of the lymphatic valve increase, which results in a larger fluid flux. The fluid flux into the lymphatic system per primary lymphatic valve was calculated in Hypothesis 1 to be 1×10^{-14} m^2/s and in Hypothesis 2 to be 3.5×10^{-12} m^2/s. Due to the varied data set for the fluid flux values in the literature, our fluid flux values from both hypotheses are comparable to the literature. However, the flux

value for Hypothesis 2 is a better fit to the experimental data.

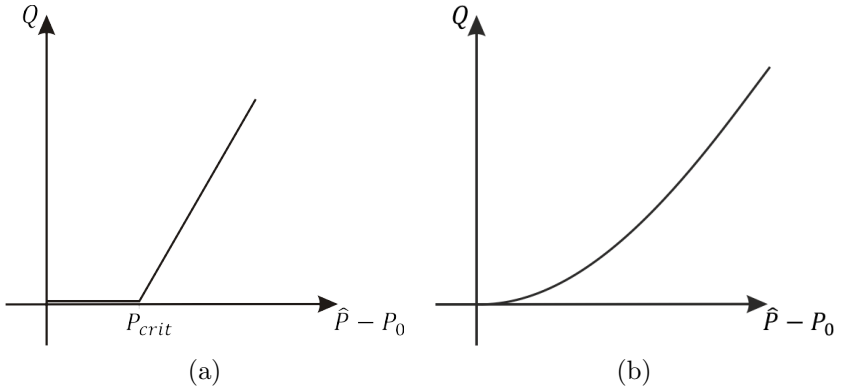

Figure 5.1: The fluid flux per unit length through the interstitial space and the initial lymphatics as a function of the pressure difference between the blood and lymphatic lumen $\widehat{P} - P_0$ for Hypothesis 1 is displayed in (a) and for Hypothesis 2 is displayed in (b).

The importance of the models presented in this thesis is that they give insight into how the primary lymphatic system functions. The first method explored the lymphatic valve opening in response to pressure differences between the interstitium and the lymphatic lumen. The second method was entirely novel, and explored solving the governing equations of fluid flow and poroelasticity to model the opening of lymphatic valves, where they open in response to interstitial deformations; to the author's knowledge, this has not been explored before.

On consideration of the results of both models we believe that Hypothesis 2 (lymphatic valve opening in response to interstitial deformations) is better able to represent the experimental data than Hypothesis 1. In particular, its results correlated better with the fluid flux values in the experimental literature than those of Hypothesis 1. Also, the experimental data (electron micrographs) illustrate lymphatic capillaries changing shapes (shear forces), from circular to oval, in a 2-D cross sectional view. This is due to the quantity of fluid drainage and the surrounding interstitial deformations. Since Hypothesis 2 includes this, we conclude that it is the better model of primary lymphatic drainage and hope future models take this into consideration.

In conclusion we have shown that by stripping biological processes back to simpler forms we can derive mathematical models that accurately replicate the in vivo and in vitro experiments. As a result of this work, new methods now exist for modelling primary lymphatic valves.

Finally we observe that there is scope for future work if we use asymptotic methods for the model in Hypothesis 2. In the future it is hoped that asymptotic methods (based on the disparity in the scales between the radii of both capillary networks and capillary separation) can be used to derive simple ODE models for the drainage process. The simplicity of these models should help us to more easily explore their results. Also it will enable us to see how drainage properties change as parameters are varied more easily. For example, it could allow us to investigate perturbations about the steady state as the lymphatic lumen pressure is varied.

Appendix A

Proof of the Schwarz–Christoffel's Formula

This proof is quoted from Driscoll's and Trefethen's book [33].

The Schwarz–Christoffel formula is

$$f(z) = A + C \int^{z} \prod_{k=1}^{n-1} (\zeta - z_k)^{\alpha_k - 1} d\zeta. \tag{A.0.1}$$

For simplicity, we can treat just the case where all prevertices are finite and the product ranges over indices 1 to n. By the Schwarz reflection principle, the mapping function f can be analytically continued into the lower half plane; the image continues into the reflection of the polygon about one of the sides. By reflecting again about a side of the new polygon, we can return analytically to the upper half plane; the same can be done for a even number of reflections of P. Let A and C be any complex constants, then,

$$\frac{(A + Cf(z))''}{(A + Cf(z))'} = \frac{f''(z)}{f'(z)}. \tag{A.0.2}$$

Therefore, the function f''/f' can be defined by continuation as a single–valued

analytic function everywhere in the closure of the upper half plane, except at the prevertices of the polygon (where derivatives may fail to exist). Similarly, considering odd numbers of reflections, we see that f''/f' is single–valued and analytic in the lower half plane as well.

At a prevertex z_k, we can rewrite equation (A.0.1) as $f'(z) = (z - z_k)^{\alpha_k - 1}\psi(z)$ for a function $\psi(z)$ analytic in a neighborhood of z_k. Therefore, f''/f' has a simple pole at z_k with residue $\alpha_k - 1$, and

$$\frac{f''}{f'} - \sum_{k=1}^{n} \frac{\alpha_k - 1}{z - z_k} \tag{A.0.3}$$

is an entire function. Because all the prevertices are finite, f is analytic at $z = \infty$, and a Laurent expansion implies that $f''/f' \to 0$ as $z \to \infty$. By Liouville's theorem, it follows that the expression in equation (A.0.3) is identically zero. Expressing f''/f' as $(ln(f'))'$ and integrating twice results in the formula (A.0.1).

Appendix B

Derivation of the Non–Linear Beam Equation

We describe the valve deformation using arc length s along the beam and the angle $\theta(s)$ between the beam and the x–axis, as shown in Figure B.1a, and assume the beam to be inextensible, so that the arc–length is conserved by the deformation [54]. The transverse displacement is given parametrically by $x = x(s)$, $y = y(s)$, where

$$\frac{\mathrm{d}x}{\mathrm{d}s} = \cos\theta, \qquad \frac{\mathrm{d}y}{\mathrm{d}s} = \sin\theta. \tag{B.0.1}$$

To obtain the nonlinear loaded beam equation we first consider a small element of the lymphatic valve of length ds, and derive the equations that govern the balance of forces and moments on this element. The element is held under tension T at each end. A force Fds is applied in the direction normal to the valve, with a tangential component, Gds. M is the bending moment at each end of the valve and N is the normal force at the ends of the valve [54]. The forces acting on the lymphatic valve are summarized in Figure B.1b.

By carrying out a force balance in the standard fashion, we obtain an expression for the resultant forces acting in the x and y directions. Since damping forces

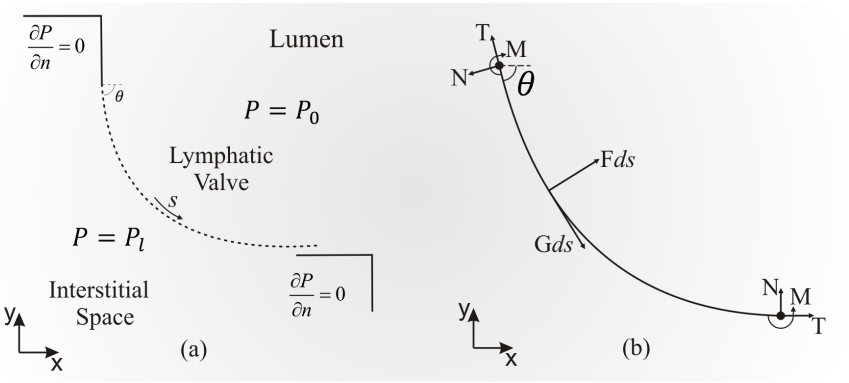

Figure B.1: (a) A geometrical view of the lymphatic valve. (b) The forces acting on a small section of the lymphatic valve.

are large we assume a quasistatic configuration in which the resultant forces are both zero, so that

$$\frac{d}{ds}(T\cos(\theta) - N\sin(\theta)) = F\sin(\theta) - G\cos(\theta), \tag{B.0.2}$$

$$\frac{d}{ds}(T\sin(\theta) + N\cos(\theta)) = -F\cos(\theta) - G\sin(\theta). \tag{B.0.3}$$

Using the product rule to expand the above equations, multiplying equation (B.0.2) by $\cos(\theta)$ and adding it to equation (B.0.3) multiplied by $\sin(\theta)$, leads to

$$\frac{dT}{ds} - N\frac{d\theta}{ds} = -G. \tag{B.0.4}$$

Similarly, taking the product of equation (B.0.2) with $\sin(\theta)$ and adding this to the product of equation (B.0.3) and $\cos(\theta)$, gives

$$\frac{dN}{ds} + T\frac{d\theta}{ds} = -F. \tag{B.0.5}$$

In order to derive a moment balance equation, we assume that the infinitesimal section of the lymphatic valve, see Figure B.1b, is approximately straight and of length ds. Balancing moments about the left hand point of the valve in Figure

B.1b, gives

$$N = -\frac{dM}{ds}. \tag{B.0.6}$$

As a constitutive relation we expect the bending moment (M) to be proportional to the valve curvature, which is given by $d\theta/ds$. Since we consider small strains in the geometrically nonlinear beam, we assume that the constant of proportionality is the same as in a linear case, that is

$$M = D\frac{d\theta}{ds}, \tag{B.0.7}$$

where D (kgμm$^2 s^{-2}$) is the flexural rigidity of the valve. We use plate theory to describe the flexural rigidity of the lymphatic valve in terms of the Young's modulus (E), the Poisson's ratio (ν) and the beam thickness (ι) by $D = E\iota^3/12(1-\nu^2)$.

We seek an equation that only depends on the angle θ and the arc length s. To achieve this we eliminate N, T and M from the force balance equations (B.0.4)-(B.0.7) and equate F, the normal force acting on the lymphatic valve, with the pressure drop across the initial lymphatics, $P_l - P_0$. Assuming the no slip boundary condition on the exterior of the lymphatic valve (no shear force) results in the tangential force G applied on the valve to be zero. It follows that

$$\frac{\mathrm{d}^3\theta}{\mathrm{d}s^3} + \frac{1}{2}\left(\frac{\mathrm{d}\theta}{\mathrm{d}s}\right)^3 = \frac{P_l - P_0}{D}. \tag{B.0.8}$$

Equation (B.0.8) is the Euler–Bernoulli beam equation for large deformations in terms of angle and arc–length.

Glossary

- **Afferent lymph vessels** The lymphatic vessels that enter at all parts of the periphery of lymphatic nodes.
- **Basal lamina** The surface on which epithelial cells are attached to.
- **Cisterna chyli** A dilated sac at the lower end of the thoracic duct into which lymph from trunks flow.
- **Cytokines** Small proteins that are important in cell signaling.
- **Schwarz reflection principle** A way to extend the domain of definition of an analytic function of a complex variable F, which is defined on the upper half–plane and has well–defined and real number boundary values on the real axis. In that case, writing * for complex conjugate, the extension of F to the rest of the complex plane is $F(z^*)^*$ or $F(z^*) = F^*(z)$.
- **Desmosome** A cell structure specialized for cell–to–cell adhesion.
- **Efferent lymph vessels** The lymphatic vessels that exit at all parts of the periphery of lymphatic nodes.
- **Elephantiasis** A disease that is characterized by the thickening of the skin and underlying tissues.
- **Erysipelas** A bacterial infection in the outer most layer of the skin (epidermis).

- **Extravasation** Is the leakage of a fluid out of its container.
- **Iliac vein** A vein that drains blood from the pelvis and lower limbs.
- **Jugular** Veins that bring deoxygenated blood from the head back to the heart.
- **Lacteals** Lymphatic capillaries that absorbs dietary fats in the small intestine.
- **Lobe** A clear anatomical division or extension that can be determined without the use of a microscope.
- **Lumen** The inside space of a tubular structure.
- **Lymphocytes** A type of white blood cell.
- **Mediastinum** It is the central compartment of the thoracic cavity, surrounded by loose connective tissue.
- **Mediated immune responses** A immune response that involves the activation of phagocytes, antigen–specific cytotoxic T–lymphocytes, and the release of various cytokines in response to an antigen.
- **Mesentery** The double layer of a smooth membrane that forms the lining of the abdominal cavity, which suspends the middle section of the small intestine and the final section from the posterior wall of the abdomen.
- **Metastasis** The process by which cancer spreads from the place at which it first arose as a primary tumour to distant locations in the body.
- **Nodules** A relatively hard, roughly spherical abnormal structure.
- **Osmotic pressure** The pressure that must be applied to a solution to prevent the inward flow of water across a semipermeable membrane.

- **Peristalsis** The propulsion of lymph due to alternate contraction and relaxation of smooth muscles.
- **Phagocyte** Are cells that protect the body by ingesting harmful foreign particles, bacteria, and dead or dying cells.
- **Plexus** A part of the nervous system.
- **Retroperitoneal** The anatomical space in the abdominal cavity behind the membrane that forms the lining of the abdominal cavity.
- **Scalenus anterior muscle** A muscle that lies at the side of the neck.
- **Situ** A polymerization mixture.
- **Sternum** A long flat bone shaped like a capital "T" located in the center of the thorax.
- **Subclavian** Two large veins, one on either side of the body.
- **Vena cava** A large vein that carries de–oxygenated blood from the body into the right atrium of the heart.
- **Venule** A small blood vessel in the microcirculation that allows deoxygenated blood to return from the capillaries to the larger blood vessels called veins.
- **Viscera** The organs contained within the abdominal cavity.

Bibliography

[1] D.I. Abramson and P.B. Dobrin. *Blood Vessels and Lymphatics in Organ Systems*. Academic Press, INC. Harcourt Brace Jovanovich, 1^{st} edition, 1984.

[2] N. Anim-Nyame, J. Gamble, S. Sooranna, M. Johnson, and P. Steer. Microvascular permeability is related to circulating levels of tumor necrosis factor - α in pre-eclampsia. *Cardiovascular Res*, 58:162–169, Dec 2003.

[3] K. Aukland and G. Nicolaysen. Interstitial fluid volume: Local regulatory mechanism. *Physiol Rev*, 61:556–643, July 1981.

[4] P. Baluk, F. Jonas, H. Hashizume, T. Romano, E. Lashnits, S. Butz, D. Vestweber, M. Corad, C. Molendini, E. Dejana, and D.M. McDonald. Functionally specialized junctions between endothelial cells of lymphatic vessels. *Journal of Experimental Medicine*, 204:2349–2362, Oct 2007.

[5] S.I. Barry and G.K. Aldis. Flow induced deformation from pressureized cavities in absorbing porous tissues. *Bulletin of Mathematical Biology*, 54:977–997, July 1992.

[6] S.I. Barry and G.K. Aldis. Radial flow through deformable porous shells. *J Austral Math Soc Ser B*, 34:333–354, Sep 1993.

[7] P.J. Basser. Interstitial pressure, volume, and flow during infusion into brain tissue. *Microvascular Research*, 44:143–165, Jan 1992.

[8] G. Bastian. *The Lymphatic and Immume Systems*. HarperCollins College Publishers, 1^{st} edition, 1993.

[9] D. Bates. Vascular endothelial growth factors and vascular permeability. *Cardiovasc Res*, 87:202–271, April 2010.

[10] L. Baxter and R. Jain. Transport of fluid and macromolecules in tumors. ii. role of heterogeneous perfusion and lymphatics. *Microvascular Research*, 40:246–263, September 1990.

[11] M.A. Biot. General solutions of the equations of elasticity and consolidation for a porous material. *Journal of Applied Mechanics*, 78:91–96, March 1956.

[12] R. Bowen. Incompressible porous media models by use of the theory of mixtures. *International Journal of Engineering Science*, 18:1129–1148, 1980.

[13] A.C. Burton. On the physical equilibrium of small blood vessels. *American Physiological Society*, 164:319–329, Jan 1951.

[14] S.L. Butler, S.S. Kohles, R.J. Thielke, C. Chen, and R. Vanderby Jr. Interstitial fluid flow in tendons or ligaments: a porous medium finite element simulation. *Journal of Vascular Research*, 35:742–746, Nov 1987.

[15] J. Casley-Smith. The functioning and interrelationships of blood capillaries and lymphatics. *Cellular and Molecular Life Sciences*, 32:1–12, 1976.

[16] J.R. Casley-Smith. The role of the endothelial intercellular junctions in the functioning of the initial lymphatics. *Journal of Vascular Research*, 9:106–131, Sep 1972.

[17] A. Castenholz. Morphological characteristics of initial lymphatics in the tounge as shown by scanning electron microscopy. *Scan Electron Microsc*, pages 1343–1352, 1984.

[18] A. Castenholz. The endothelium of initial lymphatics during postnatal development of the rat tongue. *Scan Electron Microsc*, pages 1201–1208, 1985.

[19] A. Castenholz. Corrosion cast technique in lymphatic pathways. *Scan Electron Microsc*, pages 599–605, 1986.

[20] A. Castenholz. Structural and functional properties of initial lymphatics in rat tounge: Scanning electron microscopic findings. *Lymphology*, 20:112–125, Sep 1987.

[21] A. Castenholz. Interpretation of structural patterns appearing on corrosion casts of small blood and initial lymophatic vessels. *Scanning Microscopy*, 3:315–325, March 1989.

[22] A. Castenholz. Functional microanatomy of initial lymphatics with special consideration of the extracellular matrix. *Lymphology*, 31:101–118, 1998.

[23] H. Chen, H. Granger, and A. Taylor. Interaction of capillary, interstitial, and lymphatic forces in the canine hindpaw. *Circ Res*, 39:245–254, Aug 1976.

[24] L. Cueni and M. Detmar. The lymphatic system in health and disease. *Lymphat Res Biol*, 6:109–122, 2008.

[25] P. Danias, N. Tritos, M. Stuber, R. Botnar, K. Kissinger, and W. Manning. Comparison of aortic elasticity determinded by cardiovascular magnetic resonance imaging in obese versus lean adults. *The American Journal of Cardiology*, 91:195–199, Jan 2003.

[26] M. Davis, A. Davis, C. Ku, and A. Gashev. Myogenic constriction and dilation of isolated lymphatic vessels. *Am J Physiol Heart Circ Physiol*, 296:293–302, Feb 2009.

[27] M. Davis, M. Lane, A. Davis, D. Durtschi, D. Zawieja, M. Muthuchamy, and A. Gasher. Modulation of lymphatic muscle contractility by the neuropeptide substance p. *Am J Physiol Heart Circ Physiol*, 295:587–597, June 2008.

[28] M. Ding, M. Dalstra, C. Danielsen, J. Tabel, I. Hvid, and F. Linde. Age variations in the properties of human tibial trabecular bone. *J. Bone Joint Surg*, 79:995–1002, May 1997.

[29] J. Dixelius, T. Makinen, M. Wirzenius, M. Karkkainen, C. Wernstedt, K. Alitalo, and L. Claesson-Welsh. Ligand-induced vascular endothelial growth factor recepter-3 (vegfr-3) heterodimerization with vegfr-2 in primary lymphatic endothelial cells regulates tyrosine phosphorylation sites. *Journal of Biological Chemistry*, 278:40975–40979, July 2003.

[30] J. Dixon. Lymphatic lipid transport: Sewer or subway. *Trends Endocrinol Metab*, 21:480–487, Aug 2010.

[31] J.B. Dixon, S.T. Greiner, A.A. Goshev, G.L. Cote, J.E. Moore Jr, and D.C. Zawieja. Lymph flow, shear stress, and lymphocyte velocity in rat mesenteric prenodal lymphatics. *Microcirculation*, 13:597–610, June 2006.

[32] K. Dowlatshahi, F. Ming, H. Snider, and F. Habib. Lymph node micrometastases from breast carcinoma: Reviewing the dilemma. *Cancer*, 80:1188–1197, Nov 2000.

[33] T.A. Driscoll and L.N. Trefethen. *Schwarz-Christoffel Mapping*. Cambridge University Press, 1^{st} edition, 2002.

[34] J. Eisenhoffer and M. Johnston. Importance of valves and lymphangion contractions in determining pressure gradients in isolated lymphatics exposed to elevations in outflow pressure. *Microvasc Res*, 49:97–110, 1995.

[35] M.Y.Z. Fanous, A.J. Phillips, and J.A. Windsor. Mesenteric lymph: The bridge to future management of critical illness. *Journal of the Pancreas*, 8:374–399, July 2007.

[36] R. Florence and M. Sabin. On the development of the superficial lymphatics in the skin of the pig. *American Journal of Anatomy*, 3:183–195, June 1904.

[37] A. Flyvbjerg, F. Dagnaes-Hansen, A. De Vriese, B. Schrijvers, R. Tilton, and R. Rasch. Amelioration of long term renal changes in obese type 2 diabetic mice by a neutralizing vascular endothelial growth factor antibody. *Diabetes*, 51:3090–3094, Oct 2002.

[38] M. Francois, A. Caprini, B. Hosking, F. Orsenigo, D. Wilhelm, C. Browne, K. Paavonen, T. Karnezis, R. Shayan, M. Downes, T. Davidson, D. Tutt, K. Cheah, S. Stacker, G. Muscat, M. Achen, E. Dejana, and P. Koopman. Sox18 induces development of the lymphatic vasculature in mice. *Nature*, 456:643–647, Dec 2008.

[39] J. Fraser, W. Kimpton, T. Laurent, R. Cahill, and N. Vakakis. Uptake and degradation of hyaluronan in lymphatic tissue. *Biochem J*, 256:153, Nov 1988.

[40] C. Friedman, D. Danforth, C. Herbosa-Encarnacion, L. Arbogast, B. Alak, and D. Seifer. Follicular fluid vascular endothelial growth factor concentrations are elevated in women of advanced reproductive age undergoing ovulation induction. *Fertility and Sterility*, 68:607–612, Oct 1997.

[41] N. Gale, R. Prevo, J. Espinosa, D. Ferguson, M. Dominguez, G. Yancopoulos, G. Thurston, and D. Jackson. Normal lymphatic development and function in mice deficient for the lymphatic hyaluronan receptor lyve-1. *Mol Cell Biol*, 27:595–604, Jan 2007.

[42] P. Galie and R.L. Spilker. A two-dimensional computational model of lymph transport across primary lymphatic valves. *Journal of Biomechanical Engineering*, 131:1297–1307, Nov 2009.

[43] S. Gandhi, J. Powers, A. Nomeir, K. Fowle, D. Kitzman, K. Rankin, and W. Little. The pathogenesis of acute pulmonary edema associated with hypertension. *N Engl J Med*, 344:17–22, Jan 2001.

[44] S.B. Geleff, A. Soleiman, H. Kowalski, R. Horvat, G. Amann, E. Kriehuber, K. Diem, W. Weninger, E. Tschachler, K. Alitalo, and D. Kerjaschki. Angiosarcomas express mixed endothelial phenotypes of blood and lymphatic capillaries. *American Journal of Pathology*, 154:385–394, Feb 1999.

[45] P. Gershkovich and A. Hoffman. Uptake of lipophilic drugs by plasma derived isolated chylomicrons: Linear correlation with interstinal lymphatic bioavailability. *Eur J Pharm Sci*, 26:394–404, July 2005.

[46] C. Halin, N. Tobler, B. Vigl, L. Brown, and M. Detmar. Vegf- a produced by chronically inflamed tissue induces lymphamgrogenesis in draining lymph nodes. *Blood*, 110:3158–3167, Nov 2007.

[47] A. Hargens and B. Zweifach. Contractile stimuli in collecting lymph vessels. *Am J Physiol*, 233:57–65, July 1977.

[48] A. Hawley, L. Illum, and S. Davis. Preparation of biodegradable, surface engineered plga nonospheres with enhanced lymphatic drainage and lymph node uptake. *Pharmaceutical Research*, 14:657–661, Dec 1996.

[49] C.W. Heppell, G Richardson, and T Roose. A model for fluid drainage by the lymphatic system. *Bull Math Biol*, 75:49–81, Nov 2012.

[50] D. Hill, Q. Crews Jr, and P. Walsh. Prostate carcinoma: Radiation treatment of the primary and regional lymphatics. *Cancer*, 34:156–160, July 1974.

[51] T. Hitchcock and L. Niklason. Lymphatic tissue engineering progress and prospects. *Ann N Y Acad Sci*, 1131:44–49, Dec 2008.

[52] R. Hogan and J. Unthank. The initial lymphatic as sensors of interstitial fluid volume. *Microvascular Research*, 31:317–324, May 1986.

[53] M. Holmes. Finite deformation of soft tissue: analysis of a mixture model in uni-axial compression. *Journal of Biomechanical Engeering*, 108:372–381, Nov 1986.

[54] P. Howell, G Kozyreff, and J Ockendon. *Applied Solid Mechanics*. Cambridge University Press, 1^{st} edition, 2009.

[55] R. Huggenberger, S. Siddiqui, D. Brander, S. Ullmann, K. Zimmermann, M. Antsiferoua, S. Werner, K. Alitalo, and M. Detmar. An important role of lymphatic vessel activation in limiting acute inflammation. *Blood*, 117:4667–4678, April 2011.

[56] F. Ikomi, J. Hunt, G. Hanna, and G.W. Schmid-Schönbein. Interstitial fluid, plasma protein, colliod, and leukocyte uptake into initial lymphatics. *Journal of Applied Physiology*, 81:2060–2067, Nov 1996.

[57] D. Jackson, R. Prevo, S. Clasper, and S. Banerji. Lyve-1 the lymphatic system and tumor lymphangiogenesis. *Trends Immunol*, 22:317–321, June 2001.

[58] R.K. Jain, R.T. Tong, and L.L. Munn. Effect of vascular normalization by antiangiogenic therapy on interstitial hypertension, peritumor edema, and lymphatic metastasis: Insights from a mathematical model. *American Association for Cancer Research*, 67:2729–2735, March 2007.

[59] M. Jensen, L. Simonsen, T. Karlsmark, and J. Bulow. Lymphedema of the lower extremities - background, pathophysiology and diagnostic considerations. *Clin Physiol Funct Imaging*, 30:389–398, Nov 2010.

[60] D. Jones and M. Wang. An overview of lymphatic vessels and their emerging role in cardiovascular disease. *J Cardiovasc dis Res*, 2:141–152, Sep 2011.

[61] M. Kaczmarek, R. Subramaniam, and S. Neff. The hydromechanics of hydrocephalus: Steady-state solutions for cylindrical geometry. *Bulletin of Mathematical Biology*, 59:295–323, March 1997.

[62] K. Kajiya, S. Hirakawa, B. Ma, I. Drinnenberg, and M. Detmar. Hepatocyte growth factor promotes lymphatic vessel formation and function. *EMBO J*, 24:2885–2895, Aug 2005.

[63] H. Kärkkäinen, H. Saarelainen, P. Valtonen, T. Laitinen, O. Raitakari, M. Juonala, M. Kähönen, N. Hutri-Kähönen, S. Heinonen, and T. Laitinen. Carotid artery elasticity decreases during pregnancy - the cardiovascular risk in young finns study. *BMC Pregnancy and Child Birth*, 14:98–108, 2014.

[64] T. Keaveny and W. Hayes. A 20-year perspective on the mechanical properties of trabecular bone. *J. Biomech Eng*, 115:534–542, Nov 1993.

[65] M. Klanchar and J.M. Tarbell. Modeling water flow through arterial tissue. *Bulletin of Mathematical Biology*, 49:651–669, Jan 1987.

[66] D. Krag, D. Weaver, T. Ashikagu, F. Moffat, V. Klimberg, C. Shriver, S. Feldman, R. Kusminsky, M. Gadd, J. Kuhn, S. Harlow, and P. Beitsch. The sentinel node in breast cancer - a multicenter validation study. *The New England Journal of Medicine*, 339:941–946, Oct 1998.

[67] V. Kumar, A.K. Abbas, and N. Fausto. *Pathologic Basis of Disease*. W.B. Saunders Company, 7^{th} edition, 1999.

[68] A. Kvanter, P. Algvere, L. Berglin, and S. Seregard. Subfoveal degeneration express vascular endothelial growth factor. *Investigative Ophthalmology and Visual Science*, 37:1929–1934, Aug 1996.

[69] J.M. Lauweryns and J.H. Baert. The role of the pulmonary lymphatics in the defenses of the distal lung: Morphological abd experimental studies of the transport mechanisms of intratracheally instillated particles. *Annals of the New York Academy of Sciences*, 221:244–275, Feb 1974.

[70] L. Leak and J. Burke. Fine structure of the lymphatic capillary and the adjoining connective tissue area. *Am J Anat*, 118:785–809, May 1966.

[71] L.V. Leak. Electron microscopic observations on lymphatic capillaries and the structural components of the connective tissue-lymph interface. *Microvascular Research*, 2:361–391, June 1970.

[72] L.V. Leak. Studies on the permeability of lymphatic capillaries. *The Journal of Cell Biology*, 50:300–323, Feb 1971.

[73] L.V. Leak. The structure of lymphatic capillaries in lymph formation. *Federation proceedings*, 35:1863–1871, June 1976.

[74] L.V. Leak and J.F Burke. Ultrastructural studies on the lymphatic anchoring filmants. *The Journal of Cell Biology*, 36:129–149, Jan 1968.

[75] J.S. Lee. Tissue fluid pressure, lymph pressure, and fluid transport in rat intestinal villi. *Microvascular Research*, 31:170–183, Feb 2004.

[76] J.R. Levick. Flow through interstitium and other fibrous matrices. *Journal of Experimental Physiology*, 72:409–439, March 1987.

[77] P. Lynch, F. Delano, and G.W. Schmid-Schobein. The primary valves in the initial lymphatics during inflammation. *Lymphatics Research and Biology*, 5:3–10, May 2007.

[78] A.J. Macdonald, K.P. Arkill, G.R. Tabor, N.G. McHale, and C.P. Winlove. Modeling flow in collecting lymphatic vessels: one-dimensional flow through a series of contractile elements. *American Journal of Physiology: Heart and Circulatory Physiology*, 295:305–313, May 2008.

[79] M. Macedo, D. Luminoso, M. Savvidou, C. McEniery, and K. Nicolaides. Pregnancy, hypertension, and preeclampsia. *Hypertension*, 51:1047–1051, 2008.

[80] K.N. Margaris and R.A. Black. Modelling the lymphatic system: challenges and opportunities. *Journal of The Royal Society Interface*, 9:601–612, Jan 2012.

[81] S. Mathanson. Insights into the mechanisms of lymph node metastasis. *Cancer*, 98:413–423, May 2003.

[82] A. Mattei, F. Fuechsel, N. Dhar, S. warnike, G. Thalmann, T. Krause, and U. Studer. The template of the primary lymphatic landing sites of the prostate should be revisted: Results of a multimodality mapping study. *european Urology*, 53:118–125, July 2008.

[83] M.C. Mazzoni, T.C. Skalak, and G.W. Schmid-Schönbein. Structure of lymphatic valves in the spinotrapezius muscle of the rat. *Medical and biological engineering and computing*, 24:304–312, Sept 1997.

[84] G. McNeill, M. Witte, C. Witte, W. Williams, J. Hall, D. Patton, G. Pond, and J. Woolfendon. Whole body lymphangioscintigraphy: Preferred method for initial assessment of the peripheral lymphatic system. *RSNA, Radiology*, 172:495–502, Aug 1989.

[85] E. Mendoza and G.W. Schmid-Schönbein. A model for mechanics of primary lymphatic valves. *Journal of Biomechanical Engineering*, 125:407–414, June 2003.

[86] V. Montel, T. Huang, E. Mose, K. Pestonjamasp, and D. Tarin. Expression profiling of primary tumors and mached lymphatic and lung metastases in a xenogentic breast cancer model. *Am J Pathol*, 166:1565–1579, May 2005.

[87] D. Morton, D. Wen, J. Wong, J. Economou, L. Cagle, F. Storm, L. Foshag, and A. Cochran. Technical details of intraoperative lymphatic mapping for early stage melanoma. *Archives of Surgery*, 127:392–399, April 1992.

[88] E. Mouhayer and A. Salahudeen. Hypertension in cancer patients. *Tex Heart Inst J*, 38:263–265, 38.

[89] P.A. Netti, L.T. Baxter, Y. Boucher, R. Skalak, and R.K. Jain. Macro- and microscopic fluid transport in living tissues: application to solid tumors. *AIChE Journal*, 43:818–834, March 1997.

[90] P.A. Nicoll and A.E. Taylor. Lymph formation and flow. *Ann Rev Physiol*, 39:73–95, July 1977.

[91] L. Niklason, J. Koh, and A. Solan. Tissue engineering of the lymphatic system. *Ann N Y Acad Sci*, 979:27–34, Dec 2002.

[92] M. Nipper and J. Dixon. Engineering the lymphatic system. *Cardiovasc Eng Technol*, 2:296–308, Dec 2011.

[93] B. O'Hea, A. Hill, A. Shirbing, S. Yeh, P. Rosen, D. Coit, P. Borgen, and H. Cody. Sentinel lymph node biopsy in breast cancer: Initial experience at memorial sloan kettering cancer center. *Journal of the American College of Surgeons*, 186:423–427, April 1998.

[94] G. Oliver. Lymphatic vasculature development. *Nature reviews immunology*, 4:35–45, 2004.

[95] G. Oliver and M. Detmar. The rediscovery of the lymphatic system: Old and new insights into the development and biological function of the lymphatic vasculature. *Genes Dev*, 16:773–783, April 2002.

[96] J. Pusenjak and D. Miklavcic. Modeling of interstitial fluid pressure in solid tumor. *Simulation Practice and Theory*, 8:17–24, January 2000.

[97] K. Rahmouni, M. Correia, w. Haynes, and A. Mark. Hypertension highlights, obesity-associated hypertension new insights into mechanisms. *Hypertension*, 45:9–14, Decl 2005.

[98] N. Reddy. Effects of mechanical stress on lymph and interstitial fluid flows. *Clinical Practice and Scientific Approach*, 5:203–220, July 1990.

[99] N.P. Reddy and K. Patel. A mathematical model of flow through the terminal lymphatics. *Medical Engineering and Physics*, 17:134–140, Jan 1994.

[100] S.T Reddy, D.A Berk, R.K Jain, and M.A Swartz. A sensitive in vivo model for quantifying interstitial convective transport of injected macromolecules and nanoparticles. *Journal of Applied Physics*, 101:1162–1169, May 2006.

[101] S. Rockson. Lymphedema. *Am J Med*, 110:288–295, Mar 2001.

[102] S. Rockson. Lymphatics: Where the circulation meets the immune system. *Lymphatic Research and Biology*, 11:115–115, Sep 2013.

[103] T. Roose and A. Fowler. Network development in biological gels: roles in lymphatic vessel development. *Bull Math Biol*, 70:1772–1789, Aug 2008.

[104] T. Roose and M. Swartz. Multiscale modeling of lymphatic drainage from tissues using homogenization theory. *J Biomech*, 45:107–115, Jan 2012.

[105] T. Roose and G. Tabor. Multiscale modelling of lymphatic drainage. *Multiscale Modelling of Lymphatic Drainage*, 14:149–176, Jan 2013.

[106] A. Rossi, E. Weber, G. Sacchi, D. Maestrini, F. Di Cintio, and R. Gerli. Mechanotransduction in lymphatic endothelial cells. *Lymphology*, 40:102–113, Sep 2007.

[107] F.R. Sabin. The origin and development of the lymphatic system. *Baltimore: Johns Hopkins Press*, 17:347–348, Dec 1913.

[108] M. Sarntinoranont, F. Rooney, and M. Ferrari. Interstitial stress and fluid pressure within a growing tumor. *Biomedical Engineering Society*, 31:327–335, March 2003.

[109] B. Sauter, D. Foedinger, B. Sterniczky, K. Wolff, and K. Rappersberger. Immunoelectron microscopic characterization of human dermal lymphatic microvascular endothelial cells: Differential expression of cd31, cd34, and type iv collagen with lymphatic endothelial cells vs blood capillary endothelial cells in normal human skin, lymphangioma, and hemangioma in situ. *Journal of Histochemistry and Cytochemistry*, 46:165–176, February 1998.

[110] G.W. Schmid-Schönbein. Microlymphatics and lymph flow. *Physiological Reviews*, 70, 1990.

[111] G.W. Schmid-Schönbein and B.W. Zweifach. Fluid pump mechanisms in initial lymphatics. *Physiology*, 9:67–71, April 1994.

[112] S. Schulte-Merker, A. Sabine, and T. Petrova. Lymphatic vascular morphogenesis in development, physiology, and disease. *J Cell Biol*, 193:607–618, May 2011.

[113] R. Shayan, M.G. Achen, and S.A. Stacker. Lymphatic vessels in cancer metastasis: bridging the gaps. *Carcinogenesis*, 27:1729, Sep 2006.

[114] M. Sherratt. Tissue elasticity and the ageing elastic fibre. *Age*, 31:305–325, Dec 2009.

[115] T. Skalak, G.W. Schmid-Schönbein, and B.W. Zweifach. New morphological evidence for a mechanism of lymph formation in skeletal muscle. *Microvasc*, 28:95–112, July 1984.

[116] M. Skobe and M. Detmar. Structure, function, and molecular control of the skin lymphatic system. *Journal of Investigative Dermatology*, 5:14–19, June 2000.

[117] C.H. Sloop, L. Dory, and P.S. Roheim. Interstitial fluid lipoproteins. *Journal of Lipid Research*, 28:225–237, March 1987.

[118] J. sorof and S. Daniels. Obesity hypertension in children a problem of epidemic proportions. *Hypertension*, 40:441–447, Aug 2002.

[119] J. Sowers, M. Epstein, and E. Frohlich. Diabetes, hypertension, and cardiovascular disease an update. *Hypertension*, 37:1053–1059, 2001.

[120] S.A. Stacker, M.G. Achen, L. Jussila, M.E. Baldwin, and K. Alitalo. Lymphangiogensis and cancer metastasis. *Nature Reviews. Cancer*, 2:573–583, Aug 2002.

[121] N. Staub. Pulmonary edema due to increased microvascular permeability to fluid and protein. *Circulation Res*, 43:143–151, Aug 1978.

[122] M.A. Swartz. The physiology of the lymphatic system. *Advanced Drug Delivery Reviews*, 50:3–20, Aug 2001.

[123] M.A. Swartz, D.A. Berk, and R.K. Jain. Transport in lymphatic capillaries.i. macroscopic measurements using residence time distribuation theory. *Studies in Mechanobiology, Tissue Engineering and Biomaterialsl*, 270:324–329, Jan 1996.

[124] M.A Swartz and K.C. Boardman J_R. The role of interstitila stress in lymphatic function and lymphangiogenesis. *Annals of the New York Academy of Sciences*, 979:197–210, Dec 2002.

[125] M.A. Swartz and M.E. Fleury. Interstitial flow and its effects in soft tissue. *Annu Rev Biomed Eng*, 9:229–256, April 2007.

[126] M.A. Swartz, A. Kaipainen, P.A. Netti, C. Brekken, Y. Boucher, A.J. Grodzinsky, and R.K. Jain. Mechanics of interstitial-lymphatic fluid transport: theoretical foundation and experimental validation. *Journal of Biomechanics*, 32:1297–1307, Dec 1999.

[127] A. Szuba and S. Rockson. Lymphedema: Anatomy, physiology and pathogenesis. *Vasc Med*, 2:321–326, Nov 1997.

[128] A. Taylor and H. Gibson. Concentrating ability of lymphatic vessels. *Lymphology*, 8:43–49, June 1975.

[129] D.P. Theret, M.J. Levesque, M. Sato, R.M. Nerem, and L.T. Wheeler. The applications of a homogeneous half-space model in the analysis of endothelail cell micropipette measurements. *Biomechanical Engineering*, 110:190–199, 1988.

[130] J. Unthank and H. Bohlen. Lymphatic pathways and role of valves in lymph propulsion from small intestine. *Am. J. Physiol.*, 254:389–398, 1988.

[131] P. Von der Weid and D. Zawieja. Lymphatic smmoth muscle: The motor unit of lymph drainage. *Int J Biochem Cell Biol*, 36:1147–1153, July 2004.

[132] H. Wang, S. Patel, M. Carey, and D. Wang. Quantifying anomalous intestinal sterol uptake, lymphatic transport, and biliary secretion in abcg8 mice. *Hepatology*, 45:998–1006, March 2007.

[133] R. Wilaman, R. Mackey, A. Bostom, T. thompson, and K. Sulton-tyrrell. Measures of obesity are associated with vascular stiffness in young and older adults. *Hypertension*, 42:408–473, Sep 2003.

[134] J. Wong, L. Cagle, and D. Morton. Lymphatic drainage of skin to a sentinel lymph node in a feline model. *Ann Surg*, 214:637–641, Nov 1991.

[135] D. Zawieja. Lymphatic biology and the microcirculation past present and futre. *Microcirculation*, 12:141–150, Jan 2005.

[136] D. Zawieja. Contractile physiology of lymphatics. *Lymphat Res Biol*, 7:87–96, 2009.

[137] B. Zweifach and J. Prather. Micromanipulation of pressure in terminal lymphatics in the mesentery. *Am. J. Physiol.*, 228:1326–1335, 1975.

[138] B. Zweifach and A. Siberberg. The interstitial lymphatic flow system. *Int Rev Physiol*, 18:215–260, Jan 1979.